The different functions of sEV-derived miR-574-5p in PGE_2-dependent tumors correlate with the tetraspanin composition on the sEV envelope

vom Fachbereich Biologie der Technischen Universität Darmstadt

zur Erlangung des akademischen Grades

Doctor rerum naturalium

(Dr. rer. nat.)

Dissertation

von M. Sc. Eva Pröstler

Erstgutachterin: Dr. Meike Julia Saul

Zweitgutachterin: Prof. Dr. Beatrix Süß

Darmstadt 2023

Eva Pröstler: The different functions of sEV-derived miR-574-5p in PGE_2-dependent tumors correlate with the tetraspanin composition on the sEV envelope

Darmstadt, Technische Universität Darmstadt

Jahr der Veröffentlichung der Dissertation auf TUprints: 2023
URN: urn:nbn:de:tuda-tuprints-246018

Tag der mündlichen Prüfung: 22.09.2023

Der Fortgang der wissenschaftlichen Entwicklung ist im Endeffekt eine ständige Flucht vor dem Staunen. – Albert Einstein

Table of Contents

List of Figures

List of Tables

Summary

Small extracellular vesicles (sEV) are essential for intracellular communication in the tumor microenvironment (TME). They can transport biological molecules, such as proteins or nucleic acids, including microRNAs (miRs), a class of short non-coding RNAs. MiRs can exert various functions in gene regulation of target cells. This work aimed to elucidate the transferability of the diverse functions of miR-574-5p to different tumor models. For this purpose, the two prostaglandin E_2 (PGE_2)-dependent tumor types, non-small cell lung cancer (NSCLC) and neuroblastoma (NB), were investigated. In NSCLC, miR-574-5p regulates the microsomal prostaglandin E_2 synthase 1 (mPGES-1)-dependent PGE_2 synthesis, which contributes to tumor progression. At the intracellular level, miR-574-5p binds to the CUG-RNA binding protein 1 (CUGBP1), thereby upregulating the synthesis of mPGES-1 and its enzymatic product PGE_2. In this thesis, this function of intracellular miR-574-5p was also shown in NB with 11q deletion. Furthermore, NB cells were shown to specifically secrete miR-574-5p into their sEV upon stimulation with PGE_2, similar to NSCLC cells. The autocrine role of sEV-derived miR-574-5p in mPGES-1 regulation was not confirmed in NB. However, sEV-miR-574-5p derived from NB cells was shown to exert a novel paracrine role by specific upregulation of the differentiation marker α-smooth muscle actin (α-SMA) of fibroblasts in the TME via Toll-like receptors (TLR) 7/8. Another point investigated in this study was the influence of the tetraspanins CD9, CD63, and CD81 on the functional transfer of sEV-miR-574-5p. In both tumor types, NB and NSCLC, inhibition of specific tetraspanins was shown to alter the function of sEV-miR-574-5p. A difference in the rate of internalization of sEV was excluded as the cause of this functional change. The link between tetraspanins and the functional mediation of sEV-derived miRs is a novel and promising aspect of cancer research.

Overall, this work revealed a new paracrine function of sEV-miR-574-5p, regulating the α-SMA levels of fibroblasts in the TME. Furthermore, the transferability of intracellular and extracellular miR-574-5p functions to different tumor models were analyzed. The interaction of miR-574-5p and CUGBP1 was shown to be transferable from NSCLC to NB, whereas the role of sEV-derived miR-574-5p differed. Investigating the transferability of miR functions to different tumor types is an important approach to maximize the therapeutic benefit of miRs with the least effort and the greatest impact.

Zusammenfassung

Kleine extrazelluläre Vesikel (sEV) sind für die intrazelluläre Kommunikation in der Tumormikroumgebung (TME) von wesentlicher Bedeutung. Sie können biologische Moleküle wie Proteine oder Nukleinsäuren transportieren, darunter auch mikroRNAs (miRs), eine Klasse kurzer nicht-kodierender RNAs. MiRs können verschiedene Funktionen bei der Genregulation in Empfängerzellen ausüben. Ziel dieser Arbeit war es, die Übertragbarkeit der vielfältigen Funktionen von miR-574-5p auf verschiedene Tumormodelle zu untersuchen. Zu diesem Zweck wurden die beiden Prostaglandin-E_2 (PGE_2) -abhängigen Tumorarten nicht-kleinzelliger Lungenkrebs (NSCLC) und Neuroblastom (NB) untersucht. Im NSCLC reguliert miR-574-5p die mikrosomale Prostaglandin-E_2-Synthase 1 (mPGES-1)-abhängige PGE_2-Synthese, die zur Tumorprogression beiträgt. Auf intrazellulärer Ebene bindet miR-574-5p an das CUG-RNA-bindende Protein 1 (CUGBP1), wodurch die Synthese von mPGES-1 und die seines enzymatischen Produkts PGE_2 hochreguliert wird. In dieser Arbeit wurde diese Funktion der intrazellulären miR-574-5p auch bei NB mit 11q-Deletion bestätigt. Außerdem wurde gezeigt, dass NB-Zellen bei Stimulation mit PGE_2 spezifisch miR-574-5p in ihre sEV sezernieren, ähnlich wie NSCLC-Zellen. Die autokrine Rolle von in sEV übermittelter miR-574-5p bei der Regulation von mPGES-1 wurde im NB nicht bestätigt. Allerdings wurde hier eine neuartige parakrine Rolle entdeckt, welche die sEV-miR-574-5p aus NB-Zellen ausübt, indem es über Toll-like-Rezeptoren (TLR) 7/8 spezifisch den Differenzierungsmarker *α-smooth muscle actin* (α-SMA) von Fibroblasten in der TME induziert. Ein weiterer Punkt, der in dieser Studie untersucht wurde, war der Einfluss der Tetraspanine CD9, CD63 und CD81 auf die Funktionsübertragung von sEV-miR-574-5p. Es zeigte sich, dass sowohl in NB als auch in NSCLC die Blockierung bestimmter Tetraspanine auf der sEV-Hülle zu einer Veränderung der Funktion von sEV-miR-574-5p führte. Eine Veränderung der Internalisierungsrate von sEV wurde als Ursache für diese Funktionsänderung ausgeschlossen. Die Verbindung zwischen Tetraspaninen und der funktionellen Vermittlung von sEV-vermittelten miRs ist ein neuer und vielversprechender Aspekt der Krebsforschung.

Insgesamt wurde in dieser Arbeit eine neue parakrine Funktion von sEV-miR-574-5p aufgedeckt, welche den α-SMA-Spiegel von Fibroblasten im TME reguliert. Darüber hinaus wurde die Übertragbarkeit der intrazellulären und extrazellulären miR-574-5p-Funktionen auf verschiedene Tumormodelle analysiert. Es zeigte sich, dass die Interaktion zwischen miR-574-5p und CUGBP1 von NSCLC auf NB übertragbar ist, während die Rolle von sEV-übermittelter miR-574-5p unterschiedlich ist. Die Untersuchung der Übertragbarkeit von miR-Funktionen auf verschiedene Tumortypen ist ein wichtiger Ansatz, um den therapeutischen Nutzen von miRs mit dem geringsten Aufwand und der größten Wirkung zu maximieren.

1. Introduction

1.1. Small extracellular vesicles

Communication between different cell types can occur via different pathways. There is direct communication via cellular contacts, like filopodial bridges or gap junctions [1,2], or via soluble factors like cytokines, as transforming growth factor-β (TGFβ) [3]. Another pathway is communication via extracellular vesicles (EV), which are secreted by various cell types and can mediate multiple paracrine physiological functions [4]. Finally, even distant cells can be reached in the organism via distribution through the bloodstream or other bodily fluids, such as saliva [5,6]. They offer the physiological advantage that combinations of ligands can be transferred between cells, even without cell-cell contact. In addition, membrane elements can be exchanged easily without having to be released from the membrane [7].

EV can be classified into different subtypes, based primarily on size and biogenesis (Figure 1) [8]. Oncosomes are large vesicles with a diameter of 1-10 µm and can contain many biologically active components, such as metalloproteinases, ribonucleic acid (RNA), or caveolin-1 [9]. Apoptotic bodies are also large EV ranging in size from 1 to 5 µm and are released by dying cells during apoptosis [10,11]. Migrasomes are shedded by retraction fibres of migrating cells [12]. Microvesicles (often called ectosomes) are about 100-1000 nm in size and are directly shedded by the plasma membrane, while exosomes are 30-100 nm in size and are released by the fusion of multivesicular bodies (MVBs) with the plasma membrane [13,14]. A group of EV discovered only recently in 2018 due to their small size are extracellular nanoparticles called exomeres [15]. These particles have a maximum diameter of only 50 nm. Despite their small size, exomeres also contain and transfer functional cargo [16].

The definition of the EV subtypes often differs depending on the literature [17]. In line with the 2018 minimal information for studies of extracellular vesicles (MISEV) guidelines, this work will refer to exosomes and microvesicles alike as small EV (sEV) [18] because there is no way to differentiate between the two with the most commonly used purification methods, such as ultracentrifugation [13].

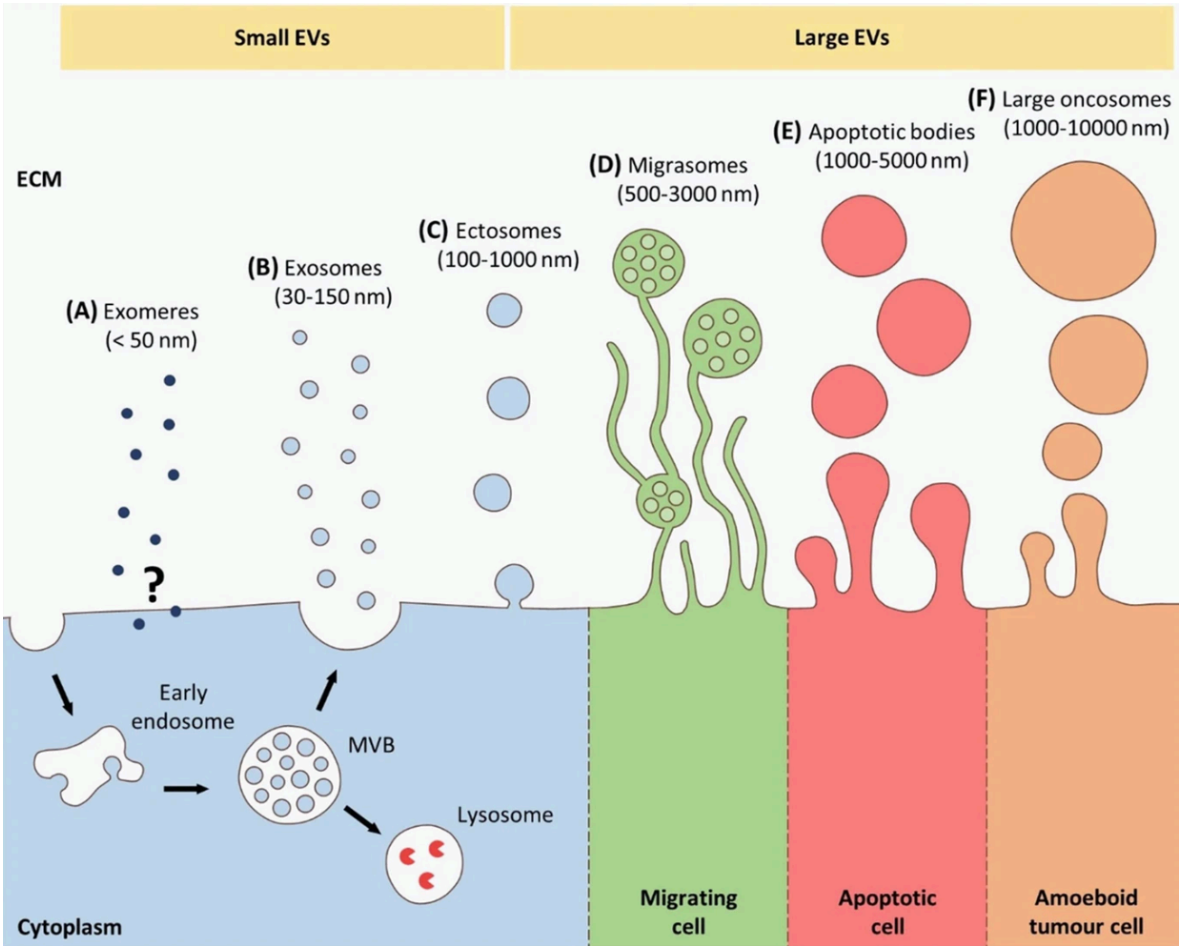

Figure 1: Different subtypes of EV.

There are various subtypes of extracellular vesicles (EVs) secreted by cells. (A) Exomeres are non-membranous nanoparticles with a size under 50 nm and currently unknown functions. (B) Exosomes are originating from the endosome and of a size around 30 – 150 nm. (C) Microvesicles or ectosomes are shed directly into the extracellular space from the cell membrane. (D) Migrasomes are secreted during cell migration by retraction fibres and belong to the large EVs. (E) Apoptotic bodies are directly shed into the extracellular space by apoptotic cells. (F) Large oncosomes are around 1 – 10 µm and derived from amoeboid tumor cells and carry oncogenic cargo [12].

1.1.1. Small extracellular vesicle content

SEV are membrane vesicles with a complex structure, consisting of many exchangeable elements (Figure 2). These include various proteins, lipids, and various nucleic acids as DNA including histones, mRNA, non-coding RNA and microRNA (miR) [19]. The most abundant proteins include tetraspanins, which fulfill a function in vesicle formation, invasion, and fusion; heat shock proteins (HSPs), which contribute to the stress response; and MVB formation proteins, which play a role in sEV release. Many of these proteins are also used as markers for sEV (e.g., CD9, CD63, Alix, HSP70) [20].

Not only does the protein content of sEV differ, but also the lipid composition. Depending on the cellular origin of sEV, the presence and levels of cholesterol, glycosphingolipids, or sphingomyelin vary between sEV subpopulations [21,22]. In addition, bioactive lipids like

prostaglandin E $(PGE)_2$ can also be transported via sEV and exert functions on other cells [23,24]. It has been shown that leukotriene biosynthesis can occur in sEV and thus affect targeted cells [25]. Another group of molecules that can exert functions on other cells are miRs [26]. MiRs are the most abundant type of RNA in human plasma-derived exosomal RNA, with 76.20% of all mappable reads besides ribosomal RNA, transfer RNA, or long non-coding RNA [26]. They are reported to play a role in exosome-based cell-cell communication and can influence angiogenesis, exocytosis, or tumorigenesis [27–29]. In the context of the tumor microenvironment, the exchange of sEV between tumor cells and the surrounding non-tumor cells may contribute decisively to cancer progression [30].

1.1.2. Biogenesis of small extracellular vesicles

As mentioned previously, there are two main pathways of sEV biogenesis. While microvesicles directly originate from the plasma membrane, exosomes are released from MVBs [4,13]. MVBs or multivesicular endosomes (MVEs) are intracellular organelles that are formed, for example, during endocytosis by invagination of the cell membrane [31]. They are derived from the early endosome, which can internalize biomolecules and thereby ensure their sorting [32]. In this way, MVBs can be used by the cell for the degradation, recycling, or exocytosis of proteins, lipids, or nucleic acids [33]. By invagination of the MVB membrane, intraluminal vesicles (ILV) are created within the MVB, containing internalized biomolecules. By fusion of MVBs with the cell membrane, the ILVs are released into the extracellular space and, from then on, called exosomes (Figure 2) [13].

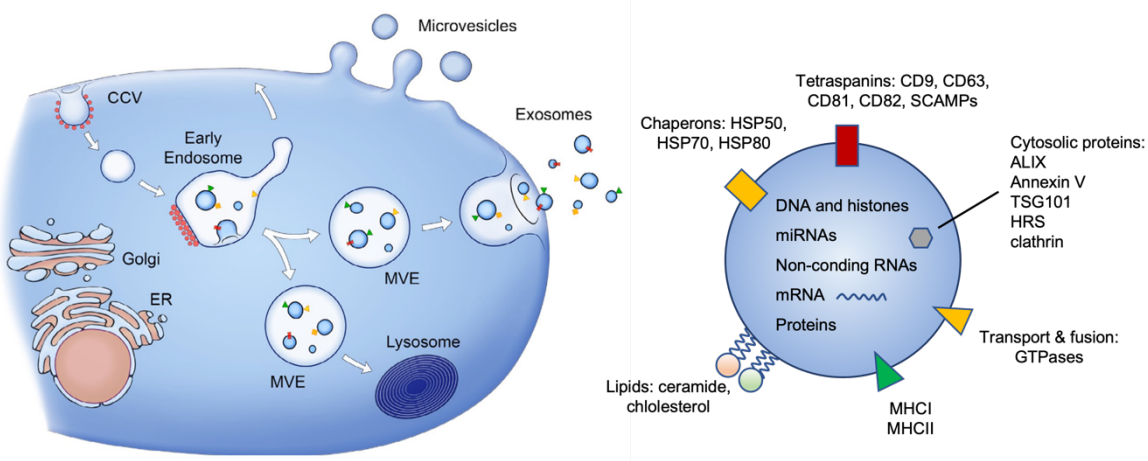

Figure 2: The origin of sEV.

The two subtypes of small extracellular vesicles (sEV) are microvesicles and exosomes. While microvesicles are released from the cell membrane, exosomes are formed by the fusion of multivesicular bodies (MVB, also called multivesicular endosome, MVE) with the cell membrane. MVBs originate at the early endosome by the uptake of intraluminal vesicles. MVBs can then either fuse with the plasma membrane and release exosomes or fuse with lysosomes. SEV contain different nucleic acids like DNA, miR, and mRNA and cytosolic proteins like ALIX, Annexin V, and HRS. The membrane contains various transmembrane proteins, such as tetraspanins, chaperones, or GTPases. Adapted from [4,13].

The endosomal sorting complex required for transport (ESCRT) plays a crucial role in the sEV biogenesis [34]. This protein complex consists of four main complexes (ESCRT-0, -I, -II, and -III) that, together with other proteins (Vacuolar protein sorting-associated protein 4A (VPS4A), vesicle trafficking 1 (VTA1), apoptosis-linked gene 2 interacting protein X (ALIX)) promote ILV and MVB biogenesis [4]. In the first step, ESCRT-0 recognizes ubiquitinated domains of endosomal membrane proteins, like hepatocyte growth factor-regulated tyrosine kinase substrate protein (HRS), and recruits ESCRT-I and -II to the MVB membrane. Then, ESCRT-I and -II initiate the budding of ILVs into the MVBs. ESCRT-III/VPS4 complex is involved in the final steps of ILV release within the MVB by stabilizing and cleaving the bud [34]. Since ESCRT-0 generally recognizes and binds ubiquitinated proteins, proteins can also be sorted into exosomes as cargo via this pathway [35]. The ESCRT complex can be recycled and reassembled for further ILV formation. Many proteins associated with ESCRT are also found in exosomes, including, for example, syntenin or ALIX [36].

In the end, MVBs are either transported to the plasma membrane to release ILVs as exosomes into the extracellular space via exocytosis or transported to the lysosome to be degraded [13]. This is mainly decided by the cholesterol content of the MVB membrane [37]. Cholesterol-rich MVBs are transported to the cell membrane, whereas cholesterol-poor MVBs are subjected to lysosomal degradation. The transport of MVBs to the plasma membrane relies on the cell's cytoskeleton. Here, actin and microtubules interact with the MVBs [38,39]. In addition, Rat sarcoma viral oncogene homologue-associated binding (Rab) proteins play a role in transporting MVBs to the membrane [40,41]. They generally influence membrane trafficking, vesicle formation, and membrane fusion [42].

The membrane fusion process needed for exocytosis is mediated by the soluble N-ethylmaleimide-sensitive-factor attachment receptor (SNARE) proteins [37]. Firstly, the transmembrane proteins synaptobrevin and syntaxin with SNARE motifs establish the initial interaction of both membranes. Then, the SNARE complex is formed by the two proteins and two more synaptosomal-associated protein of 25 kDa (SNAP-25) proteins (SN1 and SN2), enhancing proximity. The lipids mix and new formations occur until all lipids of the vesicular membrane are incorporated into the cell membrane [7,43].

The ESCRT-dependent biogenesis pathway is well described, but there are other ESCRT-independent pathways of exosome biogenesis [4]. Tetraspanins are enriched in exosomes and play a role in ESCRT-independent exosome release [44]. For example, CD63 is known to play a role in ESCRT-independent sorting of ILVs [45,46]. It was observed that the knockdown of CD63 resulted in reduced secretion of sEV. Additionally, not only proteins but also lipids are essential for vesicle formation [42]. Inhibition of neutral sphingomyelinase 2 (nSMase2), which

forms ceramides from sphingomyelin, resulted in a reduction of exosome release [47]. However, ceramides do not affect exosome secretion in all cell lines [45,48].

The amount of secreted sEV varies significantly between different cell types [33]. Cellular stress like irradiation [49] or hypoxia [50] can increase exosome secretion. This is not only valid for sEV in general but also for the cargo of sEV, which can change specifically by inflammatory triggers or hypoxia [51,52]. Initially, it was assumed that sEV generally transport waste products out of the cell [53,54]. However, since the discovery that T lymphocytes can be activated by sEV from B lymphocytes in 1996, sEV have been known to exert physiological functions [55]. Since the early 2000s, sEV have been known to transfer biological cargo between cells and more functions have been discovered [30,56]. Thus, they play a crucial role in intercellular communication [57]. The impact of the transported cargo, however, is highly dependent on the uptake mechanism of sEV by target cells.

1.1.3. Uptake mechanisms of small extracellular vesicles

There are different mechanisms of sEV uptake [58]. Firstly, sEV can interact with target cells without transferring cargo to the cell. For example, surface proteins can interact with receptors on the target cell to trigger signaling cascades [59]. An example is the activation of T-cell receptors on T lymphocytes by peptide complexes on sEV secreted by dendritic cells [60]. Also, several other ligands expressed on the surface of sEV, such as tumor necrosis factor (TNF) or Fas ligand (FasL), can bind to TNF receptors on tumor cells and thereby trigger caspase-mediated apoptosis [61].

However, there are also several uptake routes through which sEV cargo can be internalized by a cell (Figure 3). SEV can fuse with the plasma membrane of the target cell and thus release their cargo into the cytosol. This pathway is not well understood, but presumably, SNARE and proteins of the Rab family, which are already involved in membrane fusion for the release from the host cell, again play a role [43,62]. In addition, tetraspanins are thought to influence fusion, but so far, this has been shown mainly for viral fusion with the cell [63,64].

A better-studied uptake mechanism is endocytosis. There are several endocytotic pathways that are temperature- and energy-dependent, require a functioning cytoskeleton and can proceed very rapidly [58]. Several studies are describing first internalization only 30 min after addition of sEV [65–67]. During this process, sEV are first internalized, which is then followed by cargo release. When sEV are taken up via clathrin-mediated endocytosis, clathrin-coated vesicles are formed in the target cells [68]. These are then further processed by uncoating and fusing with the endosome. Clathrin-mediated endocytosis involves the guanosine-5'-triphosphate (GTP)ase Dynamin-2, which is required in order to uncouple the clathrin-coated vesicle from the membrane [69,70]. Caveolin-dependent endocytosis is a clathrin-independent

pathway, but similar to clathrin-dependent endocytosis. Here, invaginations are formed in the membrane that are later taken up by the cell. These invaginations are also called caveolae and consist of membranes rich in cholesterol, sphingolipids, and caveolins [71,72]. This pathway is sensitive to cholesterol and Caveolin-1 depletion [58,73]. Caveolin-1 is shown to be enriched in clusters in these caveolae and forms complexes with other caveolins, cholesterol, and fatty acids [74,75]. It is also thought that Dynamin-2 has a function in caveolin-dependent endocytosis, but this cannot be precisely determined due to its function in clathrin-mediated endocytosis [69,76].

Endocytosis pathways also include macropinocytosis and phagocytosis. Macropinocytosis involves the formation of membrane invaginations, actin-driven lamellipodia that internalize extracellular components into intracellular compartments such as the endosome [62,77]. Fusion of lamellipodia with other membrane extensions or the plasma membrane results in the inclusion of extracellular areas. These may contain sEV or ligands that will not need to interact directly with the cell [58]. However, this uptake pathway is probably either a pathway that does not occur frequently or is only used by specific cell types, as this mechanism often does not play a role in internalization experiments [78–80]. Phagocytosis, on the other hand, is an endocytotic pathway that is receptor-mediated [81]. During this process, larger particles are internalized the same way as bacteria or fragments of apoptotic cells [77]. Cells have been shown to take up particles as small as 85 nm, which is within the size range of larger sEV [82]. Phagocytosis is mainly used by specialized cells, such as macrophages, monocytes, and neutrophils [83]. In this context, activation of the Fc receptor triggers the extension of filopodia around the particle, followed by rac1-dependent internalization [81,84]. The phagocytosed particles are internalized into actin-lined membranes and can be transferred to either the endosome or released into the cytoplasm [85,86].

Lipid rafts are yet another membrane component that is involved in different endocytosis pathways [83]. Lipid rafts are detergent-resistant membrane microdomains enriched in cholesterol, sphingolipids, glycosylphosphatidylinositol-anchored proteins and transmembrane proteins [58]. Since lipid rafts are concentrated and tightly packed regions of lipids, they are less fluid, but float in the membrane [87]. Lipid rafts are known to be involved in clathrin-independent endocytosis pathways, due to their high levels of cholesterol. At the same time, they are enriched in flotillins, proteins which mediate endocytosis independent of clathrin and caveolin [48,88].

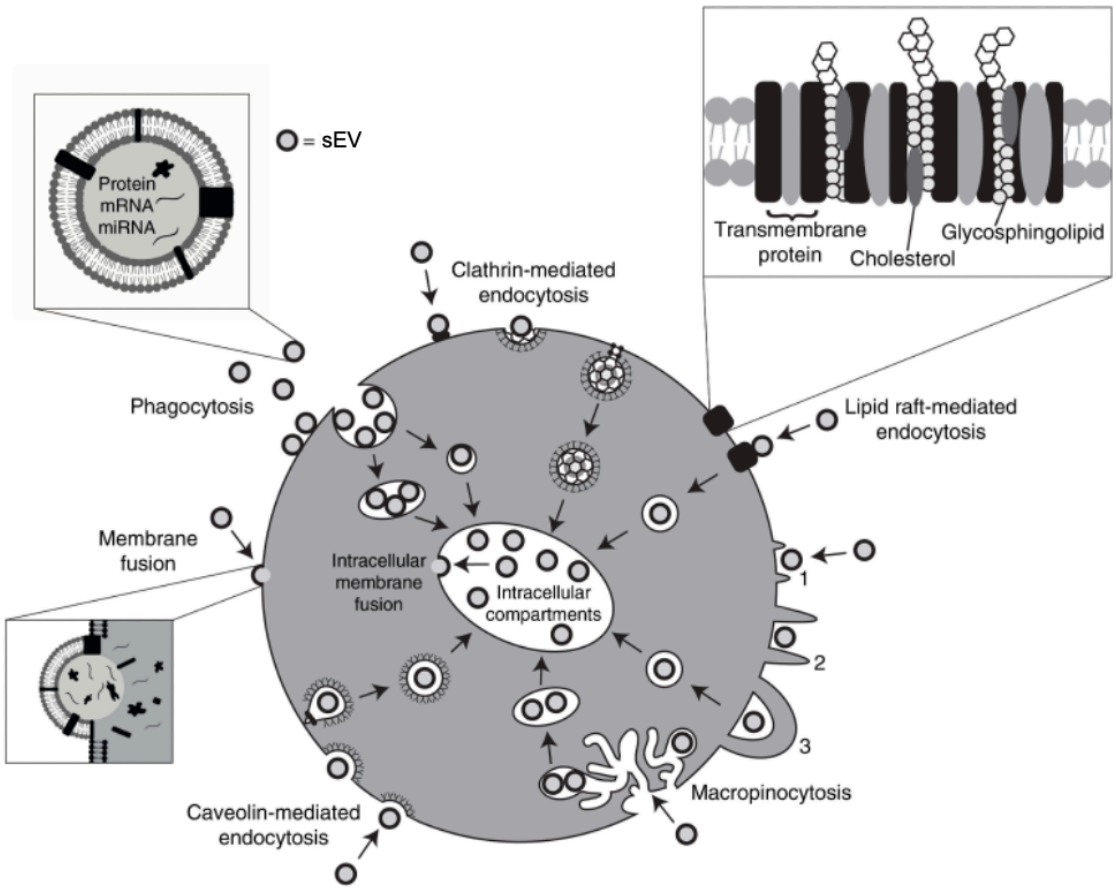

Figure 3: The different uptake mechanisms of sEV.

Internalization of sEV can occur via several uptake mechanisms. During membrane fusion, the cargo of sEV is directly released into the cytoplasm. For the endocytosis pathways, which include the caveolin-mediated, lipid raft-mediated, clathrin-mediated or macropinocytosis and phagocytosis subtypes, the entire sEV, including its cargo, is internalized. Inside the cell, the cargo can then be transferred to intracellular compartments. Modified from [58].

These different modes of sEV uptake can co-exist within the same target cell [62]. For example, in ovarian tumor or melanoma cells, sEV were mainly internalized via cholesterol-associated lipid rafts, but clathrin-mediated endocytosis, phagocytosis, and macropinocytosis were also observed [65,89,90].

Depending on how sEV are internalized, their cargo can enter the cytoplasm or intracellular compartments like the endosome, nucleus, and endoplasmic reticulum, or sEV can be targeted to the lysosome [91]. Alternatively, sEV may be recycled and released back into the extracellular space. This has been shown for fibroblast-derived CD81-positive sEV. They are taken up and released by breast cancer cells, which positively affects cell motility [92].

1.1.4. Tetraspanins and their role in the internalization of small extracellular vesicles

Tetraspanins are an essential group of sEV marker proteins that also play a role in sEV biogenesis as well as recognition and uptake by target cells [93]. In addition, tetraspanins are thought to play a role in the sorting of miRs and proteins into sEV [94]. These highly conserved membrane proteins occur in clusters on the sEV surface as "tetraspanin-enriched microdomains". Since tetraspanins are associated with cholesterol and gangliosides, they also are enriched in the microdomains, similar to lipid rafts [95,96]. Other components of these tetraspanin-enriched microdomains include integrins, adhesion receptors, and transmembrane receptor proteins, which make them predestined for the interaction with target cells [97]. Tetraspanins consist of four transmembrane domains, a small conserved extracellular loop and a large extracellular loop including a disulphide-stabilized variable region (Figure 4) [98]. Intracellular palmitoylation of cysteines in the transmembrane domains leads to association with other proteins within tetraspanin-enriched microdomains, for example integrins [99].

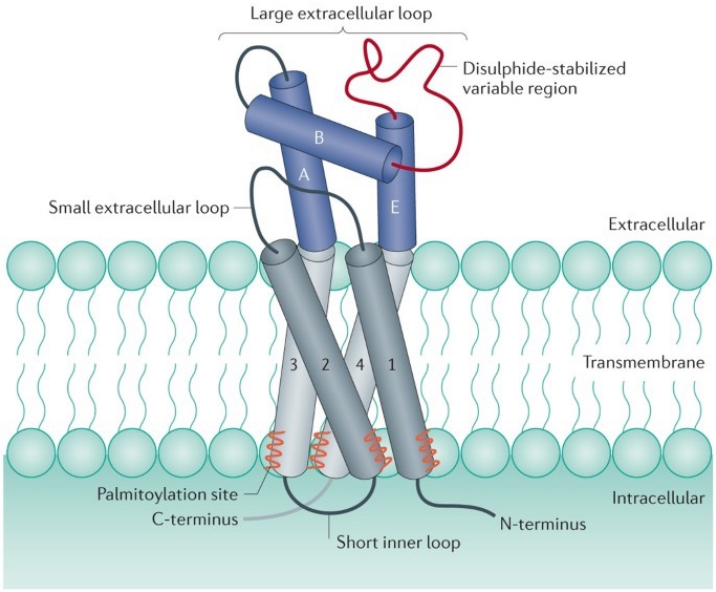

Figure 4: The typical tetraspanin structure.

Tetraspanins are transmembrane proteins with four transmembrane helices (grey), a small conserved extracellular loop, and a large extracellular loop consisting of 3 conserved helices A, B, and E (blue) and a variable disulphide-stabilized variable region (red). Intracellular palmitoylation of membrane-proximal cysteines (orange) leads to association of tetraspanins with other proteins within tetraspanin-enriched microdomains [100].

Because they are highly enriched in sEV (7 to 124-fold) compared to their host cells, tetraspanins are commonly used as sEV markers, which include CD9, CD63, CD37, CD81, and CD82 [93]. The tetraspanin composition is distinct for each sEV subpopulation [101]. This specificity of sEV is hypothesized to influence the targeting and uptake of sEV and, thus, its function [93]. For example, high expression of tetraspanin 8 (Tspan8) increases the sorting of vascular cell adhesion molecule 1 (VCAM-1) and integrins into sEV, which results in increased

binding of sEV to endothelial cells [102,103]. The effect of the tetraspanins on the internalization of sEV has not been studied in detail, but there is described an alternative endocytosis pathway of viruses via tetraspanin-enriched microdomains in the cellular membrane [104]. In addition, via the microdomains various fusion processes, such as viral uptake or sperm-egg fusion, are regulated [63,64,105]. Furthermore, in the treatment of viral infections, neutralizing antibodies against tetraspanins are used to inhibit viral uptake by cells via tetraspanin-enriched microdomains [106,107]. For example, hepatitis C infection can be treated with the addition of CD81-targeted antibodies, which are dependent on CD81 for cellular uptake [108]. In summary, tetraspanins play a crucial role in the biogenesis and function of sEV, but most of the mechanisms remain unclear. A deeper understanding of tetraspanins will help to understand the specificity of sEV functions.

1.2. MicroRNAs

MiRs are highly conserved non-coding RNAs of about 22 nucleotides (nts) in length and are considered key regulators of post-transcriptional gene expression [109]. These small single-stranded RNAs can exert important roles in various biological processes, for example, cell proliferation or differentiation [110]. The first miR, called lin-4 was discovered in *Caenorhabditis elegans* (*C. elegans*) in 1993 [111]. When discovered, miRs were thought to be rare exceptions found only in nematodes [112–114]. In 2001, three independent publications reported that several hundred of these small non-coding RNAs were found not only in nematodes, but also in mouse and human cells. Since then, many more miRs have been discovered, most of them highly conserved across different species [115]. Currently, more than 38.500 miRs have been identified [116], although the functions of many of them are still unknown [117].

1.2.1. Biogenesis of microRNAs

MiRs are formed via precursors called pri-miRs, which are transcribed from genes and processed into shorter pre-miRs by the microprocessor complex in the nucleus (Figure 5) [118]. This complex consists of the RNA-binding protein DiGeorge Syndrome Critical Region 8 (DGCR8) and the ribonuclease III enzyme Drosha [119]. The processed pre-miR is then exported from the nucleus to the cytoplasm by Exportin 5 and RanGTP while protecting it from degradation by nucleases [120]. Removal of the terminal loop from the pre-miR by the RNA polymerase III Dicer finally results in the formation of a mature miR duplex [121]. Only one strand of this miR duplex is introduced into a larger complex called the RNA-induced silencing complex (RISC), together with Argonaute 2 (AGO2) [122]. The passenger strand is usually degraded [121]. Which strand will be degraded strongly depends on the cell type and cellular environment [123]. Often, the strand selection is also based on the thermodynamic stability at

the 5'-end. The directionality of the miR strand determines the name of the mature miR. While the 5p strand arises from the 5'-end of the hairpin, the 3p form originates from the 3'-end [124].

The miR biogenesis pathway described above is the canonical and most common pathway. However, there are also several non-canonical biogenesis pathways [109] that involve the same proteins, Drosha, Dicer, AGO2, and Exportin 5. An example for miRs that originate from a non-canonical pathway are the 7-methylguanosine-capped pre-miRs [125]. These RNAs are not cut by Drosha but exported directly into the cytoplasm by Exportin 5. There is a strong tendency towards the 3p strand, most likely due to the 7-methylguanosine cap preventing loading of the 5p strand into AGO2. Studies have also shown that a large fraction of miRs are present in so-called miRtrons and are processed by the spliceosome via a non-canonical pathway (Figure 5) [126,127]. After splicing, the pre-miRs are exported to the cytoplasm by Exportin 5 and processed by Dicer to mature miRs. MiRtrons and canonical miRs can be distinguished based on various features, such as guanine content, hairpin-free energy, or hairpin length [128].

MiRs can exert different functions, which are cell-specific and also depend on their intracellular location [52].

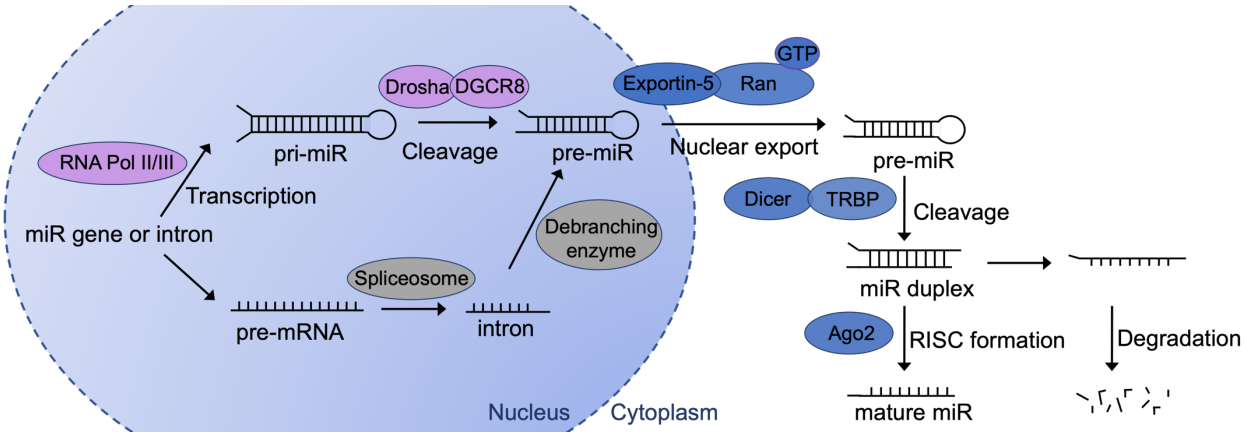

Figure 5: MiR biogenesis.

MiRs are either transcribed via the canonical pathway from miR genes or non-canonically spliced from intronic sequences of host genes. The non-canonical pathway requires the spliceosome and debranching enzyme. In the canonical pathway, the pri-miR is processed by Drosha and DiGeorge Syndrome Critical Region 8 (DGCR8). In both pathways, the pre-miR is further exported into the cytoplasm and there processed by Dicer and Argonaute (AGO)2, to finally generate a mature miR. Figure adapted from [129,130].

1.2.2. Post-transcriptional gene expression regulation by microRNAs

The functions of miRs are also divided into canonical and non-canonical functions. Conventionally, miRs were thought to act as global gene expression repressors [131]. Once a miR is loaded into the RISC after canonical biogenesis and one strand of the miR duplex has been removed by AGO2, only the leading strand is active [123]. This miR can then bind to a

target sequence, which is often located in the 3' untranslated region (UTR) of an mRNA, resulting in endonucleolytic cleavage, translational repression or deadenylation of the mRNA transcript [110]. The complementarity between a miR and its target sequence plays a major role in this process. If the miR is entirely complementary to the target sequence, AGO2 endonuclease activity is induced and mRNA degradation occurs [132]. However, in animal cells, compared to plant cells, the sequences are often not completely complementary, which inhibits AGO2 endonuclease activity [133]. In this case, AGO2 acts as a mediator for RNA interference (RNAi), resulting in translational repression [132].

If the miR-RISC complex binds to mRNA regions other than the 3'UTR, e. g. within a promoter region, the miR may also have a non-canonical function and transcription may be induced [134,135]. If the miR is created via a RISC-independent non-canonical pathway, it is not loaded into the RISC and also can perform other functions. For example, miRs can play a role in miR biogenesis. It has been shown that in *C. elegans*, the miR let-7 positively regulates its own maturation together with AGO2 by binding its pri-miR [136]. A miR can also bind RISC-independently to an RNA-binding protein (RBP) and thereby prevent the binding of the RBP to its target RNA. This function as an RNA-decoy was first shown for miR-328 and the heterogeneous nuclear ribonucleoprotein (hnRNP) E2 [137,138]. The interaction of miR-328 and hnRNP E2 regulates the gene expression of several targets, such as CCAAT/enhancer-binding protein alpha (CEBPA), high-mobility group protein B1 (HMGB1), and 141 other predicted proteins [139]. Since it has been observed even in different cell types, this decoy appears to have a global effect on a variety of targets.

Another non-canonical function is the binding of miRs to Toll-like receptor (TLR) 7/8 (murine TLR7; human TLR8) [131]. TLR7/8 receptors are localized intracellularly in the membranes of the endolysosomal compartment, where their main function lies in the induction of cytokines which makes them a crucial part of the immune response [140]. They can recognize foreign nucleic acids, such as viral or bacterial desoxyribonucleic acid (DNA) or RNA [141–143]. The binding of endogenous miRs to TLR 7/8 can occur when GU-rich miRs are transported within sEV and taken up by the endosome of target cells [140]. In lung cancer (LC), sEV-derived miR-21 and miR-29a can bind to TLR7/8, thereby inducing cytokine expression as a pro-inflammatory immune response [144]. The binding of sEV-derived miR-21 and miR-29a to TLR7/8 was also confirmed in several other models like neuroblastoma or Alzheimer's disease [145,146]. Another miR that can act as an RNA-decoy and bind to TLR7/8 is miR-574-5p, whose function will be described later.

1.2.3. MicroRNA sorting into small extracellular vesicles

Interestingly, the concentration of certain miRs was shown to be much higher in sEV than in their host cells, suggesting a specific secretion of miRs in sEV [147]. In recent years, more and more proteins have been found to play a role in the sorting of miRs. A closer look at the underlying mechanisms revealed that the miR sequence plays an important role in the sorting process. For example, miRs can be specifically sorted into sEV if they exhibit so-called EXO motifs, which include sequences like CAUG or CNGGNG. These EXO motifs are bound by the proteins Aly/REF export factor (Alyref) and fused in sarcoma (Fus), which are responsible for the recognition and export of miRs [148]. CELL motifs, on the other hand, lead to intracellular retention of miRs [148]. HnRNPs, for example, hnRNPA2B1 can also recognize and bind certain miR sequences, including the EXO motif GGCU and CELL motif UGCA [149]. Posttranslational modifications of hnRNPs, for example, SUMOylation can lead to increased binding and sorting of miRs into sEV [149]. There also appear to exist some 3'UTR sequences in mRNA transcripts, which are also present in miRs and appear to be specific for the sorting into sEV [150].

Another miR sorting pathway appears to be via RISC and the associated protein AGO2. AGO2 can specifically bind miRs and sort them into exosomes [151,152]. But there seem to be several other proteins playing a role in the sorting of miRs into exosomes. Y-box protein 1 was shown to sort miRs in exosomes [153], and as well synaptotagmin-binding cytoplasmic RNA-interacting protein (SYNCRIP) plays a role in miR sorting in hepatocytes [149].

In general, the field of DNA and RNA sorting into sEV is a relatively new field that has gained more attention in recent years. In particular, miRs are of high interest due to their potential use as biomarkers for several diseases, including cancers.

1.2.4. MicroRNAs as diagnostic and prognostic biomarkers

In the organism circulating miRs are ideal candidates as biomarkers because they have high availability and stability [154]. They were first established as biomarkers for cancer in 2008 in the serum of B-cell lymphoma patients [155,156]. Since then, they have been detected in body fluids, such as blood, urine, or saliva as biomarkers for various diseases, including different types of cancer [157]. Especially the occurrence in urine and saliva makes the use of biomarkers perfect as a minimal-invasive and sensitive method of early disease detection [117]. Another advantage is that different markers can be used at once as a multimarker panel, which significantly improves the possibility of diagnosis for example in breast cancer [158]. Another application of miRs besides as diagnostic biomarkers is as prognostic biomarkers [159]. By the detection of the miR, conclusions can be drawn about tumor progression, metastasis, and other pathological characteristics, as well as survival outcome [160].

MiR-574-5p is a miR that's potential as a diagnostic or prognostic maker has recently gained increasing interest. It has been proposed as a diagnostic biomarker in adenocarcinoma and other early-stage non-small cell lung cancers (NSCLCs) [161–163]. In addition, miR-574-5p is described as a prognostic marker in breast cancer, squamous cell carcinoma of the esophagus, or small cell lung cancer (SCLC), where it correlates with metastasis or treatment response [164–166].

1.3. MiR-574-5p and prostaglandin E_2 in the tumor microenvironment

1.3.1. MiR-574-5p

MiR-574-5p is recently described as a novel upregulated target in different pathological states, especially cancers [167]. This miR is formed by the non-canonical miR-biogenesis pathway by the spliceosome. The host mRNA of miR-574-5p is nervous system overexpressed protein 20 (NOXP20) [168]. NOXP20 is overexpressed in the brain and the spinal cord during neural differentiation and may play a role during neural cell development [169,170]. Particularly in miR biogenesis of miR-574-5p is that one strand is not completely degraded as usual, but both strands are present, and the 5p/3p ratio may vary and contribute to pathogenesis [171,172]. Such arm-selection preferences have also been observed previously for other miRs in breast or gastric cancer, as for hsa-miR-193a, hsa-miR-136, or hsa-miR-423 [173,174].

Functions of miR-574-5p are described in various studies, but some describe the miR as a tumor suppressor and some as an oncogene [167]. Therefore, the effects, for example on proliferation, migration, invasion, metastasis, or angiogenesis, seem to be highly tumor- and context-dependent. In breast cancer, miR-574-5p represses tumor cell proliferation, migration, and epithelial-mesenchymal transition [175]. In addition, miR-574-5p was shown to inhibit tumor growth and metastasis *in vivo* [164,175]. In contrast, tumor-promoting functions of miR-574-5p were found in gastric cancer. Inhibition of miR-574-5p resulted in reduced viability, migration, invasion, and tube formation of human umbilical vein endothelial cell lines [176]. In addition, both miR-574-5p and -3p were also shown to be involved in angiogenesis in gastric cancer development [171,177]. The tumor-promoting role of miR-574-5p has also been described in other tumor types, such as cervical cancer, nasopharyngeal carcinoma or colorectal cancer [178–180]. First, miR-574-5p was described in 2012, as a tumor promoter that plays a role in immunosuppression via TLR9 [181]. Meanwhile, it is known that miR-574-5p plays a critical role in microsomal PGE synthase-1 (mPGES-1)-mediated PGE_2 regulation in NSCLC [52].

1.3.2. Prostaglandin E_2 biosynthesis

PGE_2 is the most abundant prostaglandin found in many tumors, such as lung, colon and breast cancer, and is often associated with a poor prognosis [182–184]. PGE_2 stimulates the tumor growth by establishing an inflammatory microenvironment [23]. This promotes cancer proliferation, invasion and metastasis and induces the angiogenic process [185].

Furthermore, PGE_2 is upregulated in several inflammatory diseases, including arthritis and cancer [186]. Together with the other prostanoids PGI_2, Thromboxane A2 (TXA_2), PGD_2, or PGF_{2a}, it belongs to the group of eicosanoids [23]. These are formed from arachidonic acid by cyclooxygenases (COX)-1 and-2. COX-1 is constitutively expressed, which results in basal expression levels of the prostaglandins, while COX-2 is an immediate response gene that is not normally present in most cells, but is strongly induced at sites of inflammation and during tumor progression [187,188]. Both together secure the homeostasis in the body and mediate pain and inflammation [189]. After the conversion of arachidonic acid to PGH_2 by COX-1 and -2, different synthases are further processing PGH_2 to the prostaglandins (Figure 6). PGE_2 is formed by the mPGES-1, mPGES-2, and cytosolic PGE synthase (cPGES) [190,191]. COX-2 and mPGES-1 are often linked and upregulated together upon inflammation [190,192]. After synthesis, PGE_2 is either degraded by the 15-PG dehydrogenase (HPGD) or secreted from the cells [193]. There, PGE_2 can bind autocrine or paracrine to the E-type prostanoid (EP) receptors. These G-protein coupled transmembrane receptors can trigger various downstream pathways via stimulatory ($G\alpha_s$) or inhibitory ($G\alpha_i$) subunits to the levels of Ca^{2+} via phospholipase C enzymes (PLC), cyclic adenosine monophosphate (cAMP), or inositol phosphate [194,195]. EP1 is known to increase the PLC and cytosolic Ca^{2+} levels, which induces nuclear factor-kappaB (NFκB) and protein kinase C (PKC) [196]. EP2 and EP4 increase the formation of cAMP, and therefore also activate protein kinase A (PKA) [194,197]. EP3 can due to its coupling with different G proteins decrease cAMP levels, but also increase Ca^{2+} levels [198,199].

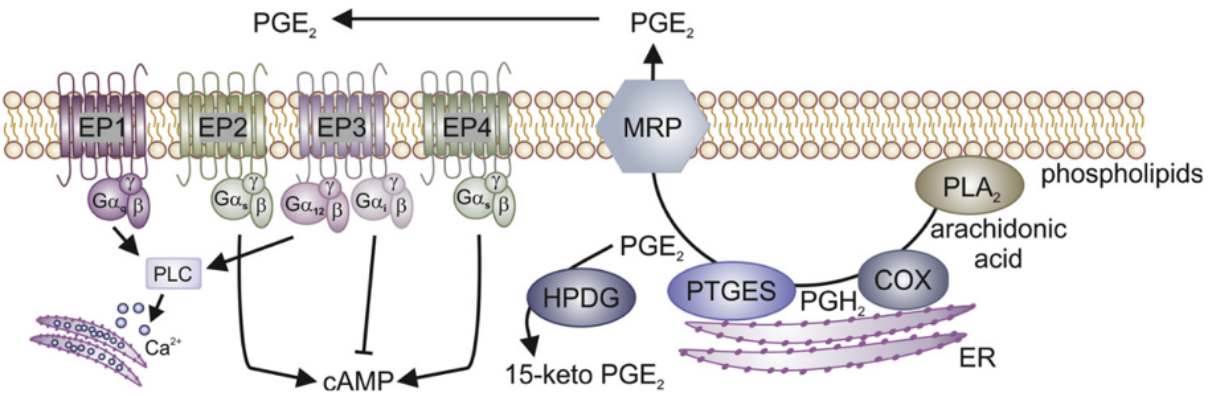

Figure 6: PGE_2 biosynthesis and signaling via EP receptors.

PGE_2 is formed from arachidonic acid. The two cyclooxygenases (COX) form PGH_2, which in turn is converted to PGE_2 by microsomal prostaglandin E synthase 1 (mPGES-1 or PTGES). PGE_2 is either degraded by 15-PG dehydrogenase (HPDG) or secreted by multi-drug restistance proteins (MRP) and can trigger downstream processes via the E-type prostanoid receptors (EP1-4) through the regulation of cyclic adenosin monophosphate (cAMP), or calcium via phospholipase C enzymes. EP2 and 4 have a cAMP stimulatory subunit (Gαs), whereas EP3 has an inhibitory subunit (Gαi). Adapted from [193].

Non-steroidal anti-inflammatory drugs (NSAIDs) are often used to treat PGE_2. These inhibit COX-1 and -2, which is often associated with side effects [200,201]. However, mPGES-1-dependent PGE_2 also plays a major role in pathological conditions such as inflammation, pain, fever, or tumorigenesis [202–205]. Therefore, mPGES-1 is a potential target for the development of therapeutic agents for the treatment of various diseases [191,206].

1.3.3. Cancer-associated fibroblasts in the tumor microenvironment

The inflammatory environment created by PGE_2 in tumors promotes tumor progression through enhanced angiogenesis, metastasis, or invasion [185]. Various cell types can be involved in these effects [193]. The progression of a tumor depends on genetic alterations of the tumor cells and on the crosstalk between the different cells in the tumor microenvironment (TME) [207]. Genetic alterations include upregulation of oncogenes and downregulation of tumor suppressors, which are contributing to the hallmarks of cancer, for example angiogenesis, immune destruction, or proliferative signaling [208,209]. The TME includes the cells that make up a tumor, such as cancer cells, fibroblasts, endothelial cells, and immune cells such as macrophages or lymphocytes (Figure 7) [210].

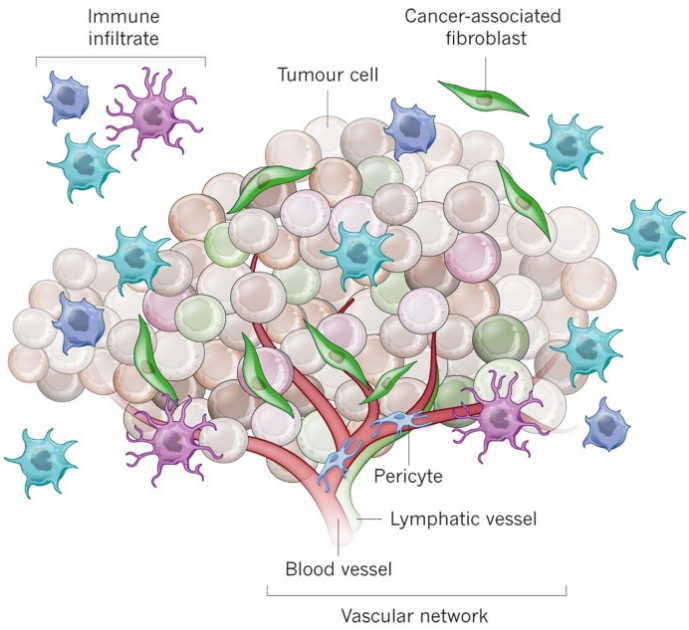

Figure 7: The tumor microenvironment.

Many different cell types are present in the tumor microenvironment (TME). These include tumor cells, immune cells, blood vessels, and cancer-associated fibroblasts (CAFs). All cell types in the TME communicate with each other, producing an extracellular matrix (ECM) contributing to the tumor progression [211].

Furthermore, the TME includes an extracellular matrix (ECM) consisting of components that hold the tumor together such as collagen, fibronectin, hyaluronans, or laminin [212]. Changes in the ECM can activate stromal cells or support the tumor development and metastasis [213]. In addition, the tumor cells can communicate with the non-cancerogenic cells via the ECM, which results in these performing tumor-promoting functions [214]. Here, signaling by various inflammatory mediators, as cytokines interleukin (IL)-1, -10, -22 or TNF-α, and matrix-remodeling enzymes as matrix metalloproteinases play a role [215]. Some inflammatory mediators are as well inhibiting the tumor promotion, for example IL-12. Cells can exchange these inflammatory mediators by direct contact, or via the exchange of EV [216,217]. As mentioned above, PGE_2 is also one of the inflammatory mediators that contribute to tumor progression [185]. The paracrine and autocrine effects on cells in the TME create an inflammatory tumor environment. Thus, all cells in the TME work together to drive forward tumorigenesis, cancer development, angiogenesis, and metastasis [218]. A better understanding of the interaction of all cells in the TME could be useful in developing new therapeutic strategies. These strategies include, for example, inhibiting the interaction between tumor cells and other cells in the TME to inhibit metastasis and tumor progression [219].

Another option is to deplete fibroblast activation to cancer-associated fibroblasts (CAFs), which play a central role in the tumor development [220]. In the TME, fibroblasts can be chronically activated into CAFs (Figure 8) [221]. Similar to in wounds, fibroblasts are activated by

inflammatory mediators, such as TGFβ. TGFβ can be secreted by tumor cells and induces CAF proliferation, expansion, and differentiation [222,223]. Although PGE_2 is one of the major inflammatory factors in the carcinogenesis of many tumor types, the effect of PGE_2 signaling on CAF activation is not yet clear and differs tumor type-dependent [193]. In many solid tumors, CAFs are the most abundant type of stromal cells, including breast and pancreatic tumors [224,225]. They share common features with myofibroblasts, such as the expression of α-smooth muscle actin (α-SMA) or enhanced ECM synthesis [221]. However, compared to myofibroblasts, CAFs are resistant to cell death and proliferate and persist in the activated state [193]. In tumors, activation of fibroblasts into CAFs may occur during tumor development, which is often associated with a poor prognosis [226,227]. This is due to their various tumor-promoting properties. CAFs ensure fast tumor growth through the secretion of growth factors or proinflammatory factors and the remodeling of ECM, which increases cancer cell invasion [214,228,229]. They induce the formation of collagen crosslinks in the ECM, which also enhances migration and invasion of tumor cells [230]. They can also communicate with other cells to recruit myeloid cells and lymphocytes [231]. Altered sEV and intracellular miR expression patterns were also detected in CAFs, which affects also communication with other cell types [232]. The up- and down-regulation of different miRs vary depending on the tumor type [233]. These represent potential markers for CAFs. Intensive research is still ongoing in this field, as most known markers are upregulated in differentiated myofibroblasts as well as in CAFs [221]. The best-known marker is α-SMA, although other cytoskeletal markers such as vimentin, desmin, or smooth muscle myosin can also be used to distinguish differentiated fibroblasts from normal fibroblasts [234–236]. These can be combined with additional markers, such as ECM components, like collagens and fibroblast specific protein (FSP)1 [237,238], growth factors and cytokines, such as TGFβ or IL-6 [229,237] or with receptors like platelet-derived growth factor receptors (PDGFRs) or fibroblast activation protein (FAP) [229,239,240]. However, the variety of markers used for different studies reveals there is no one ideal marker that exclusively detects activation to CAFs [241].

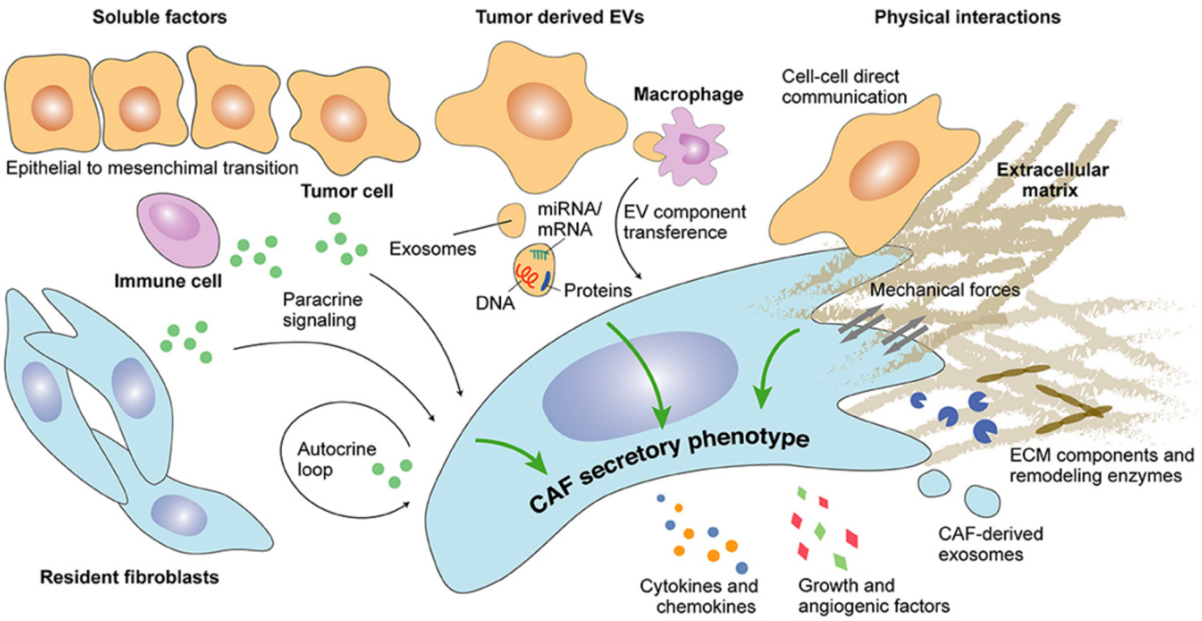

Figure 8: The activation of fibroblasts to cancer-associated fibroblasts (CAFs).

In the tumor microenvironment (TME), fibroblasts can be influenced by tumor cell-derived soluble factors, tumor-derived extracellular vesicles, or physical interactions with tumor cells. Thus, the secretory profile of CAFs is influenced, for example by the secretion of cytokines, growth factors or CAF-derived sEV [242].

1.4. Prostaglandin E_2 regulation in non-small cell lung cancer

LC is the most fatal cancer worldwide [243]. The most common cause of LC, accounting 90% in men and 70-80% in women is smoking [244]. Nevertheless, there are several other factors regarding the environment, such as air pollution or genetic predisposition, for example, mutations in the tumor suppressor protein 53 (*TP53 gene)* [245,246]. LC is divided into SCLC and NSCLC, with NSCLC accounting for approximately 85% of all LC cases [247]. NSCLC is in turn divided into 30% AC, 37.5% squamous cell carcinoma (SCC), 19.6% neuroendocrine carcinoma, and 6.6% large-cell carcinoma, which differ in their cellular origin [248]. While SCC tumors almost always correlate with smoking, ACs are the most common LC tumors in nonsmokers [249,250]. Various genetic alterations occur more frequently in ACs. These include, for example, chromosomal changes such as the copy-number gain of chromosome 5p. This is thought to mediate the amplification of telomerase reverse transcriptase, which occurs in 18% of ACs [251]. Other genetic mutations occur in 32.2% of AC cases in the kirsten rat sarcoma viral oncogene homologue (*KRAS*) oncogene, which almost never occur in the other NSCLC types [252–254]. In addition, mutations in the gene of epidermal growth factor receptor (*EGFR)* occur in 11.3% of cases and in neurofibromatosis type 1 gene (*NF1)* in 8.3% [251,252]. There are several therapeutic options for the treatment of LC, depending on the histological subtype and stage of the disease. These are ranging from resection of the tumor to radio- and chemotherapy [247]. A novel strategy is the inhibition of programmed cell death protein ligand 1 (PD-L1), for example by using antibodies against PD-L1 or programmed cell

death protein 1 [250]. This induces the immune reaction against tumor cells with upregulated PD-L1 levels, present in approximately 60% of all NSCLC [255]. Since PD-L1 is known to be regulated by PGE_2, the inhibition of PGE_2 could also be an option to reduce PD-L1 and thus treat PD-L1-dependent tumors [256]. Another therapeutic approach could also be the targeted disruption of communication with the TME in the LC [257–259]. Several sources indicate that crosstalk between tumor cells and CAFs and their influence on angiogenesis, invasion, metastasis, and cancer progression in NSCLC [260,261]

In NSCLC, PGE_2 is regulated by a negative feedback loop implemented by different functions of miR-574-5p (Figure 9). Compared to NB, in NSCLC, it is notable that mPGES-1 is more present in the cancer cells and not in the surrounding cells [262]. The inhibition of mPGES-1 leads to decreased PGE_2 levels and a determination of tumor growth, which reveals the dependence on PGE_2 [202,263]. In the AC cell line A549, miR-574-5p was shown to bind to the CUG-RNA binding protein 1 (CUGBP1) to exert its function as RNA decoy [52,264]. CUGBP1 can thus no longer bind to the mPGES-1 mRNA, and via alternative splicing, an mPGES-1 3' UTR isoform with a higher translation rate than the mPGES-1 wild-type (WT) mRNA is generated. As a result, more mPGES-1 is produced and thus more PGE_2. *In vivo*, this leads to faster tumor growth in mice. This miR-574-5p-CUGBP1 decoy is unique in AC cells [265]. Some other studies have also described the tumor-promoting effect of miR-574-5p in NSCLC. Inhibition of the expression of the miR-574-5p target protein tyrosine phosphatase receptor type U (PTPRU) promoted both migration and invasion of cancer cells [266]. Tumor suppression was promoted, and apoptosis was induced by miR-574-5p-dependent inhibition of the target Rho family GTPase 3 (RND3) [267]. However, miR-574-5p can also play a tumor-suppressing role in NSCLC. Increased levels of PGE_2 led to the secretion of miR-574-5p into sEV mediated via the EP1/3 receptor. The higher sEV-miR-574-5p levels were detected in AC cells 2 h after PGE_2 treatment. This sEV-miR-574-5p has a function as a TLR7/8 ligand and thus can decrease the intracellular level of miR-574-5p [52,144,268]. This also results in the formation of lower levels of mPGES-1 and PGE_2 again. This, in turn results in less PGE_2 secretion and self-regulation of PGE_2 synthesis mediated by miR-574-5p. Interestingly, in other NSCLC cells, namely squamous cell carcinoma cell line 2106T, the secretion of miR-574-5p in sEV was also triggered by PGE_2 after 8 h. However, the sEV-miR-574-5p had no function as a TLR7/8 ligand here. It was suggested that a different tetraspanin composition on the sEV envelope mediates a different uptake of the sEV, resulting in a different function of miR-574-5p [52].

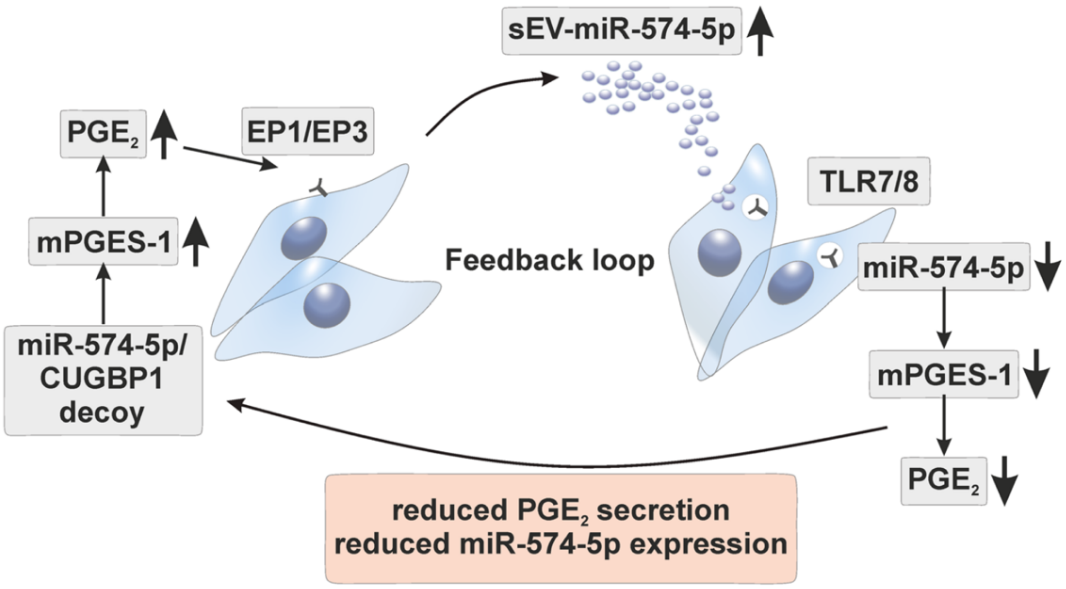

Figure 9: PGE_2 is regulated via a feedback loop in non-small cell lung cancer.

The miR-574-5p-CUGBP1 decoy increases mPGES-1 and PGE_2 levels. PGE_2 triggers the miR-574-5p secretion via EP1/3 in A549 cells. By binding of TLR7/8 lead increased levels of sEV-miR-574-5p to a negative regulation of intracellular miR-574-5p, mPGES-1 and PGE_2 levels, which in turn lead to decreased PGE_2 secretion and miR-574-5p expression [52].

1.5. Prostaglandin E_2 in neuroblastoma

1.5.1. Neuroblastoma

In this study, NSCLC was compared with another PGE_2-dependent tumor model, neuroblastoma (NB), to further explore the role of miR-574-5p. NB is a tumor of the sympathetic nervous system that occurs mostly in children under 10 years old [269]. It corresponds to 6-10% of all tumors appearing in children but corresponds to approximately 15% of all deaths in children [270,271]. Most children of more than one year at diagnosis have a poor overall prognosis [272]. NBs presumably arise from progenitor cells of the neural crest that differentiate into sympathetic ganglion cells and adrenal catecholamine-secreting chromaffin cells (Figure 10) [273,274].

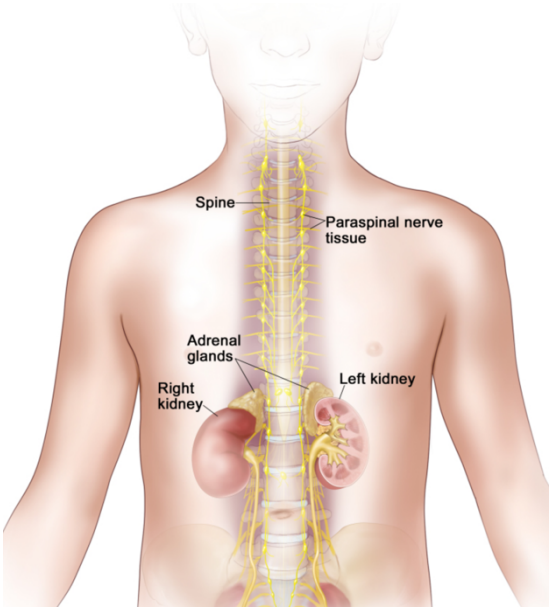

Figure 10: Locations where neuroblastomas may arise.

Neuroblastoma may be found in the adrenal glands and paraspinal nerve tissue and arises from cells in the nerve tissue of the adrenal gland, neck, chest, or spinal cord [275].

These tumors are characterized by their high heterogeneity. Spontaneous regressions, or tumor progression despite therapy, may occur [276]. Therefore, age at diagnosis, different genetic markers, chromosomal alterations, grade of tumor differentiation, and histological appearance are used to classify risk groups, which differ in the prognosis of cure [277]. Unique to NBs among human cancers is the possibility of spontaneous regression, which often occurs even without therapy [276]. In addition to chemotherapeutic agents, retinoic acid is frequently used in the treatment of NBs to induce cancer cell differentiation and thus tumor regression [278]. Histological markers for the identification of NB cells include disialoganglioside (GD2) and the tropomyosin receptor kinase (Trk)A and TrkB [234,235]. In addition, there are many genetic alterations that are also used as markers. Low-risk NBs often showed hyperdiploidy of the chromosomes of the tumor cells [281]. High-risk NBs, on the other hand, often show only partial alterations of chromosomes or single genes. One of the most common is an amplification of the *MYCN* proto-oncogene. *MYCN* amplification occurs in approximately 25% of all high-risk NBs and is associated with poor outcome [282]. The MycN protein is required in the development of the neural crest but is usually gradually reduced while maturation [283,284]. It is suggested as sufficient for NB development and as a major oncogenic driver in NBs [269]. Chromosomal alterations are also frequently present, such as the hemizygous deletion of 11q [270]. The 11q deletion occurs in about 30-40% of NB patients [285–287]. Most of the NB tumors are mutually exclusive, not having both genetic alterations 11q deletion and *MYCN* amplification, but both are associated with a poor prognosis [286,288]. It is suspected that the 11q deletion contains NB suppressor genes [287].

1.5.2. Regulation of prostaglandin E_2 in neuroblastoma

Among many other tumor types, such as breast cancer [183,289], colorectal cancer [290,291] or prostate cancer [202,292], NBs are PGE_2-dependent tumors. It has been shown that COX-2, mPGES-1, and PGE_2 are upregulated in NBs [293]. In addition, all four EP receptors are known to be present [294]. PGE_2 treatment leads to a higher viability of NB cells [294]. Furthermore, it was shown that tumor growth was reduced in *in vivo* mice models, by inhibiting COX-2 [293]. There seems to be a special role for PGE_2 in 11q deleted tumors. Here, both mPGES-1 mRNA and PGE_2 are increased, and these patients had a lower survival rate of 10% [295]. In addition, a distinctive feature was found that NB tumor cells do not express mPGES-1 but only the surrounding cells in the TME. In further studies, it was shown that CAFs in the TME are the primary source of PGE_2, as mPGES-1 inhibition in the CAFs resulted in the suppression of PGE_2 levels and tumor growth [295,296].

1.6. Aim of the study

This study aimed to define the roles of miR-574-5p and sEV-derived miR-574-5p in NB and compare with known functions in NSCLC. In NSCLC, miR-574-5p contributes to the autocrine regulation of mPGES-1-dependent PGE_2 synthesis via a feedback loop that includes functions of miR-574-5p as a decoy for CUGBP1 and as a TLR7/8 ligand [52,264,265]. The previously unknown functions of miR-574-5p and sEV-miR-574-5p in NB were compared with those in NSCLC to gain a better understanding of cross-tumor regulation by miRs. The association of miR-574-5p and mPGES-1-dependent PGE_2 regulation has not been investigated in NB and will be investigated in this thesis. The second part of this thesis aimed to investigate the influence of different tetraspanins on the sEV surface on sEV-miR-574-5p mediated functions with a focus on the uptake rate of sEV. This may contribute to a better understanding of the intercellular regulation in the TME.

2. Materials and methods

All incubation steps were performed at room temperature (RT) if not otherwise stated. Detailed buffer compositions can be found in supplementary (Table S1).

2.1. Cell lines and cell culture conditions

All cell culture experiments were carried out under sterile and standardized cell culture conditions (37 °C, 5% CO_2, and 98% humidity). All cell culture experiments regarding sEV were carried out with sEV-depleted fetal calf serum (FCS, Sigma-Aldrich, St. Louis, USA). The FCS was centrifuged at 120 000 x g at 4 °C for 18 h in an Optima™ XPN-80 ultracentrifuge (Beckman Coulter, Brea, USA). Afterward, the bottom third of the volume was discarded to exclude contamination by endogenous sEV. The NB cell lines SK-N-AS (ATCC:CRL-2137™) and SK-N-SH (RRID:CVCL_0531) and the human lung AC cell line A549 (ATCC: CCL-185™) were cultured in Dulbecco's modified Eagle medium (DMEM, Thermo Fisher Scientific, Waltham, USA) with 10% (v/v) heat-inactivated FCS, 100 U/mL Penicillin (gibco, Thermo Fisher Scientific, Waltham, USA), 100 µg/mL Streptomycin (gibco, Thermo Fisher Scientific, Waltham, USA) and 1 mM sodium pyruvate (Thermo Fisher Scientific, Waltham, USA). The human lung fibroblast cell line HFL1 (CCL153, ATCC, Manassas, USA) was cultured in Kaighn's modification of Ham's F-12 medium (F-12K, gibco, Thermo Fisher Scientific, Waltham, USA) with 10% (v/v) FCS, 100 U/mL Penicillin and 100 µg/mL Streptomycin. The human pulmonary squamous cell carcinoma cell line 2106T (CLS Cell Lines Service GmbH, Eppelheim, GER) was cultured in 50% DMEM and 50% F-12K with 5% (v/v) FCS, 100 U/mL Penicillin, and 100 µg/mL Streptomycin, 0.5 mM sodium pyruvate and 15 mM HEPES (Sigma-Aldrich, St. Louis, USA). All cell lines were passaged twice a week. Cells were briefly washed with 5 mL prewarmed 1x phosphate buffered saline (PBS) and then detached using 5 mL 0.05% Trypsin-EDTA (TE, Thermo Fisher Scientific, Waltham, USA) in 1x PBS at 37 °C. The reaction was stopped by adding 5 mL fresh cell culture medium, and $2x10^6$ SK-N-AS and SK-N-SH or $5x10^5$ A549, 2106T or HFL1 cells were put in a new T75 flask (Greiner Bio-One, Kremsmünster, AUT) into 15 mL fresh cell culture medium. The cancer cell lines were used until they reached a passage of 30, while the cell line HFL1 was only used for experiments from passages 4 to 11.

All cell lines are stored as cryo-stocks in a nitrogen tank, which can be thawed to obtain cells within lower passages. To freeze the cells, they were detached, and $1x10^6$ cells were combined with 10% (v/v) dimethyl sulfoxide (DMSO, Carl Roth, Karlsruhe, GER) in a total volume of 1 mL in a cryo-vial /VWR, Radnor, USA). Then, cells were frozen at -80 °C for 24 h and transferred to the nitrogen tank. For thawing, cryo-vials were briefly prewarmed at RT. Subsequently, 10 mL of prewarmed cell culture medium was used to rinse the tube until the whole cell

suspension was thawed. Next, cells were transferred into a 50 mL reaction tube and spun down at 1 200 rpm for 5 min in an Eppendorf Centrifuge 5702. Afterward, the supernatant containing dimethyl sulfoxide (DMSO, Carl Roth, Karlsruhe, GER) was carefully aspirated, and cells were resuspended in fresh cell culture medium and transferred into a T75 flask for cultivation.

2.1.1. SK-N-AS and SK-N-SH stimulation

For sEV-derived miR-574-5p measurements, SK-N-AS and SK-N-SH cells were seeded in 6-well plates (Greiner Bio-One, Kremsmünster, AUT) at a density of $5x10^5$ cells per well in a total volume of 2 mL 24 h prior stimulation. Cells were stimulated with 5 nM PGE_2, 5 nM Butaprost, 5 nM Sulprostone (all Sigma-Aldrich, St. Louis, USA), 5 nM L-902,688 (Cayman Chemicals, Ann Arbor, USA), or vehicle DMSO for 30 min, 1 h, and 2 h. For this purpose, cells were washed briefly with 1x PBS. Afterward, 2 mL fresh medium containing the stimulation reagents was added. For harvesting, the cell supernatant was transferred into a 2 mL reaction tube and centrifuged at 17 000 x g for 5 min. Then, 1.5 mL of the supernatant was transferred into a fresh tube, and the remaining cellular debris was discarded. The supernatants were stored at -80 °C until sEV isolation.

To analyze the function of sEV-miR-574-5p, SK-N-AS cells were seeded in 6-well plates as described above. Cells were washed briefly with 1x PBS and then stimulated with 2 µg/mL purified miR-574-5p oe or ScrC sEV or 100 ng/mL Resiquimod (R848, Invivogen, San Diego, USA) for 24 h. Then, cells were briefly washed with 1x PBS, and then 500 µL TE was added per well to detach the cells. After 10 min, the reaction was stopped by adding 500 µL cell culture medium. Cells were pelleted at 17 000 x g and 4°C for 5 min. Protein or RNA was extracted as described below.

2.1.2. Transient CD81 knockdown in SK-N-AS cells

Transient knockdown of CD81 was performed using siRNA oligonucleotides against CD81. A combination of siRNA oligonucleotides SASI_Hs01_00181702 and SASI_Hs01_00181703 (Merck, Darmstadt, GER) against CD81 was used. As a control, naturally not expressed siRNA oligonucleotides against GFP were used (5´-UCUCUCACAACGGGCAUUU-3´). SK-N-AS cells were seeded in a 12-well plate at a density of $2.6x10^5$ cells per well the day before transfection. Prior to transfection, cells were washed with 1x PBS. Transfection was performed with 4.5 µL Lipofectamine™ RNAiMAX (Invitrogen, Karlsruhe, GER) and 20 pmol siRNA per transfection in OptiMEM according to the manufacturer's instructions. After 4 h, the medium was aspirated and replaced to FCS-depleted cell culture medium. Cells and supernatants were harvested 24 h after the transfection, as described in section 2.1.1.

2.1.3. HFL1 stimulation

HFL1 cells were seeded in 12-well plates at a density of $1x10^5$ cells per well 24 h before stimulation. Cells were washed briefly with 1x PBS and then stimulated with 2 µg/mL purified miR-574-5p oe or ScrC sEV, 10 ng/mL TGFβ (PeproTech, Rocky Hill, USA), 100 ng/mL Resiquimod (R848, Invivogen, San Diego, USA), or 200 nM ODN 2088 Control (ODN 2087) (Miltenyi Biotec, Bergisch-Gladbach, GER) in sEV-depleted cell culture medium for 72 h. Afterward, cells were washed and harvested as described in section 2.1.1. Protein or RNA was extracted as described below.

2.1.4. Tetrazolium reduction assay in HFL1 cells

The effects of sEV treatment on cell proliferation and viability were analyzed using a 3-(4,5-dimethylthiazol-2-yl)-2,5-diphenyltetrazoliumbromide (MTT) tetrazolium reduction assay (Carl Roth, Karlsruhe, GER). Therefore, HFL1 cells were seeded in 96-well plates (Greiner Bio-One, Kremsmünster, AUT) at a density of $1x10^4$ cells per well 24 h before stimulation. After 24 h, cells were treated with 2 µg/mL isolated miR-574-5p oe or ScrC sEV or with 10 ng/mL TGFβ for 72 h. Untreated cells or cells only treated with TGFβ were used as controls. After 72 h, MTT was added to each well at a final concentration of 5 mg/mL. Next, cells were incubated for 3h at 37°C. At this time, MTT should be reduced by the cells to purple formazan, which should correlate with the number of live and proliferating cells. After 3 h of incubation, the medium was aspirated, 100 µL DMSO was added to each well, and the cells were resuspended. The released formazan was detected using a Tecan Infinite M 200 plate reader (Tecan Group, Männedorf, CHE) at 570 nm. The non-specific background was measured at 630 nm and subtracted from the formazan amount. Treated samples were normalized to untreated or only TGFβ-treated controls.

2.2. SEV methods

2.2.1. Overexpression of miR-574-5p in sEV

To investigate the physiological function of miR-574-5p in the sEV, an overexpression (oe) of miR-574-5p and a scrambled control (ScrC) sequence in the sEV for the different cell lines was established. These sEV can be used to determine the cell-specific function after purification of the sEV and subsequent stimulation of target cells. To get the miR-574-5p overexpression sEV, the XMIRXpress Lenti system (System Biosciences, Palo Alto, USA) was used. In addition, a respective negative control was generated with the XMIRXP-NT system (System Biosciences, Palo Alto, USA). Both constructs were used to transfect LC or NB cell lines A549, 2106T, SK-N-AS, and SK-N-SH.

A549 or SK-N-AS cells were seeded in 6-well plates at a density of $5x10^5$ cells per well in a total volume of 2 mL 24 h before transfection. The cells were briefly washed with 1 mL 1x PBS per well. Both cell lines were transfected with either 2 µg miR-574-5p oe or ScrC plasmids in 250 µL Opti-MEM (gibco, Thermo Fisher Scientific, USA) using Lipofectamine 2000 (Invitrogen, Karlsruhe, GER) following the manufacturer's instructions. While SK-N-AS cells were incubated overnight in exosome-depleted DMEM, A549 cells were incubated in Opti-MEM.

2106T or SK-N-SH cells were seeded in 12-well plates (Greiner Bio-One, Kremsmünster, AUT) at a density of $1x10^5$ cells per well in a total volume of 1 mL 24 h before the transfection. SK-N-SH cells were transfected with 3 µg plasmid per well using polyethyleneimine (PEI, 1 g/L, Sigma-Aldrich, Germany) (pH 7). For this purpose, 6 µL PEI was mixed with 100 µL DMEM without supplements. Plasmids were mixed with 100 µL DMEM without supplements, then united with the PEI mix and incubated at RT for 15 min. 2106T cells were transfected using the same protocol with 2 µg plasmids per well and PEI (pH 10).

After 18 h, supernatants containing engineered sEV were transferred in a fresh tube, spun down at 2 000 x g for 20 min, and supernatants were stored at -80 °C.

2.2.2. SEV isolation via ultracentrifugation

Cell supernatants were thawed on ice and then transferred to 1.5 mL polypropylene tubes (Beckman Coulter, Brea, USA). At first, samples were centrifuged at 21 000 x g and 4 °C for 1 h with the Optima XPN 80 ultracentrifuge and the 70.1.Ti rotor (Beckman Coulter, Brea, USA). The supernatant was transferred into a new polypropylene tube, followed by a second centrifugation step at 100 000 x g and 4 °C for 1 h. Then the supernatant was discarded, the sEV resuspended in 20 µL 1x PBS for stimulation experiments, or the RNA was extracted directly.

2.2.2. SEV characterization with the ExoView R100 platform

The sEV were characterized using the ExoView R100 platform (NanoView Biosciences, Boston, USA). This system is a chip-based system and can be used to analyze sEV population directly from unpurified supernatants. The tetraspanin chips (NanoView Biosciences, Boston, USA) are labeled with antibodies against the tetraspanins CD9, CD63, and CD81 or IgG control. The sEV are immobilized by binding to the anibodies. Subsequently, vesicle size and immunostaining of surface markers or cargo can be determined [101,297].

For the experiment, unpurified cell culture supernatants of SK-N-AS, SK-N-SH, or HFL1 cells were added to the chips and incubated overnight for approximately 18 h. Tetraspanins on the sEV surface were stained according to the manufacturer's instructions. Chips were washed, and sEV were blocked and then stained with antibodies against CD9 (CF®488A-labeled), CD63 (CF®647-labeled), and CD81 (CF®555- labeled) diluted 1:600 in blocking solution (all NanoView Biosciences, Boston, USA). After staining, chips were air-dried and imaged using the ExoView R100 platform. Data analysis was performed using the nanoViewer software, version 2.8 (NanoView Biosciences, Boston, USA).

2.2.3. Particle measurements with the nCS1™

To analyze the sEV concentration and size distribution, cell culture supernatants of PGE_2-treated SK-N-AS cells were analyzed using the microfluidic resistive pulse sensing technology-based nCS1™ Nanoparticle Analyzer (Spectradyne LLC, Signal Hill, USA) kindly provided for use by Merck (Darmstadt, GER). The supernatants were harvested as described in chapter 2.2.2. and diluted 1:10 in 1x PBS containing 1% Tween20. 3 µL of each sample was loaded into factory precalibrated TS-300 cartridges (Spectradyne LLC, Signal Hill, USA). The cartridges with a measurement range of 50-300 nm and the system were primed with running buffer containing 1x PBS and 1% Tween20. The analysis was performed using the nCS1 software version 2.5.0.249.

2.2.4. Transmission electron microscopy

Isolation of sEV was proven by transmission electron microscopy (TEM). For this purpose, isolated sEV from SK-N-AS and SK-N-SH cells were resuspended in 1x PBS. The sEV concentration was measured by Bradford assay and then adjusted to a final concentration of 0.05 mg/mL in 1x PBS. A formvar carbon-coated copper grid (Plano, Wetzlar, GER) was placed in a 15 µL drop of diluted sEV on parafilm (Bemis Company, Neenah, USA) for 10 min. Then, the grid was placed in a 15 µL drop of 2% FA in PBS for 10 min and washed 3x with MQ. Prior to imaging, samples were negatively stained with 2% uranyl acetate (Sigma Aldrich,

St. Louis, USA) for 1 min, subsequently washed 3x with MQ, and dried. All samples were imaged using a Zeiss EM109 electron microscope.

2.2.5. Triton X-100 and RNase I treatment of sEV

To verify whether miR-574-5p is inside or outside the sEV after purification, the sEV were treated with RNase and Triton X-100. For this purpose, the sEV were divided into three approaches. One approach was mixed with NEBuffer 3 only (New England Biolabs, Ipswich, USA), one was mixed with NEBuffer 3 and 2.5 U/µL RNase I, and one was additionally spiked with 1% Triton X-100 for 10 min before RNase treatment. Then, RNase treatment was performed at 37 °C for 20 min. Afterward, total RNA was isolated using the miRNeasy Mini Kit (Qiagen, Hilden, GER) following the manufacturer's instructions. The amount of miR-574-5p was analyzed via real-time quantitative polymerase chain reaction (RT-qPCR) as described in chapter 2.4.4 and all values were normalized to untreated controls.

2.2.6. Antibody treatment of sEV

Isolated miR-574-5p oe or ScrC sEV were treated with antibodies against tetraspanins CD9, CD63, and CD81 to determine the influence of tetraspanins on the functionality of sEV-derived miR-574-5pTherefore, sEV were resuspended in 1x PBS after purification, and the concentration was determined by the Bradford assay (described in chapter 0). For each condition, 1 µg sEV was mixed with 100 ng antibody against CD9 (sc-59140, Santa Cruz Biotechnology, Dallas, USA), CD63 (NBP2-42225, Novus Biologicals, Littleton, GER), CD81 (MABF2061, Sigma Aldrich, St. Louis, USA) or Mouse IgG1 Isotype control (MAB002, Novus Biologicals, Littleton, USA) in a total volume of 20 µL. Appropriate antibody concentrations were tested previously. All reactions were incubated at 4°C for 21 h. Then, the previously seeded cells were washed briefly with 1x PBS, and fresh sEV-depleted medium was added. Cells were stimulated with either sEV blocked with antibodies or with antibodies alone as a control at 37°C for 24 h. Afterwards, the cells were harvested and SDS-PAGE and Western blot analysis was performed as described in sections 2.5.3 - 2.5.4.

2.2.7. Live cell imaging

Live cell imaging experiments for the first visualization of the uptake of sEV were performed with either protocol A or B. Protocol A: SK-N-AS or SK-N-SH cells were seeded in 8-well chamber slides (IBIDI, Gräfeling, GER) at a density of $2.6x10^4$ cells per cell. After 24 h, the medium was aspirated and changed to sEV-depleted medium containing 5 µg/mL Hoechst 33258 (Sigma-Aldrich, St. Louis, USA) at 37 °C for 1 h in stain the nuclei. Isolated sEV were stained with the lipophilic tracer 3,3′- dioctadecyloxacarbocyanine perchlorate (DiO, Sigma-Aldrich, St. Louis, USA) at 37 °C for 15 min. After the first images, sEV were added, and cells

were imaged in 5 min intervals for a total duration of 30 min. Images were acquired with an UltraView VoX spinning disk system (PerkinElmer, Waltham, USA) mounted on an inverted Nikon Ti-E microscope (Nikon, Minato, Japan) equipped with a climate chamber (ACU control, Olympus, 37 °C, 5% CO_2, 60% humidity) kindly provided by Prof. Dr. Cristina Cardoso. The camera used was a cooled 14-bit Hamamatsu C9100-50 EMCCD camera with the Volocity 6.3 software (PerkinElmer, Waltham, USA). Protocol B: HFL1 or A549 cells were seeded or in µ-24-well plates with black walls (IBIDI, Gräfeling, GER) at a density of $6x10^4$ cells per well. After 24 h, the medium was aspirated and changed to an sEV-depleted medium containing 5 µg/mL Hoechst 33258 at 37 °C for 1 h in stain the nuclei. SEV were stained with DiO for 15 min and then added to the cells. Images were taken for 60 min every 5 min. Images were acquired with a Nikon Eclipse Ti equipped with a climate chamber (37 °C, 5% CO_2, 60% humidity) and a Nikon DS-Qi2 camera kindly provided by Prof. Dr. Alexander Löwer and analyzed with the NIS elements software (Nikon, Minato, Japan). Endocytosis was analyzed by additional incubation with 20 µg/mL pHrodo™ Red Dextran (Invitrogen, Karlsruhe, GER) and DiO-labeled sEV. After 1 h, cells were washed briefly with 1x PBS, and fresh cell culture medium was added. Cells were imaged within 15 min.

2.3. SEV uptake assays

In order to determine the influence of tetraspanins on the uptake of sEV by acceptor cells, two different methods to analyze the uptake were used.

2.3.1. Nano-Luciferase uptake assay

The Nano-Luciferase (NLuc)-Hsp70 plasmid and protocol for this assay were kindly provided by Dr. Gregory Lavieu (Université de Paris, FRA) [298]. In this assay, sEV containing an NLuc-Hsp70 construct was used to monitor sEV uptake by measuring NLuc internalization in acceptor cells.

The sEV-donor cells SK-N-AS or A549 were seeded in 6-well plates at a density of $5x10^5$ cells per well the day before transfection. Cells were transfected with 2 µg NLuc-Hsp70 plasmid as described in chapter 2.2.2. After 18 h, supernatants were harvested and sEV isolated (as described in 2.2.2). 2 µg sEV were blocked with 200 ng antibodies in a total volume of 40 µL as previously described in 2.2.6. Acceptor cells were seeded in 96-well plates at a density of $1.5x10^4$ cells were well 24 h before stimulation. Then, cells were stimulated in quadruplets with 0.5 µg blocked sEV at 37°C for 4 h. Afterward, the amount of taken-up NLuc was measured using Nano-Glo® Luciferase (Promega, Madison, USA) according to the manufacturer's instructions. Briefly, the cells were washed 3 times with ice-cold 1x PBS to remove the unincorporated sEV. PBS was then discarded, and 100 µL of Nano-Glo reagent was added

per well to catalyze the reaction of furimazine to furimamide, which can be quantified by luminescence. The plate was shaken in the dark for 5 min, and bubbles were busted with a lighter flame. The amount of NLuc was detected by measuring the luminescence using Tecan Infinite M 200 for 1000 ms.

2.3.2. Uptake quantification by confocal microscopy

A549 or HFL1 cells were seeded in 8-well cell culture slides (SPL life sciences, Naechon-myeon, KOR) at a density of $1.2x10^4$ cells per well the day before the uptake experiment. Isolated and with antibodies-treated sEV (performed as described in chapter 2.2.6) were stained with DiO for 30 min and then dialyzed against 5 mL 1x PBS using a 14 kDa membrane (Carl Roth, Karlsruhe, GER) for 1 h. The seeded cells were briefly washed with 1x PBS, and the medium was switched to an sEV-depleted medium containing stained sEV. After 4 h, the cells were washed twice with 1x PBS and then fixed with 3.7% FA in PBS for 15 min. Again, cells were washed twice with 1x PBS and then incubated with 100 µL 1x PBS containing 1% bovine serum albumin (BSA, Sigma Aldrich, Darmstadt, GER), 1 µg/mL 4',6-Diamidino-2-phenylindol (DAPI, Sigma-Aldrich, Darmstadt, GER) and 0.1% Phalloidin i647 (Abcam, Cambridge, UK) for 45 min. Afterward, cells were washed twice with 1x PBS, once with MQ, and mounted on a glass coverslip using Mowiol-488 (Sigma-Aldrich, Darmstadt, GER) and air-dried overnight in the dark. Stained cells were visualized with a confocal Leica DMi8 microscope. The images were analyzed with a custom ImageJ script written by Kai Breitwieser. First, the 3D multichannel microscope images were 2D max Z-projected, and the cell's dimensions to be analyzed were determined using an automatic intensity threshold based on the actin skeleton. The captured sEV within the cell were detected and counted using a classifier trained with the WEKA segmentation algorithm (doi:1093/bioinformatics/btx180). The number of sEV was normalized to the cell area to determine the relative uptake rate.

2.4. RNA methods

For all RNA methods, attention was paid to creating an RNAse-free environment. Therefore, all materials used were decontaminated with RNase-Zap (Sigma-Aldrich, Darmstadt, GER), and only plugged tips were used. Whenever possible, work was performed on ice. Unless otherwise stated, all centrifugation steps were performed at 4°C.

2.4.1. Intracellular RNA extraction

To extract RNA from cells, they were harvested as described in chapter 2.1.3, dissolved in 1 mL of TRIzol (Thermo Fisher Scientific, Waltham, USA) reagent, and samples were incubated for 5 min. To serve as a reference for later quantification of miR content in a reverse transcription-quantitative polymerase chain reaction (RT-qPCR) 20 nmol of the synthetic

ath (*Arabidopsis thaliana*)-miR-159a (5´ UUUGGAUUGAAGGGAGCUCUA-3', Sigma Aldrich, Darmstadt, GER) were spiked-in. Then, 200 µL of chloroform was added, and samples were vortexed for at least 15 s. Samples were then incubated on ice for 15 min and centrifuged at 17 000 x g and 4°C for 15 min. When the phase separation is completed, the aqueous phase containing the RNA was transferred to a new reaction tube. To precipitate the RNA, 500 µL isopropanol (VWR, Radnor, USA), 5 µL 3 M sodium acetate (pH 6.5; Carl Roth, Karlsruhe, GER), and 1 µL GlycoBlue™ (Thermo Fisher Scientific, Waltham, USA) co-precipitate were added. RNA was precipitated on ice for 15 min and then centrifuged at 17 000 x g for 15 min. The supernatant was discarded, and the RNA dissolved in 17 µL MQ. DNA was digested with Turbo™ DNase (Thermo Fisher Scientific, Waltham, USA) according to the manufacturer's instructions. RNA was then precipitated again by adding 100 µL 100% Ethanol (v/v) (EtOH, VWR, Radnor, USA), 2 µL sodium acetate, and 1 µL GlycoBlue™ and incubating the samples at -80°C for at least 30 min. Subsequently, the samples were centrifuged at 17 000 x g for 30 min. The supernatant was discarded, and the pellet was washed with 100 µL of 70% EtOH. Subsequently, the samples were centrifuged again at 17 000 x g for 10 min. The supernatant was discarded, and the RNA was resuspended in 20 µL MQ. The quality of the extracted RNA was determined by 1% agarose (Carl Roth, Karlsruhe, GER) gel electrophoresis, and the concentration was determined by UV spectroscopy using NanoDrop ND-1000 spectrophotometer (Thermo Fisher Scientific, Waltham, USA).

2.4.2. MRNA quantification via RT-qPCR

For mRNA quantification, intracellular RNA was reverse transcribed into complementary DNA (cDNA) using High-Capacity cDNA Reverse Transcription Kit (Thermo Fisher Scientific, Waltham, USA). For this purpose, 1000 ng RNA was transcribed in 10 µL MQ using the reaction mix described in Table 1 and the program described in Table 2.

Table 1: MRNA reverse transcription reaction mix

Component	Volume (µL)
10 x RT Buffer	2
25 x dNTP mix (100 mM)	0.8
10 x RT random primers	2
MultiScribe Reverse Transcriptase (50 U/µL)	1
MQ	4.2

Table 2: Reverse transcription program for mRNA

Temperature (°C)	Time (min)
25	10
37	120
85	5

Prior to RT-qPCR, reverse transcribed cDNA was diluted 1:2, and 1 µL cDNA was quantified with the RT SYBR Green FAST Kit (Thermo Fisher Scientific, Waltham, USA). Each reaction contained 10 µL SYBR green mix, 7.5 µL primer mix containing forward and reverse primers (both 1 mM), and 1.5 µL MQ. The RT-qPCR was performed with the StepOne Plus™ Real-Time PCR System (Thermo Fisher Scientific, Waltham, USA), and the program in Table 3 was used. Detailed used primer sequences are listed in Table 4.

Table 3: RT-qPCR program for mRNA

Step	Temperature (°C)	Time (s)	Repeat
Initial denaturation	95	20	1 x
Denaturation	95	3	40 x
Annealing	60	60	
	95	15	1 x
Melt curve	60 – 95 °C		

All samples were measured in duplicates and the mean was calculated. If the standard deviation exceeded 0.5, the sample was measured again. In addition, the quality of the product was ensured based on the melting curve. Relative mRNA amounts were calculated by normalizing cycle threshold (ct) values to endogenous levels of the housekeeping gene Glycerinaldehyd-3-phosphate-dehydrogenase (GAPDH), and fold inductions were calculated using the $2^{(-\Delta Ct)}$ method.

Table 4: Primers used for mRNA quantification by RT-qPCR

Target	Forward primer sequence	Reverse primer sequence
GAPDH	TGAGAACGGGAAGCTTGTCA	ATCGCCCCACTTGATTTTGG
α-SMA	GCTGTTTTCCCATCCATTGT	TTTGCTCTGTGCTTCGTCAC
mPGES1	TCCCGGGCTAAGAATGCA	ATTGGCTGGGCCAGAATTTC
COX-2	CCGGGTACAATCGCACTTAT	GGCGCTCAGCCATACAG

2.4.3. Extracellular RNA extraction

In order to isolate RNA from sEV, 200 µL of extraction buffer, 20 µL of 20% sodium dodecyl sulfate (SDS, AppliChem GmbH, Darmstadt, GER), and 200 µL of 6 M guanidinium thiocyanate (GTC, Sigma-Aldrich, Darmstadt, GER) were added to the isolated sEV pellet. Next, 200 µL of 65 °C warmed Roti®-Aqua-phenol (Carl Roth, Karlsruhe, GER) was added and samples were vortexed for at least 15 s to dissolve the sEV. Subsequently, the samples were incubated at 65 °C for 5 min. Then, 0.01 pmol synthetic ath-miR-159a was added as an internal standard for subsequent normalization, and 1 pmol synthetic cel (*Caenorhabditis elegans*)-miR-39-3p (5′-UCACCGGGUGUAAAUCAGCUUG-3′, Sigma Aldrich, Darmstadt, GER) was added to increase the precipitation efficiency of the RNA. The samples were then mixed with 200 µl chloroform: isoamyl alcohol (24:1, both Carl Roth, Darmstadt, GER) and centrifuged at 17 000 x g for 5 min. Then, the aqueous phase containing the RNA was transferred to a new reaction tube and 1.5 mL EtOH, 40 µL 3 M sodium acetate (pH 6.5), and 1 µL GlycoBlue™ were added. RNA was precipitated at -80 °C for at least 20 min and afterward centrifuged at 17 000 x g for 20 min. The supernatant was discarded, and RNA was resuspended in 17 µL MQ. The protocol was continued, and the DNA was digested, as previously described in chapter 2.4.1. Finally, the RNA was solubilized in 15 µL MQ.

2.4.4. MiR quantification via RT-qPCR

The following protocol established by Maria Fauth was used for miR miR quantification. To analyze the miR levels, 2 µL of extracted sEV-derived RNA or 200 ng intracellular RNA in a total volume of 10 µL was reverse transcribed to cDNA using E. Coli Poly-A-Polymerase (New England Biolabs GmbH, Ipswich, USA) and M-MuLV Reverse Transcriptase (New England Biolabs GmbH, Ipswich, USA). The detailed reaction mix is listed in Table 5.

Table 5: MiR reverse transcription reaction mix

Component	Volume (µL)
Poly (A) Buffer	2
Poly (A) Polymerase	0.4
M-MulV RT	0.5
ATPs (10 mM)	1.1
dNTPs (10 mM)	1
RT Primer (20 µM)	1
MQ	4

The reaction was performed at 42 °C for 60 min, followed by an incubation step at 75 °C for 5 min. The cDNA was diluted 1:3 in MQ, followed by RT-qPCR using the StepOne RT-qPCR system with the program listed in Table 6.

Table 6: RT-qPCR program for miR quantification

Step	Temperature (°C)	Time (s)	Repeat
Initial activation	95	120	1 x
Denaturation	95	10	40 x
Annealing	58	30	
Elongation	70	30	
	95	15	1x
Melt curve	60 – 95 °C		

All samples were measured in duplicates, and the mean was calculated. If the standard deviation exceeded 0.5, the sample was measured again. In addition, the quality of the product was ensured based on the melting curve. Relative mRNA amounts were calculated by normalizing cycle threshold (ct) values to spiked-in normalization control ath-miR-159a and fold inductions were calculated using the $2^{(-\Delta Ct)}$ method.

2.4.5. RNA immunoprecipitation

RNA-Immunoprecipitation (RIP) of CUGBP1 was performed to analyze the binding of mPGES-1 mRNA and miR-574-5p to CUGBP1. Briefly, 500 µL GammaBind Plus Sepharose beads (GE Healthcare, Chicago, USA) were blocked in 500 µL blocking solution containing 0.2 mg/mL BSA in PBS and 0.1 mg/mL yeast tRNA (Invitrogen, Karlsruhe, GER) at 4 °C for 1.5 h rotating in a rotary laboratory mixer (Labnet, Edison, USA). The beads were then centrifuged at 100 x g and 4 °C for 5 min, the supernatant was discarded, and the beads were resuspended in 500 µL 1x PBS. To link the beads to the antibodies, 50 µL blocked beads were mixed with 10 µg of CUGBP1 antibody (05-621 clone 3B1, Merck, Darmstadt, GER) or normal mouse IgG antibody (12-371, Merck, Darmstadt, GER) and incubated in a rotary mixer at 4 °C for 1 h.

HFL1 cells were seeded at a density of $1.6x10^6$ cells and SK-N-AS cells at $6x10^6$ cells 24 h prior to stimulation in one 15 cm dish per condition (Greiner Bio-One, Kremsmünster, AUT). Prior to stimulation, the cells were washed with 1x PBS, and the medium was changed to sEV-depleted medium. Cells were treated with 2 µg/mL miR-574-5p oe, ScrC sEV, or 5 ng/mL IL-1β (PeproTech, Rocky Hill, USA) for 24 h. Cells were then washed with ice-cold 1x PBS (gibco, Thermo Fisher Scientific, Waltham, USA) and harvested by scraping with a cell scraper in 1x

PBS with an EDTA-free protease inhibitor (Roche, Basel, CHE). The cells were centrifuged at 400 x g and 4 °C for 5 min, and the pellet was resuspended in 1 mL lysis buffer. Then, the cells were lysed for 10 min on ice and then sonicated 3x at 30% amplitude for 10 s, with a 30 s pause in between in a Branson Sonifier 250. Then, samples were centrifuged at 10 000 x g and 4 °C for 10 min to remove cell debris. The supernatant containing the proteins was transferred into a fresh tube, filled up to 1.1 mL, and 10% were separated as input samples for each condition.

The rest of the prepared lysate was divided equally into CUGBP1/- and IgG-bead mixture and incubated by rotation at 4 °C for 2 h. Then, the samples were washed sequentially with 1 mL wash buffers B1, B2, and B3 (for detailed composition, see Table S1) for each 5 min at 4 °C, with centrifugation steps of 300 x g and 5 min in between. After the last washing step, beads were resuspended in B3, and 10% were separated for Western blot analysis to validate immunoprecipitation. The remaining precipitates were spun down and resuspended in 500 µL of TRIzol reagent RNA isolation as described in section 2.1.3. Total RNA was isolated and resuspended finally in 6 µL MQ. 3 µL were reverse transcribed for miR detection using the miRCURY LNA kit (Qiagen, Hilden, GER) according to the manufacturer's instructions, and 3 µL were used for mRNA detection using the RT SYBR Green FAST Kit (described in 0).

2.5. Protein methods

2.5.1. Protein isolation

For whole protein isolation, cells were harvested as described in chapter 2.1.3. and lysed in 20 µL of tissue protein extraction reagent (T-PER, Thermo Fisher Scientific, Waltham, USA) for 30 min on ice. Samples were then sedimented at 17 000 x g and 4°C for 15 min, and the supernatant was transferred into a fresh tube.

For sEV protein isolation, purified sEV from 30 mL cell culture medium and corresponding cells were lysed in 50 µL RIPA buffer supplemented with 1x EDTA-free protease inhibitor for 30 min on ice (detailed composition can be found in Table S1). Then, samples were sedimented at 17 000 x g and 4°C for 15 min, and the supernatant was transferred into a fresh tube.

2.5.2. Bradford assay

Protein concentrations were determined by the Bradford assay (Bio-Rad Laboratories, Hercules, USA) according to manufacturer's instructions. For this purpose, standard curves containing 0 mg/mL, 0.5 mg/mL, 1 mg/mL, 2 mg/mL, 3 mg/mL, 4 mg/mL, and 5 mg/mL BSA (Sigma-Aldrich, Darmstadt, GER) were used. 10 µL of the different BSA solutions or protein samples (diluted 1:10 in MQ) were mixed in a 96-well plate. Then, 190 µL Bradford reagent was added. The absorption was measured at 595 nm in a Tecan Infinite M 200. The standard curve was used to calculate the total protein concentration according to the Beer-Lambert Law [299].

2.5.3. SDS-PAGE

The proteins were separated by sodium dodecyl sulfate-polyacrylamide gel electrophoresis (SDS-PAGE) using a 12% separating gel (see Table 7 for gel composition). 15-20 µg protein was mixed with 5 µL 4x protein loading buffer in a total of 20 µL. For sEV analysis, 50 µg protein from cells and all the volume of sEV samples were used. Samples were denatured at 95 °C for 5 min. 5 µL of the Precision Plus Protein All Blue Standard (Bio-Rad, Hercules, USA) marker was used per gel. The gel was run at 130 V for approximately 1.5 h.

Table 7: Gel composition of SDS-PAGE

Stacking gel (7.4%)	µL	Separating gel (12%)	µL
Acrylamide (30%, w/v)	266	Acrylamide (30%, w/v)	2000
Tris-HCl, 0.5 M, pH 6.8	500	Tris-HCl, 1.5 M, pH 8.8	1300
SDS (10%, w/v)	20	SDS (10%, w/v)	50
APS (10%, w/v)	12	APS (10%, w/v)	50
TEMED	3	TEMED	4
MQ	1200	MQ	1600

2.5.4. Western blotting

For Western blot analysis, the proteins were wet blotted onto a HyBond ECL nitrocellulose membrane (Amersham, Sigma-Aldrich, Darmstadt, GER) at 230 mA for 80 min. Then, the membrane was blocked for 1 h using the Odyssey blocking buffer (PBS) (LI-COR BioSciences, Lincoln, USA). Membranes were incubated with antibodies against α-SMA, mPGES-1, CUGBP1, and GAPDH as internal standard at 4 °C overnight. Then, membranes were washed in 0.1% (v/v) Tween20 (Carl Roth, Karlsruhe, GER) in 1x PBS 3 times for 5 min, followed by incubation with a suitable infrared dye conjugated secondary antibody (IRDye, LI-COR Biosciences, Lincoln, USA) for 45 min. Protein bands were detected with the Odyssey Fc chemiluminescence reader (LI-COR Biosciences, Lincoln, USA). Quantitative analysis of Western blots was performed using Image Studio Lite Software. For sEV analysis, antibodies against CD9, CD63, and CD81 were used. All used primary antibodies can be found in Table 8.

Table 8: Primary antibodies used for Western blot analysis

Target	Host	Dilution	Supplier (product no.)
α-SMA	Mouse	1:1000	Abcam, ab7817
mPGES-1	Rabbit	1:200	Cayman Chemicals, 160140
GAPDH	Rabbit	1:1000	Cell Signaling Technology, 2118
CUGBP1	Rabbit	1:500	Abcam, ab129115
CD9	Mouse	1:500	Santa Cruz Biotechnology, sc-59140
CD63	Mouse	1:1000	Novus Biologicals, NBP2-42225
CD81	Mouse	1:1000	Merck, MABF2061

2.6. Tissue samples

Prof. Dr. Per Kogner, Karolinska Institutet, Stockholm, Sweden, provided NB tumor tissue samples. Ethical approval was obtained by the Stockholm Regional Ethical Review Board and

the Karolinska University Hospital Research Ethics Committee (approval nos. 2009/1369-31/1 and 03/736). Tissue samples of in total 20 patients from different NB subtypes were stained: MYCN amplified (N=8), 11q deleted (N=5), low-risk (N=5), and 11q/MYCN (N=2) amplified.

Lung tumor tissue sections were kindly provided by Prof. Dr. Rajkumar Savai (Max Planck Institute for Heart and Lung Research in Bad Nauheim) and the UGMLC Gießen Biobank as part of the KMU-innoviativ-22 Förderprojekt (FKZ: 161B0768A). The study protocol for tissue donation was passed by the ethics committee (Ethik Kommission am Fachbereich Humanmedizin der Justus Liebig Universität Giessen) of the University Hospital Giessen (Giessen, Germany) and is in accordance with national law and with Good Clinical Practice/International Conference on Harmonization guidelines. Written informed consent was obtained from each patient or the patient's next of kin (AZ 58/15) (25–27). In total, AC tumors of 19 patients were stained.

2.6.1. Immunohistochemical staining of tissue sections

Tissue samples were analyzed with immunohistochemistry (IHC) staining of mPGES-1 and CUGBP1. For this purpose, the samples were deparaffinized by incubating in xylene (Carl Roth, Karlsruhe, GER) 3 times for each 5 min. Then, sections were rehydrated sequentially in 100% EtOH, 96% EtOH, and 70% EtOH and washed 3x in MQ for each 5 min. Antigen unmasking was performed by heating the sections for 3x 5 min in 1 x citrate buffer at 1100 W in the microwave. Afterward, the slides were allowed to cool down for about 30 min to RT. Tissue sections were then washed 3 times for each 3 min in 1x PBS. Next, a hydrophobic barrier pen was applied, and blocking was performed with 3% BSA in PBS for 30 min. After that, the primary antibody solution was applied and incubated at 4 °C overnight. On the next day, slides were washed 3 times in 1x PBS-T (Tween20, 0.01%, v/v) for each 5 min. Then, endogenous oxidases were blocked with 3% H_2O_2 (Sigma-Aldrich, Darmstadt, GER) in PBS for 10 min, and slides were washed 3 times in 1x PBS again. A secondary antibody diluted in blocking solution was applied at RT for 1 h. Afterward, slides were washed in PBS-T 3 times for each 5 min. Then, a 3,3′-Diaminobenzidine (DAB) substrate kit (Abcam, Cambridge, UK) was used to develop the immunostaining following the manufacturer's instructions, resulting in a brown substrate staining. Counterstaining was performed using Hematoxylin Gill 3 (Sigma-Aldrich, Darmstadt, GER) for 15 s. To stop the reaction, slides were briefly dipped in tap water and washed under running tap water for 10 min. Finally, tissue sections were dehydrated in 70% EtOH, 96% EtOH, and 100% EtOH for each 1 min and briefly incubated in xylene to remove the hydrophobic barrier pen. All slides were mounted in EUKITT (VWR, Radnor, USA) and air-dried overnight. Negative control staining was performed without a primary antibody to exclude any unspecific binding of the secondary antibody. Additionally, IgG control staining

with an antibody from the same host-animal was performed to exclude unspecific binding of the primary antibody. A detailed list of the used antibodies can be found in Table 9. The stained sections were imaged using an Aperio CS2 slide scanner (Leica, Wetzlar, GER) and the Aperio ScanScope Software (Leica, Wetzlar, GER) with a magnitude of 20x. Images of tissue sections were analyzed with the Aperio ImageScope software (version 12.3.2.8013, Leica, Wetzlar, GER).

2.6.2. *In-situ* hybridization of tissue sections

For the colocalization studies, *in-situ* hybridization (ISH) of miR-574-5p was also performed on the paraffin-embedded tissue sections. A double fluorescein-labeled miR-574-5p probe was used for this purpose. First, the tissue sections were deparaffinized as described in chapter 2.6.1 and incubated in 1x PBS for 5 min. The tissue was permeabilized with 3 µg/µL proteinase K (Qiagen, Hilden, GER) diluted in proteinase K buffer in staining chambers at 37 °C for 10 min. Subsequently, the sections were washed 3 times in 1x PBS for 5 min each. The sections were then prehybridized in hybridization buffer (Qiagen, Hilden, GER) for 20 min at 54 °C. Hybridization was performed using 100 nM customized miR-574-5p-complementary locked nucleic acid (LNA)-probes in hybridization buffer at 54 °C for 1 h. The specificity of the miR-574-5p ISH was controlled using a digoxygenin (DIG) labeled scramble control probe (negative control) and a DIG-labeled U6 small nuclear RNA probe (positive control, all Qiagen, Hilden, GER). To increase the binding specificity, the sections were stringently washed with different concentrations of saline-sodium citrate (SSC) buffers. First, tissue sections were incubated once in 5x SSC and then twice in 1x SSC buffer at 54 °C. Subsequently, they were washed twice in 0.2x SSC at 54 °C and once at RT. Then, the sections were incubated in 1x PBS for 5 min to remove salt residues. Afterward, the hydrophobic barrier pen was applied, and tissue was blocked with ISH blocking buffer for 15 min. The miR-574-5p-probes were detected with alkaline phosphatase (AP)-labeled antibody against FAM. U6 and ScrC probes were detected with an AP-labeled antibody against DIG. For this purpose, tissue sections were incubated with the antibodies diluted 1:500 in ISH antibody buffer for 1 h. Then, tissue sections were washed with PBS-T three times for 3 min and once with 1x PBS. The staining was developed using the AP substrate nitro blue tetrazolium/ 5-Bromo-4-chloro-3-indolyl-phosphate (NBT/BCIP, Roche, Basel, CHE) following the manufacturer's instructions at 30 °C for 2 h. The substrate solution was supplemented with 0.2 mM levamisole (Sigma-Aldrich, Darmstadt, GER) to block endogenous phosphatases. After substrate development, the reaction was stopped by washing twice in KTBT buffer and once in tap water for each 5 min. Counterstaining was performed with nuclear fast red (Vector Laboratories, Burlingame, USA) for 60 s. To stop the staining reaction, slides were briefly dipped in tap water and washed under running tap water for 10 min. Finally, tissue sections were dehydrated, mounted, digitalized,

and analyzed as described above (chapter 2.6.1). A detailed list of the antibodies used can be found in Table 9.

Table 9: Antibodies used for IHC and ISH

Target	Host	Dilution	Supplier (product no.)
CUGBP1	Rabbit	1:100	Abcam (ab129115)
mPGES-1	Rabbit	1:200	Cayman Chemicals (160140)
rabbit-IgG-HRP-labeled	Goat	1:300	Abcam (ab7090)
DIG AP labeled	Sheep	1:500	Roche (11 093 274 910)
FAM AP labeled	Sheep	1:500	Roche (11 426 338 910)

2.7. Statistics

All results are shown as mean + standard error of mean (SEM) of at least three independent experiments. Statistical analysis was carried out by Student's unpaired t-test (two-tailed) or one-way ANOVA with Tukey's multiple comparison test using GraphPad Prism 6.0. Experimental differences were considered as significant for $p \leq 0.05$ (indicated as * for $p \leq 0.05$, ** for $p \leq 0.01$, *** for $p \leq 0.001$, and **** for $p \leq 0.0001$, or § for $p \leq 0.05$, §§ for $p \leq 0.01$, §§§ for $p \leq 0.001$, and §§§§ for $p \leq 0.0001$).

3. Results

3.1. The role of intracellular miR-574-5p in neuroblastoma

3.1.1. Two PGE_2-dependent tumor types have different miR-574-5p expression patterns

This study aimed to determine the role of miR-574-5p in NB and compare it with its functions in NSCLC. In NSCLC, miR-574-5p was found to function as a decoy for CUGBP1 in mPGES-1-dependent PGE_2 regulation. Therefore, we focused on the comparison between NSCLC and NB. Firstly, we compared the cellular location of miR-574-5p, mPGES-1, and CUGBP1 between NB and NSCLC tissues by staining serial sections from 19 patients with AC. For each tumor, immunostaining for mPGES-1 and CUGBP1 and *in-situ* hybridization for miR-574-5p was performed (Figure 11). The tumor cells in the LC sections had high levels of miR-574-5p (black arrows). The miR-574-5p is present in the cell nuclei, where the miR-574-5p-CUGBP1 decoy occurs [264]. As expected, the tumor cells were also positive for mPGES-1 and CUGBP1 (black arrows). MPGES-1 is not present in the nuclei here but rather in the rest of the cell. This also corresponds to the localization in the endoplasmic reticulum described in the literature [300]. The localization of CUGBP1 cannot be determined as precisely as for the other targets, but it seems to be present in the nucleus for the most part, like miR-574-5p in most tissue sections. The literature also describes that CUGBP1 can be present in different cellular compartments, including the nucleus, depending on the cellular constitution [301,302]. The colocalization of miR-574-5p and CUGBP1 in the nuclei suggests that the miR-574-5p-CUGBP1 decoy is present in the cancer cells [52,264]. However, the surrounding cells in the TME, presumably connective tissue, including fibroblasts, had lower amounts of miR-574-5p (white arrows). Differences were also visible between the individual tumor patients. 2 of the 19 patients had no signal for miR-574-5p, with one patient as well negative for mPGES-1 and CUGBP1.

NB tumor sections of 4 different tumor subtypes were stained. In total, tumors from 20 different NB patients were stained, 8x MYCN amplified, 5x 11q deleted, 5x low-risk, and 2x 11q deleted, and MYCN amplified were stained for mPGES-1, CUGBP1, and miR-574-5p. Strikingly, compared to the NSCLC sections, less miR-574-5p is present in the cancer cells in the NB sections. Nevertheless, in the tumor sections of the subtypes with 11q deletion and low-risk, low levels of miR-574-5p are present in larger tumor cells, to be determined by their histology as presumably differentiated cancer cells (Figure 12A,C, black arrows) [303]. In both tumor subtypes, mPGES-1 and CUGBP1 are also present in these cells. While miR-574-5p is less present in NB, CUGBP1 appears to be more abundant than in NSCLC, which is consistent with the results of 3D cell culture experiments that were gained in my master's thesis and were continued during this thesis [304]. NBs with MYCN amplification did not express miR-574-5p

and mPGES-1. However, they expressed higher levels of CUGBP1 (Figure 12B). In the sections with MYCN amplification, no differentiated cancer cells were found. Notably, mPGES-1 is strongly present in the other cells of the TME in the sections with 11q deletion. These cells were identified as fibroblasts or CAFs (white arrows) based on their histologic structure. These are strongly positive for mPGES-1 but negative for CUGBP1 and miR-574-5p, in agreement with the findings of Larsson et al. in 2015 [295].

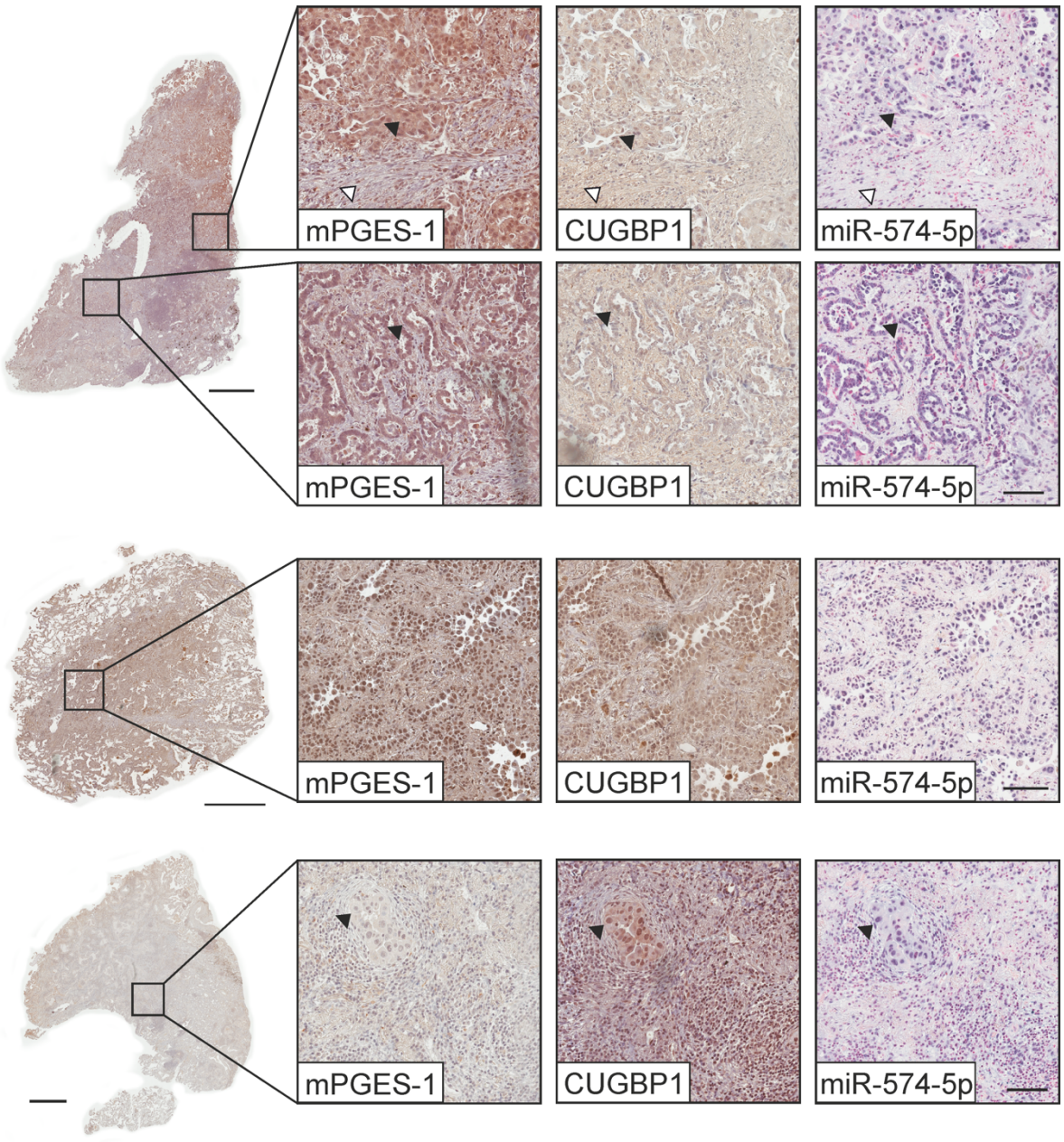

Figure 11: MPGES-1 and CUGBP1 immunostaining (IHC) and *in-situ* hybridization (ISH) of miR-574-5p in paraffin-embedded lung adenocarcinoma (AC) tumor sections.

IHC (brown) was performed using antibodies against mPGES-1 and CUGBP1, and sections were counterstained with hematoxylin (blue). ISH was performed using a miR-574-5p-probe (blue), and sections were counterstained with nuclear fast red (red). Fibroblasts (white arrows) and cancer cells (black arrows) are highlighted. Cancer cells express high levels of miR-574-5p. Exemplary images of 3 stained AC tumors are shown (N=19). Scale bars: 2 mm, magnified images: 100 µm.

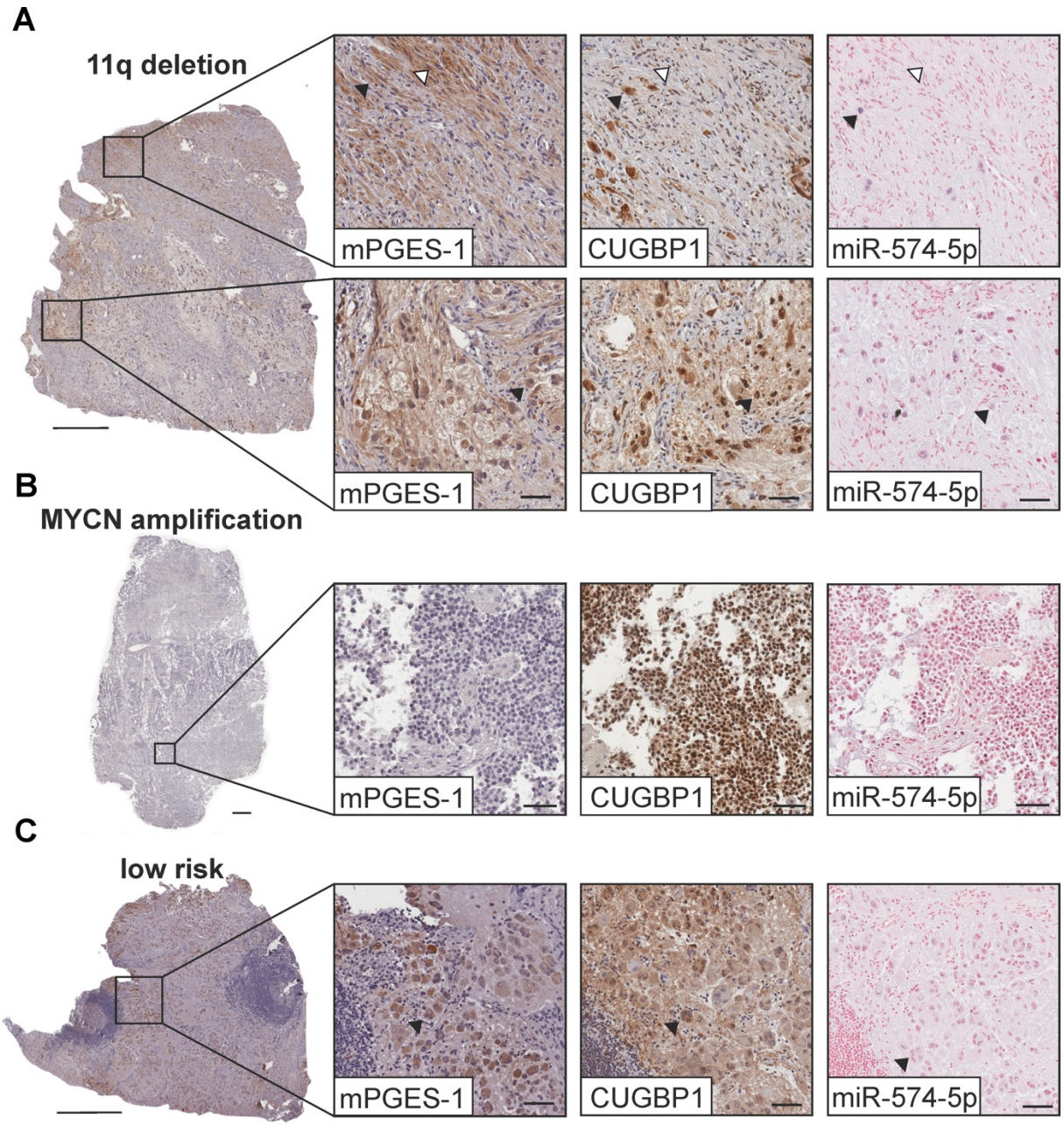

Figure 12: MPGES-1 and CUGBP1 immunostaining (IHC) and *in-situ* hybridization (ISH) of miR-574-5p in paraffin-embedded neuroblastoma (NB) tumor sections.

IHC (brown) was performed using antibodies against mPGES-1 and CUGBP1, and sections were counterstained with hematoxylin (blue). ISH was performed using a miR-574-5p-probe (blue) and sections were counterstained with nuclear fast red (red). Exemplary tumor sections of NB tumor subtypes with (A) 11q deletion (N=5), (B) MYCN amplification (N=8), and (C) of the low-risk subtype (N=5) are shown. Fibroblasts in the 11q deleted subtype (white arrows) are positive for mPGES-1, and differentiated cancer cells (black arrows) are positive for mPGES-1, CUGBP1 and miR-574-5p. Scale bars: 0.5 mm, magnified images: 50 µm.

The negative controls showed no signal from the secondary antibody, and there was as well no false positive signal in the *in-situ* hybridization (Figure 13). In summary, there were visible differences between NSCLC and NB and subtype-specific differences in NB. In both cancer types, miR-574-5p, mPGES-1, and CUGBP1 colocalize in the cancer cells, but NSCLC had higher levels of miR-574-5p and NB higher levels of CUGBP1. In NB, there were higher levels

of mPGES-1 and CUGBP1 in the cancer cells and mPGES-1 in the fibroblasts, indicating communication between different cell types. The results were summarized in Table 10.

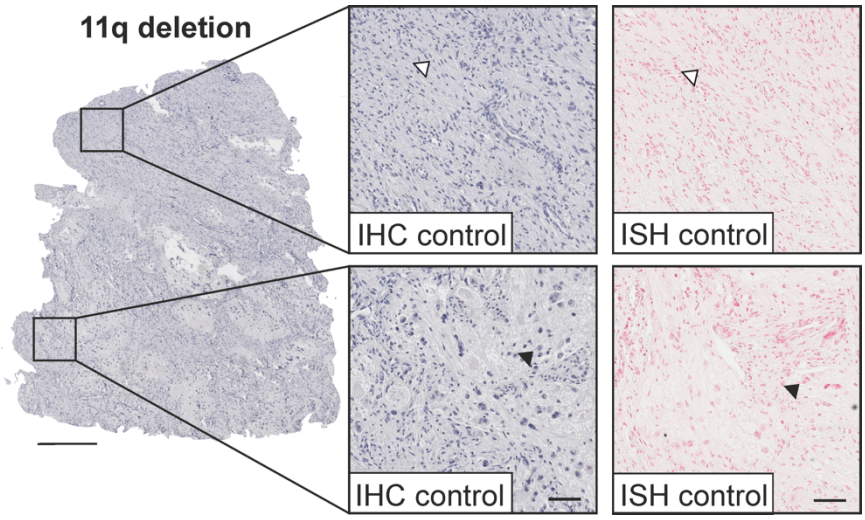

Figure 13: Negative controls for immunostaining (IHC) and *in-situ* hybridization (ISH) in paraffin-embedded neuroblastoma (NB) tumor sections.

Control IHC was performed using a rabbit IgG antibody and was counterstained with hematoxylin (blue). Control ISH was performed using an ScrC-probe (blue) and sections were counterstained with nuclear fast red (red). Fibroblasts (white arrows) and differentiated cancer cells (black arrows) are highlighted. Scale bars: 0.5 mm, magnified images: 50 µm.

Table 10: Overview of staining intensities in AC and NB tissue sections

	mPGES-1	**CUGBP1**	**miR-574-5p**
AC	– in cancer cells	– in cancer cells	↑ in cancer cells
NB	– in CAFs and cancer cells	↑ in cancer cells	↓ in cancer cells

3.1.2. Interaction of miR-574-5p and CUGBP1 regulates PGE_2 in neuroblastoma cells

In NSCLC, miR-574-5p as well as CUGBP1 and mPGES-1 colocalize in cancer cells, which is required for the interaction of miR-574-5p and CUGBP1 leading to the regulation of PGE_2 [52]. Now, colocalization of miR-574-5p, CUGBP1 and mPGES-1 was also shown in NB cancer cells. In addition, mPGES-1 was shown to be similarly regulated in NSCLC and NB *in vitro*, supporting the presence of the miR-574-5p-CUGBP1 decoy [304]. In order to show that miR-574-5p interacts with CUGBP1 to regulate the expression of mPGES-1, it is necessary to demonstrate the binding of miR-574-5p and the mPGES-1 mRNA to CUGBP1. Therefore, RIP experiments of CUGBP1 from the cell lysates of SK-N-AS cells was carried out. The miR-574-5p-CUGBP1 decoy is present in NSCLC in A549 cells in the inflammatory environment, which was achieved *in vitro* by stimulation with IL-1β [264]. Therefore, RIP experiments were also

performed in SK-N-AS cells with and without IL-1β to pursue a possible regulation of the interaction (Figure 14). The amounts of miR-574-5p, miR-16-5p, mPGES-1, and COX-2 mRNA bound to CUGBP1 were determined and normalized to IgG control. It was shown that the amount of miR-574-5p and mPGES-1 were significantly enriched in both conditions compared to the IgG control (Figure 14A,C). MiR-16-5p and COX-2 were used as controls and did not show any enrichment in either of the two conditions (Figure 14B,D). To validate the enrichment of CUGBP1, the lysates were analyzed by Western blot and compared to the input control (Figure 14E,F). An average immunoprecipitate recovery of 29% was observed for the unstimulated SK-N-AS cells and 41% for the cells stimulated with IL-1β.

Taken together, the RIP experiments show that both miR-574-5p and mPGES-1 bind to CUGBP1, providing the basis for a miR-574-5p-CUGBP1 decoy. Together with the 3D cell culture experiments, it is very likely that PGE_2 synthesis is also regulated in NB cancer cells via the interaction between miR-574-5p and CUGBP1 [304].

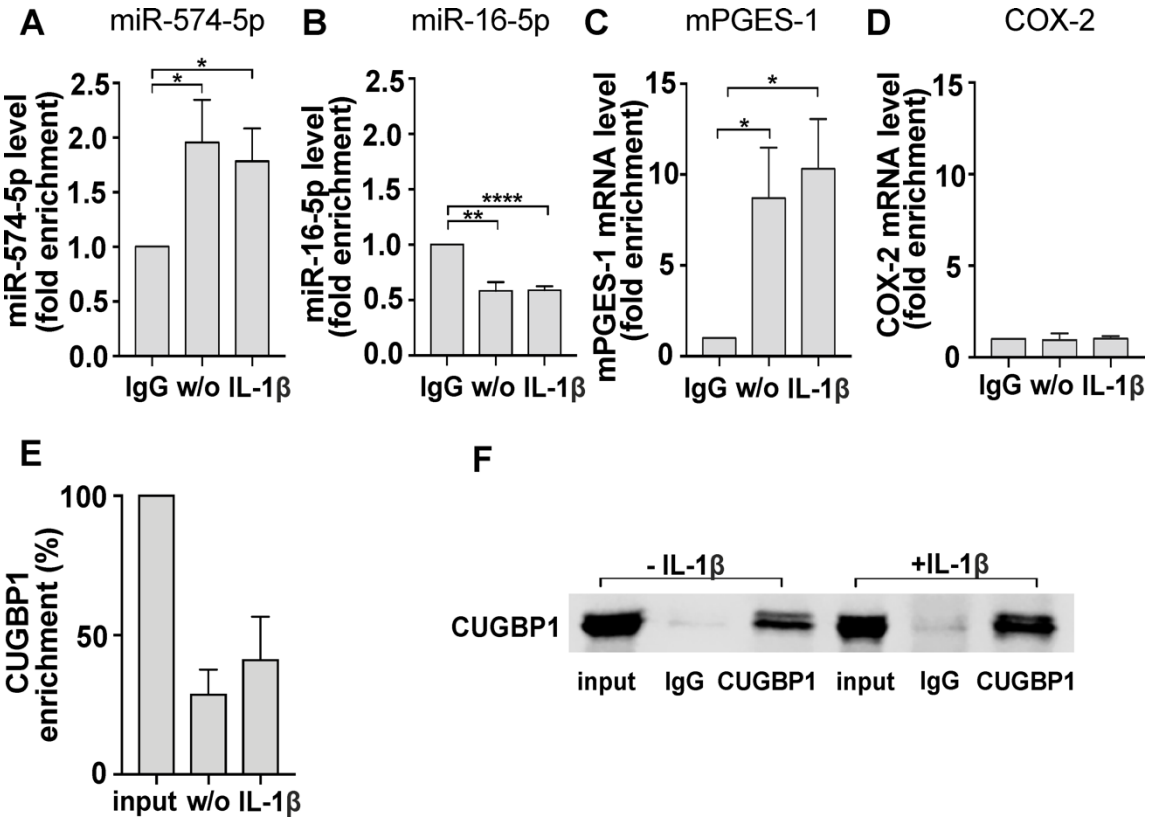

Figure 14: RNA-Immunoprecipitation (RIP) of CUGBP1 from SK-N-AS cells.

CUGBP1 was enriched from SK-N-AS cells untreated and treated with 5 ng/mL IL-1β. (A,B) MiR-574-5p was enriched 1.96-fold in the CUGBP1-immunoprecipitate of untreated cells and 1.78-fold in cells treated with 5 ng/mL IL-1β compared to IgG control. MiR-16-5p was not enriched in the CUGBP1-immunoprecipitate. (C,D) MPGES-1 mRNA was enriched 8.7-fold in the CUGBP1-immunoprecipitate of unstimulated cells and 10.31-fold in cells treated with IL-1β. COX-2 mRNA was not enriched in the CUGBP1-immunoprecipitate. (E, F) Validation of the CUGBP1-immunoprecipitation by Western blot using an α-CUGBP1 antibody. For untreated SK-N-AS cells 28.64% and for cells stimulated with IL-1β, 41.01% of the total CUGBP1 were recovered in the immunoprecipitates. A representative blot of 4 independent experiments is shown. Data are presented as mean + SEM (N=4). Unpaired t-test to IgG control, *p≤0.05; **p≤0.01; ****p≤0.0001.

3.2. The role of sEV-miR-574-5p in neuroblastoma

3.2.1. Neuroblastoma cells secrete miR-574-5p upon PGE_2 stimulation

PGE_2 can trigger the miR-574-5p secretion in AC and SCC cells. Both cell lines secrete miR-574-5p at different time points after PGE_2 treatment [52]. To compare this to NB, two different NB cell lines, SK-N-AS and SK-N-SH, were stimulated with 5 nM PGE_2 or DMSO as control. Intracellular and extracellular miR-574-5p levels were measured after 0.5, 1, and 2 h by RT-qPCR (Figure 15). Both cell lines are high-risk NB cell lines, while the cell line SK-N-AS has an 11q deletion and SK-N-SH not [288]. SK-N-AS cells secreted miR-574-5p in their sEV 0.5 h after PGE_2 stimulation (Figure 15A). In comparison, intracellular miR-574-5p levels did not change significantly (Figure 15B). SK-N-SH cell line secreted sEV-derived miR-574-5p 2 h after PGE_2 stimulation (Figure 15C) No significant effect on intracellular levels was observed (Figure 15D).

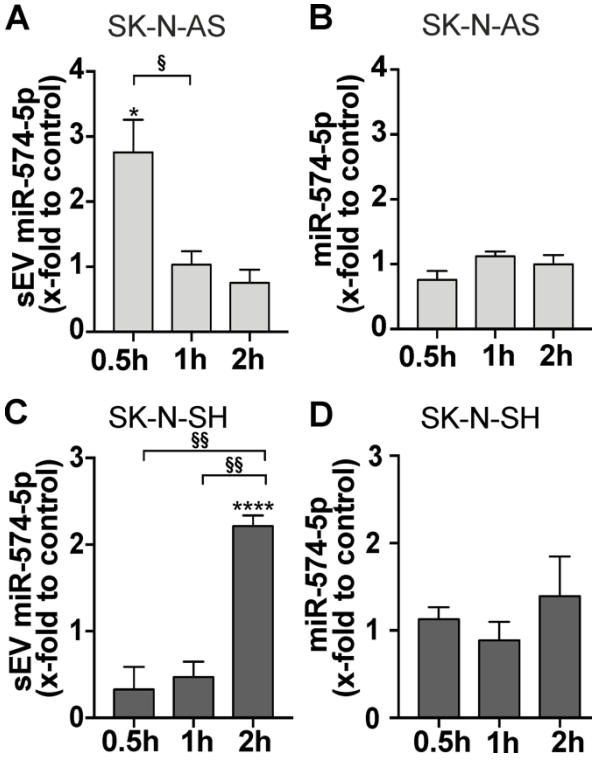

Figure 15: SK-N-AS and SK-N-SH cells secrete miR-574-5p upon PGE_2 stimulation.

Cells were stimulated with 5 nM PGE_2 for 0.5, 1, and 2 h. Then, (A) exosomal and (B) intracellular miR-574-5p level of SK-N-AS cells and (C) exosomal and (D) intracellular miR-574-5p level of SK-N-SH cells was measured. Exosomal miR-574-5p level of SK-N-AS cells was increased to 2.75-fold 0.5 h after stimulation, while the intracellular level was unaffected. Exosomal miR-574-5p level of SK-N-SH cells was increased to 2.21-fold 2 h after stimulation, and the intracellular level was also not affected. MiR levels were analyzed by RT-qPCR, normalized to the spike-in control ath-miR-159a and folded to their corresponding control. Data are shown as mean +SEM (N=3-4). Unpaired t-test to DMSO control, * $p \leq 0.05$, **** $p \leq 0.0001$. Unpaired t-test to other samples, §$p \leq 0.05$, §§$p \leq 0.01$.

SK-N-AS cells were stimulated with agonists for EP1/3, EP2, and EP4 to further analyze the secretion effect induced by PGE_2 (Figure 16). The EP1/3 agonist sulprostone induced miR-574-5p secretion after 30 min (Figure 16A). In contrast, this effect was not triggered by the addition of the agonists against EP2 butaprost (Figure 16B) and EP4 L-902,688 (Figure 16C). Thus, it could be determined that the effect of increased secretion of sEV-miR-574-5p is mediated via the EP1/3 receptors. To exclude the effect of an increase in the total number of secreted sEV, particles were measured in the supernatants of SK-N-AS cells 30 min and 60

min after PGE_2 stimulation using a microfluidic resistive pulse sensing technology-based nCS1™ nanoparticle analyzer by M. Sc. Tatjana Best (Figure 16D). The number of particles between 50 and 300 nm did not significantly change after PGE_2 stimulation.

In conclusion, PGE_2 induces the secretion of miR-574-5p into the sEV of SK-N-AS cells via EP1/3 as in NSCLC. The fact that the cell lines are all triggered by the same inflammatory mediator suggests a similar function of sEV-miR-574-5p in NB as in NSCLC.

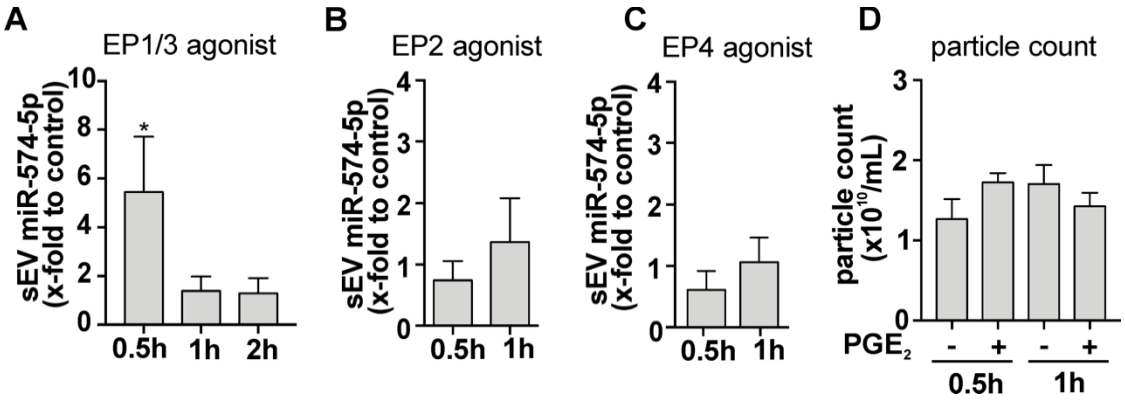

Figure 16: SK-N-AS cells secrete miR-574-5p via EP1/3.

For further analysis of PGE_2-dependent miR-574-5p secretion, SK-N-AS cells were stimulated with 5 nM (A) EP1/3 agonist sulprostone, (B) EP2 agonist butaprost and (C) EP4 agonist L-902,688 or respective control solvents. Sulprostone triggered the secretion of miR-574-5p to 5.45-fold 0.5 h after stimulation, while the other agonists did not affect the sEV-miR-574-5p levels. MiR levels were analyzed by RT-qPCR, normalized to the spike-in control ath-miR-159a, and folded to their corresponding control. Data are shown as mean +SEM (N=3-4). Unpaired t-test to corresponding control, *p≤0.05. (D) In order to analyze the effect on sEV numbers, SK-N-AS cells were stimulated with 5 nM PGE_2 or DMSO for 0.5 h, and 1 h and total particle numbers of the cell supernatants were measured with an nCS1™ nanoparticle analyzer by Tatjana Best. PGE_2 stimulation had no significant effect on the particle count. Particles of a size between 50 and 300 nm were detected (N=3).

3.2.2. Establishment of miR-574-5p oe sEV derived from neuroblastoma cells

To determine the function of sEV-derived miR-574-5p in NB, sEV with engineered miR-574-5p levels were used. For this purpose, SK-N-AS or SK-N-SH cells were transfected with the XMIR-Xpress system, and the sEV were subsequently purified. After that, the sEV-miR-574-5p levels were quantified via RT-qPCR. The miR-574-5p overexpression (oe) sEV of SK-N-AS cells (Figure 17A) and SK-N-SH cells (Figure 17B) had a nearly 10-fold increased level of miR-574-5p compared to their respective scrambled control (ScrC) sEV. A good comparability between the sEV subtypes is ensured by the similarly high oe-level.

To demonstrate that miR-574-5p is truly present in the oe sEV and not attached to the outside, a Triton X-100 assay was performed by M. Sc. Sheila Nevermann during her master's thesis under my supervision. For this reason, the purified sEV were divided into three approaches, one treated with RNase I and the other treated with RNase I and Triton X-100. The miR-574-5p present in the sEV was expected to be protected from degradation by RNase by the membrane of the sEV. The addition of Triton X-100 permeabilized the sEV membrane. As a result,

miR-574-5p was degraded by the addition of RNase. More than 70% of miR-574-5p in sEV of SK-N-AS cells (Fig. 17C) and SK-N-SH cells (Figure 17D) was shown to be protected from RNase degradation by the membrane and thus present in sEV.

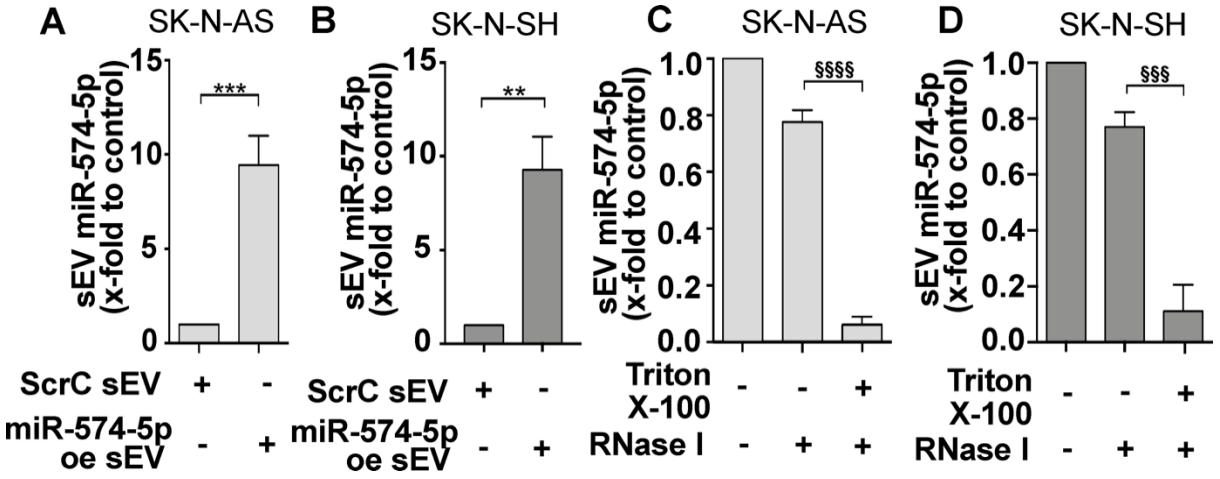

Figure 17: Establishment of miR-574-5p overexpression (oe) sEV

XMIR-Xpress-plasmids for miR-574-5p and ScrC were used to generate oe sEV of (A) SK-N-AS and (B) SK-N-SH cells. MiR-574-5p levels were analyzed via RT-qPCR, normalized to the spike-in control ath-miR-159a, and folded to their corresponding negative control (N=3). Relative changes to ScrC are shown as mean + SEM, unpaired t-test **p≤0.01; ***p≤0.001. MiR-574-5p oe sEV of (C) SK-N-AS and (D) SK-N-SH were treated with Triton X-100 and RNase I. In samples without Triton X-100, miR-574-5p was protected from RNase digest. MiR-574-5p levels were analyzed via RT-qPCR, normalized to the spike-in control ath-miR-159a and folded to their corresponding control (SK-N-AS: N=6, SK-N-SH N=5). Relative changes to RNAse I control are shown as mean +SEM, unpaired t-test §§§p≤0.001; §§§§p≤0.0001. The RNase experiment was performed by Sheila Nevermann.

To prove the uptake of sEV by their respective cells, live cell experiments were performed (Figure 18). Therefore, SK-N-AS and SK-N-SH cells were seeded, and their nuclei were stained with Hoechst. Isolated miR-574-5p oe sEV from SK-N-AS and SK-N-SH cells were stained with the lipophilic tracer DiO and then added to their respective cells. The uptake was monitored for 30 min. The experiment revealed an uptake of SK-N-AS-derived miR-574-5p oe sEV by SK-N-AS cells after 20 min (Figure 18A). SK-N-SH-derived miR-574-5p oe sEV were internalized to a lesser extent and the sEV accumulated at the cell membrane of SK-N-SH cells after 20 min (Figure 18B). Similar cell-dependent differences were previously observed between the NSCLC cell lines A549 and 2106T [52]. Moreover, when treated with each other's sEV, it was observed that the type of internalization was cell type specific and not dependent on the sEV. Here, we observed that SK-N-AS and A549 cells showed a similar pattern of internalization of their sEV, whereas SK-N-SH and 2106T cells showed a similar pattern. Therefore, the cell-specific differences between the two NB cell lines may indicate a different mode of sEV internalization by their cells.

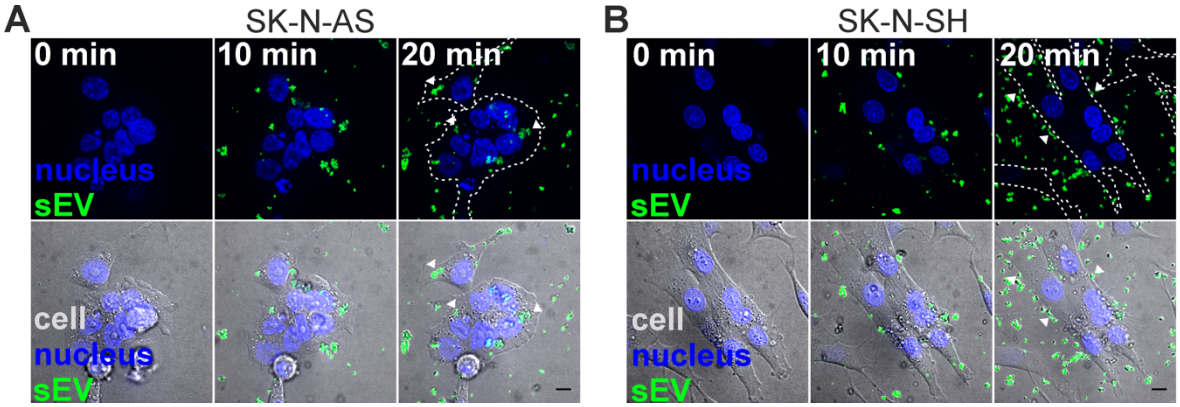

Figure 18: Live cell imaging of SK-N-AS and SK-N-SH cells with their respective miR-574-5p oe sEV.

Cell nuclei were stained with Hoechst and sEV with the lipophilic tracer DiO. SK-N-AS internalized their sEV after 20 min, while SK-N-SH sEV accumulated at the cell membrane. The experiment was performed with protocol A, described in 2.2.7. Representative images of three independent biological replicates with at least five technical replicates are shown. Scale bars: 10 µm

3.2.3. SEV-miR-574-5p has no effect on mPGES-1 levels in neuroblastoma cancer cells

The intracellular function of miR-574-5p is the same in NB as in NSCLC. Therefore, it is reasonable to assume that the function of sEV-miR-574-5p is also the same. To investigate this assumption, SK-N-AS cells were treated with 2 µg/mL of isolated sEV with miR-574-5p oe or ScrC sEV. The mPGES-1 protein and RNA levels were analyzed. In addition, R848, a TLR7/8 ligand, was included in the experiments. In A549 cells, sEV-derived miR-574-5p was shown to decrease mPGES-1 levels via TLR7/8 receptors, thereby negatively regulating PGE_2 synthesis [52]. The expectation that mPGES-1 levels would also be decreased in NB cells was not confirmed (Figure 19A). The sEV-derived miR-574-5p had no significant effect on mPGES-1 levels in SK-N-AS cells. The addition of TLR7/8 ligand R848 significantly decreased the mPGES-1 mRNA level to 0.8-fold (Figure 19B). However, sEV-derived miR-574-5p had no effect. Thus, sEV-derived miR-574-5p does not exert the same autocrine function in SK-N-AS cells as it does in A549 cells.

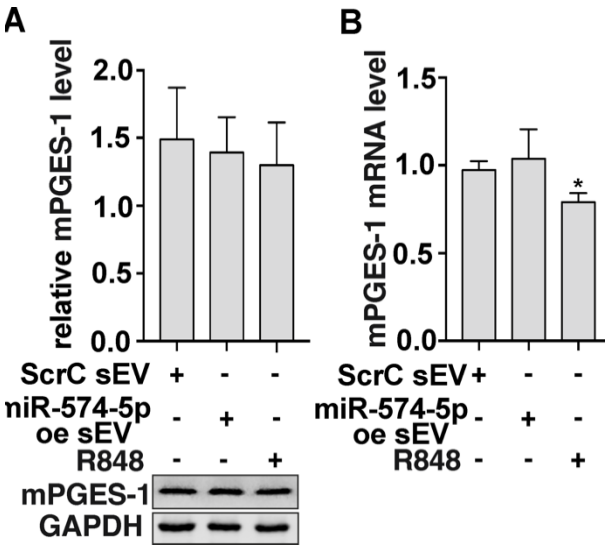

Figure 19: MPGES-1 levels of SK-N-AS cells after sEV-miR-574-5p oe and ScrC sEV stimulation.

(A) Western blot analysis of SK-N-AS cells treated with miR-574-5p oe and ScrC sEV derived from SK-N-AS cells or 100 ng/mL TLR7/8 ligand R848 in combination with 5 ng/mL IL-1β. No significant effects on mPGES-1 protein level were detected. Results are shown as mean +SEM (N=4). (B) RT-qPCR analysis of mPGES-1 mRNA of SK-N-AS stimulated with miR-574-5p oe or ScrC sEV derived from SK-N-AS cells or 100 ng/mL TRL7/8 ligand R848. sEV-miR-574-5p had no significant effect on mPGES-1 mRNA level, while R848 decreased the mPGES-1 mRNA level significantly. Results are shown as mean +SEM (N=3). Unpaired t-test to corresponding control, * p≤0.05.

3.2.4. SK-N-AS-derived sEV-miR-574-5p increases α-SMA levels in fibroblasts

CAFs generally play a central role in the NB, as they are required for the mPGES-1-dependent synthesis of PGE_2 [295,296]. For this purpose, the fibroblast cell line HFL1 was treated with miR-574-5p oe sEV isolated from SK-N-AS cells. To visualize sEV uptake by the cells, live cell microscopy experiments were performed (Figure 20). In the microscopy experiments, the fibroblasts internalized the sEV through long membrane extensions (white arrows). The sEV are ‘grabbed and pulled’ into the cells by the membrane extensions. In addition, the internalization time of sEV was visibly longer in the fibroblasts than in the SK-N-AS cells.

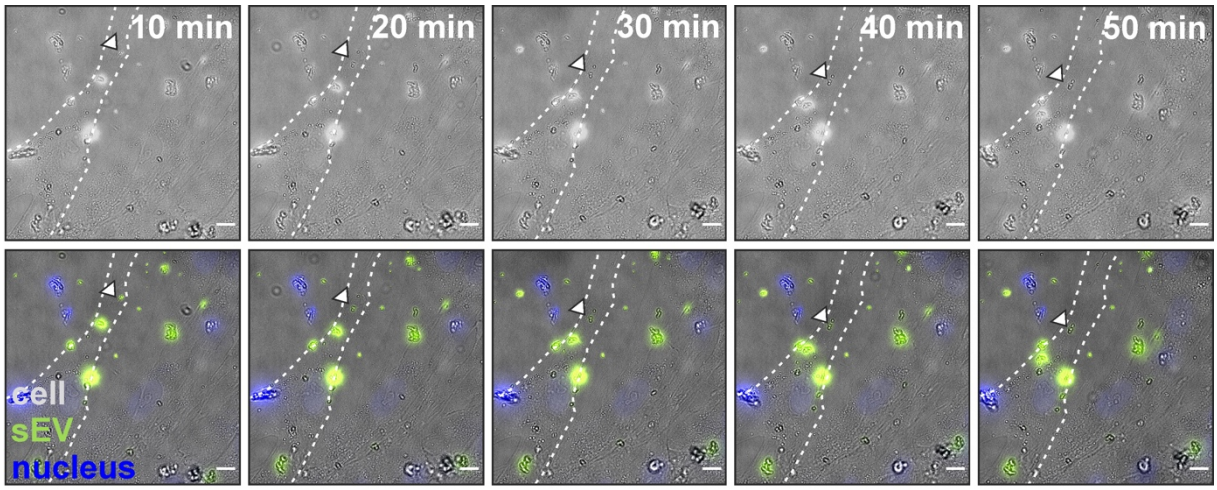

Figure 20: HFL1 cells take up SK-N-AS-derived sEV.

Live cell microscopy was performed using HFL1 cells and miR-574-5p oe sEV derived from SK-N-AS cells. The nuclei of the fibroblasts were stained with Hoechst and sEV with the lipophilic tracer DiO. Cells were incubated with the sEV for 50 min. The cells internalized the sEV via long membrane extensions (white arrows). The experiment was performed using protocol B described in 2.2.7. Representative images of three independent biological replicates with at least five technical replicates are shown. Scale bars: 10 µm

HFL1 cells were treated with miR-574-5p oe or ScrC sEV for 72 h, and the α-SMA level of the cells was analyzed by Western blot analysis to consider the differentiation of HFL1 cells into CAFs in the analyses (Figure 21). MiR-574-5p oe sEV derived from four different established cell lines SK-N-AS, SK-N-SH, 2106T, and A549 were tested [52]. The α-SMA level of fibroblasts was significantly increased by the addition of miR-574-5p oe sEV of SK-N-AS cells (Figure 21A). Simultaneous addition of TGFβ further enhanced the effect to a 1.5-fold induction (Figure 21B). The miR-574-5p oe sEV of SK-N-SH, 2106T, and A549 cell lines did not trigger a significant upregulation of α-SMA compared to ScrC sEV. On the contrary, sEV from 2106T cells significantly decreased α-SMA levels when TGFβ was added. This effect was significantly enhanced by miR-574-5p oe sEV. No such effect was observed with sEV derived from other cell lines. However, the effect of sEV-miR-574-5p from SK-N-AS seems to be specific for sEV-miR-574-5p derived from this cell line. Compared to NSCLC, there is no autocrine effect on PGE2 synthesis. Instead, there is a paracrine effect on the α-SMA level of fibroblasts.

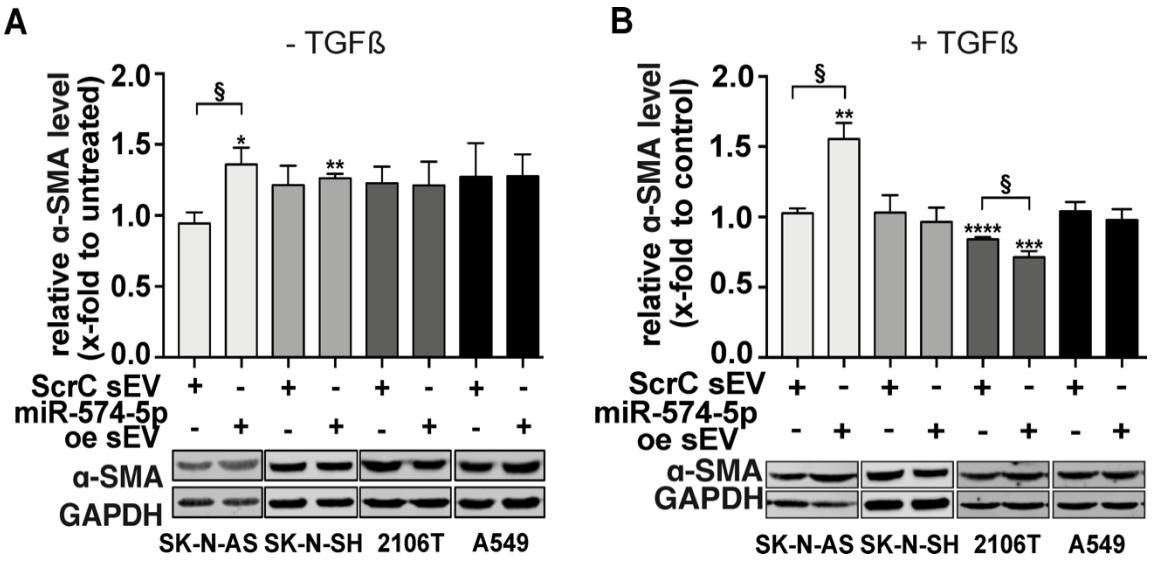

Figure 21: The α-SMA level of HFL1 cells is increased by sEV-miR-574-5p from SK-N-AS cells.

Western blot analysis of α-SMA protein levels of HFL1 cells treated with 2 µg/mL miR-574-5p overexpression (oe) or ScrC sEV derived from SK-N-AS, SK-N-SH, 2106T, or A549 cells. Cells were treated for 72 h without (A) or with 10 ng/mL TGFβ (B). α-SMA level was increased specifically by sEV-miR-574-5p derived from SK-N-AS cells compared to their respective ScrC control. α-SMA levels were normalized to GAPDH and folded to control (SK-N-AS, A549: N=3, SK-N-SH, 2106T: N=4). Results are shown as mean +SEM, unpaired t-test to control without sEV, * p≤0.05; **p≤0.01; *** p≤0.001; **** p≤0.0001. Unpaired t-test to other samples, §p≤0.05.

Together with M. Sc. Sheila Nevermann, a viability assay was performed to exclude toxic and proliferation-inhibitory effects on the cells. In this assay, HFL1 fibroblasts were again treated with the isolated miR-574-5p oe or ScrC sEV derived from SK-N-AS cells. A tetrazolium reduction assay was then performed to determine cell viability. Neither sEV alone nor sEV in combination with TGFβ affected the relative viability of the cells (Figure 22).

In summary, sEV-derived miR-574-5p of SK-N-AS cells showed a specific induction of α-SMA level of fibroblasts, which was not induced due to cell viability.

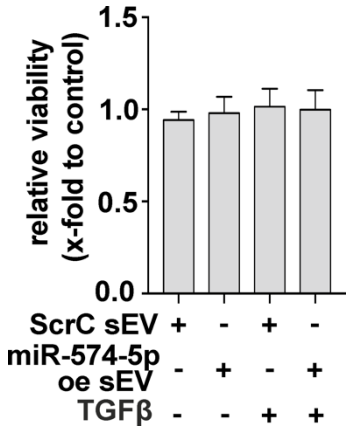

Figure 22: SK-N-AS-derived miR-574-5p oe or ScrC sEV do not affect the cell viability detected by tetrazolium reduction assay.

HFL1 cells were stimulated with 2 µg/mL miR-574-5p oe or ScrC sEV and 10 ng/mL TGFβ for 72 h. Then the cells were incubated for 3 h with 3-(4,5-dimethylthiazol-2-yl)-2,5-diphenyltetrazoliumbromide (MTT) to detect effects on the proliferation and cell viability. No cytotoxic effects of sEV were detected. Results are shown as mean +SEM (N=4). This experiment was performed together with Sheila Nevermann.

3.2.5. SK-N-AS-derived sEV-miR-574-5p increases α-SMA levels via TLR7/8

The question is how this effect, which is mediated by the sEV-miR-574-5p derived from SK-N-AS, affects HFL1. One possible hypothesis is that sEV-miR-574-5p uptake activates the miR-574-5p-CUGBP1 decoy mechanism in HFL1 cells. RIP of CUGBP1 was performed on cell lysates from HFL1 cells treated with the SK-N-AS-derived miR-574-5p or sEV or ScrC sEV to test whether miR-574-5p and CUGBP1 interact in HFL1 cells upon sEV treatment (Figure 23). CUGBP1 was isolated from HFL1 cells and miR-574-5p, miR-16-5p, mPGES-1 and COX-2 mRNA were measured in the precipitate. No significant enrichment could be detected for either miR-574-5p or miR-16-5p (Figure 23A,B). There was a significant enrichment of mPGES-1 mRNA in all conditions (Figure 23C). In untreated cells as well as in HFL1 cells treated with ScrC or miR-574-5p or sEV, mPGES-1 was enriched bound to CUGBP1. COX-2 was not significantly enriched (Figure 23D). Addition of miR-574-5p oe sEV did not affect the enrichment of RNAs compared to untreated HFL1 cells. Furthermore, a very high average enrichment of CUGBP1 of 100% was detected in miR-574-5p oe sEV treated cells. In contrast, only an average enrichment of about 50% was detected in untreated cells (Figure 23E,F). In conclusion, no miR-574-5p-CUGBP1 decoy was detected in HFL1 cells. Treatment of cells with miR-574-5p or sEV did not significantly affect the binding of CUGBP1 and miR-574-5p or mPGES-1 mRNA.

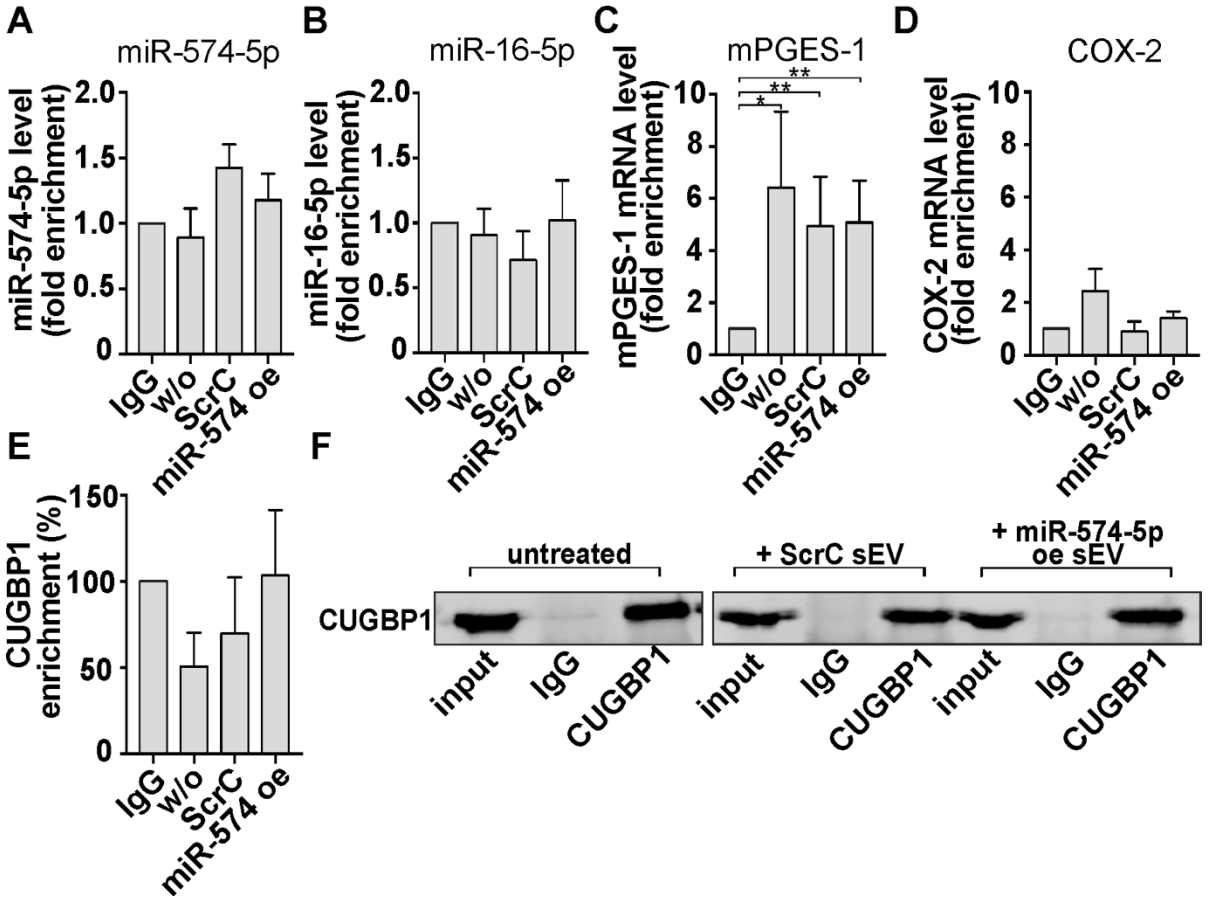

Figure 23: MiR-574-5p is not binding to CUGBP1 in HFL1 cells.

RNA-Immunoprecipitation (RIP) of CUGBP1 was performed from HFL1 cells treated with 2 µg/mL ScrC or miR-574-5p oe sEV derived from SK-N-AS cells (A,B) MiR-574-5p and miR-16-5p were not enriched in the CUGBP1-immunoprecipitate of HFL1 cells compared to IgG control. (C,D) MPGES-1 mRNA was enriched 6.4-fold in the CUGBP1-immunoprecipitate of unstimulated cells and 4.9 and 5-fold in cells treated with ScrC and miR-574-5p oe sEV from SK-N-AS cells. COX-2 mRNA was not enriched in the CUGBP1-immunoprecipitate. (E, F) Validation of the CUGBP1-immunoprecipitation by Western blot using an α-CUGBP1 antibody. For untreated HFL1 cells 50.57%, for ScrC sEV treated cells, 69.87% and for cells stimulated with miR-574-5p oe sEV, 103.35% of the total CUGBP1 were recovered in the immunoprecipitates. A representative blot of 4 independent experiments is shown. Data are presented as mean + SEM (N=4). Unpaired t-test to IgG control, *p≤0.05; **p≤0.01.

Previous studies investigating the function of miR-574-5p already showed that miR-574-5p could act as a ligand for TLR7/8 receptors [52,144,268]. Therefore, the TLR7/8 ligand R848 and the TLR7/8 inhibitor ODN 2088 were included in the experiments to investigate whether the effect on α-SMA is mediated via TLR7/8. Cells were treated with ScrC or miR-574-5p oe sEV for 72 h and additionally stimulated with TLR7/8 ligand and inhibitor. Subsequently, the α-SMA level of HFL1 cells was again determined by Western blot and RT-qPCR. The α-SMA protein level of HFL1 cells was again induced to 2.43-fold by the addition of miR-574-5p oe sEV (Figure 24A). Moreover, the upregulation to 2.28-fold was also triggered by the addition of R848. The induction of miR-574-5p oe sEV and R848 was inhibited by the addition of ODN 2088. The α-SMA mRNA was not affected by the addition of ScrC or miR-574-5p sEV, nor by the addition of R848 or ODN 2088 (Figure 24B).

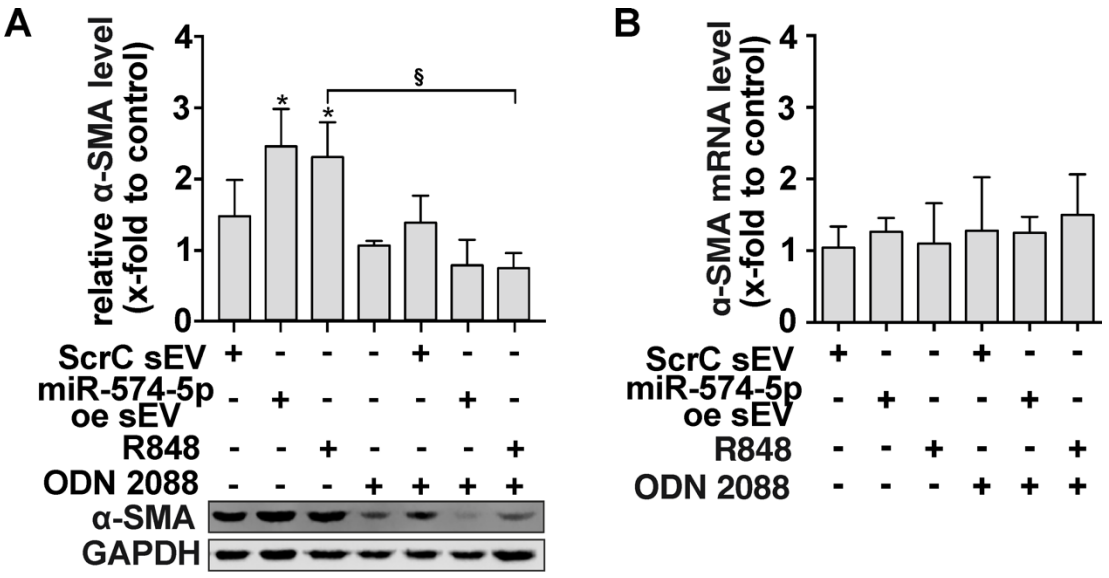

Figure 24: Effect on α-SMA-level of HFL1 by SK-N-AS-derived sEV-miR-574-5p is mediated via TLR7/8.

(A) α-SMA protein levels were detected by Western blot, and (B) RNA levels by RT-qPCR. HFL1 cells were treated with 2 µg/mL ScrC or miR-574-5p oe sEV from SK-N-AS cells, 100 ng/mL R848 (TLR7/8 ligand) or 200 mM ODN 2088 (TLR7/8 inhibitor) for 72 h. α-SMA levels were normalized to GAPDH and folded to untreated cell samples (N=4). Results are shown as mean +SEM, unpaired t-test to control without sEV, * p≤0.05. Unpaired t-test to other samples, §p≤0.05. MRNA analysis was performed together with Sheila Nevermann.

In conclusion, sEV-miR-574-5p derived from SK-N-AS have an inducing effect on α-SMA protein levels of HFL1 cells. This effect is mediated by the TLR7/8 receptor. However, this effect is not induced by sEV-derived miR-574-5p of SK-N-SH, A549, or 2106T cells. Therefore, it is likely that the sEV composition, which is individual for each sEV type and influenced by the cells of origin [8,101,216], plays a role in miR-574-5p function.

3.3. The role of tetraspanins in the physiological function of sEV-miR-574-5p

3.3.1. Analysis of sEV from neuroblastoma cell lines SK-N-AS and SK-N-SH

It is suggested that the composition of sEV plays a role in mediating the function. Since, there were visible differences in the uptake of SK-N-AS and SK-N-SH cells in the performed live cell microscopy experiments, sEV secreted by the two NB cell lines SK-N-AS and SK-N-SH, were characterized in detail. Together with M. Sc. Leon Florian Koch, TEM analyses of the purified sEV were performed. For this purpose, the sEV were fixed on a carbon grid and subsequently visualized with the electron microscope. A vesicle size of about 50-150 nm could be determined (Figure 25). Most of the sEV appear intact after the purification. Some structural differences can be observed, and the sEV of the cell line SK-N-AS seem to be larger. However, the images of the SK-N-SH sEV could be of better quality, and therefore, the TEM images were used only in addition to the analysis with the ExoView R100 platform.

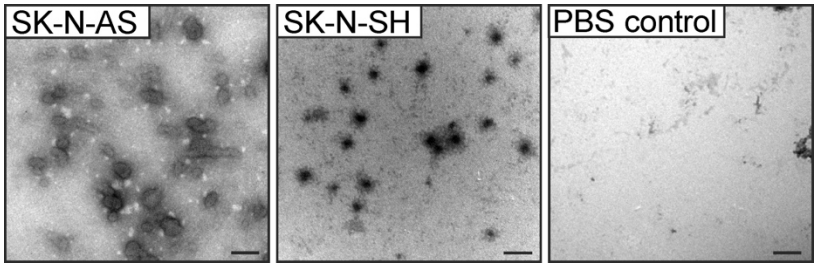

Figure 25: Transmission electron microscopy analysis of sEV secreted from NB cells.

Prove of purification of SK-N-AS and SK-N-SH sEV by TEM. SEV were isolated using differential ultracentrifugation and resuspended in 1x PBS. Scale bars: 200 nm. The experiment was performed together with Leon Florian Koch.

The unpurified sEV were analyzed using the ExoView R100 platform (Figure 26Figure 27). The cell culture supernatants are added directly to antibody-labeled chips. The sEV are immobilized with antibodies against the sEV markers CD9, CD63, and CD81, or IgG control. Subsequently, immunofluorescence staining can be performed on the surface of the fixed sEV. Again, antibodies against the surface markers CD9, CD63, and CD81 were used to analyze the colocalization profiles of the sEV populations. In addition, size determination of the immobilized sEV can be performed via light scattering. Comparing the sEV of SK-N-AS and SK-N-SH cells, similar size profiles could be determined (Figure 26). Both sEV populations had the most sEV (about 25%) of a size of 55 nm. Since smaller sEV with a size of 50 nm are also present, it is likely that even smaller particles are present, but the instrument's detection limit is 50 nm. Both sEV populations showed sEV up to a size of about 140 nm, with 0.5% SK-N-AS-derived sEV also having a size of 160 nm. NSCLC sEV from A549 and 2106T cells had similar sEV sizes of 50 nm [52].

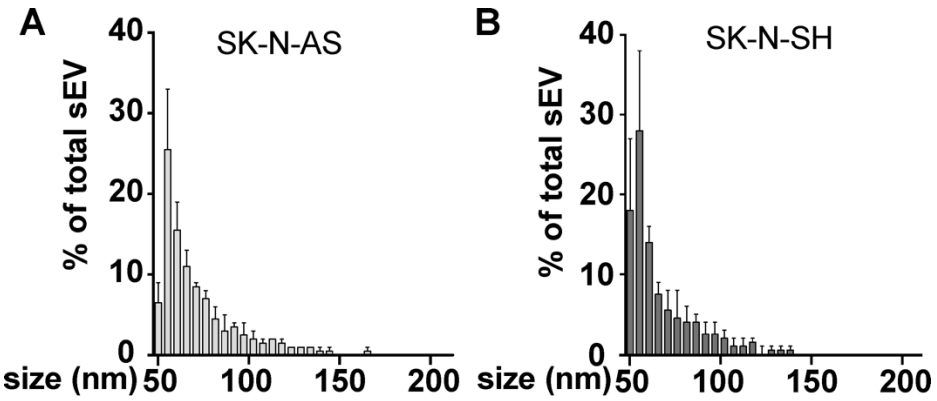

Figure 26: Size distribution of sEV derived from SK-N-AS and SK-N-SH detected with the ExoView R100.

Unpurified cell supernatants were incubated on tetraspanin CD9, CD63, and CD81 coated chips, and the size distribution of the sEV was measured by light scattering. Both sEV populations had mostly sEV with a size of 55 nm. Results are shown as mean +SEM, and experiments were performed in two biological replicates with each of 3 technical replicates.

Tetraspanin analysis of sEV strikingly showed that both sEV-populations had high levels of CD81 (Figure 27). While SK-N-AS-derived sEV were 63% bound to the CD81 spots, SK-N-SH-derived sEV were 55%. SK-N-AS-derived sEV were bound to approximately 20% at the CD9 and CD63 spots, while SK-N-SH-derived sEV had 37% bound at the CD9 spots and a smaller proportion of 8% bound at the CD63 spots. It is also striking that sEV at the CD9, and CD63 spots have similar tetraspanin colocalization patterns. In contrast, the tetraspanin colocalizations of sEV bound to CD81 differed more. While SK-N-AS-derived sEV are increasingly non-colocalizing with other tetraspanins, SK-N-SH-derived sEV have a higher proportion of triple-positive sEV. These triple-positive sEV are almost absent in SK-N-AS-derived sEV bound to CD63 or CD81. Interestingly, the tetraspanin composition is more different between the two NSCLC-derived sEV subtypes than between the two NB-derived sEV subtypes. A549-derived sEV had the most CD9, whereas 2106T-derived sEV had the most CD63 positive sEV [52].

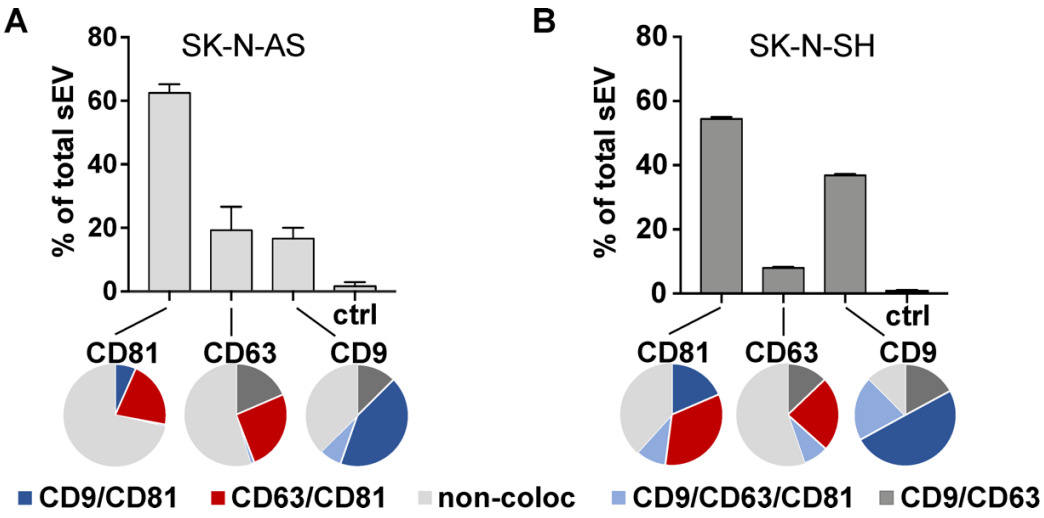

Figure 27: ExoView R100 analysis of sEV derived from SK-N-AS and SK-N-SH cells.

Unpurified sEV were captured at antibody-coated spots against the tetraspanins CD9, CD63, and CD81 (bar graphs). Further, sEV were stained with antibodies against CD9, CD63, and CD81 to analyze the tetraspanin composition on the surface (pie charts). Results are shown as mean +SEM, and experiments were performed in 2 biological replicates with each of 3 technical replicates.

In order to confirm the results of the ExoView R100 analysis, an additional Western blot analysis of the tetraspanins from sEV and the corresponding cell lysates was carried out by M. Sc. Leon Florian Koch (Figure 28). All three tetraspanins were present in sEV and cell lysates as shown by the Western blots. In addition, CD9 and CD81 appear to be present at higher levels than CD63 in both sEV subtypes. Since the same volume of supernatant was used to isolate the sEV, there appears to be less protein or less sEV in the SK-N-SH samples. To summarize, we see differences in tetraspanin composition on the envelope of different NB-derived sEV.

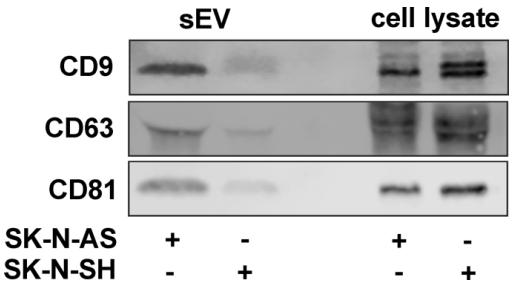

Figure 28: Western blot analysis of tetraspanins in lysates of SK-N-AS and SK-N-SH cells and corresponding sEV.

CD9, CD63, and CD81 were analyzed in protein samples of sEV and cell lysates from SK-N-AS and SK-N-SH cells. A representative Western blot of 3 independent experiments is shown. This experiment was performed by Leon Florian Koch.

3.3.2. SiRNA-mediated knockdown of tetraspanin CD81 alters sEV numbers

It is well known that tetraspanins play an essential role in sEV formation, uptake, and function [93,105,305]. To investigate the role of tetraspanin CD81 in the function of sEV-miR-574-5p, a siRNA-mediated transient knockdown of CD81 in SK-N-AS cells was established. Intracellular CD81 levels, validated by Western blot analysis, were reduced by 50% (Figure 29A).

Subsequently, the supernatants of siCD81 and siScrC transfected cells were analyzed using the ExoView R100 platform to analyze the tetraspanin composition (Figure 29B,C). However, the analysis did not confirm the hypothesis that reducing the intracellular CD81 level would decrease the CD81 level on the surface of sEV. Instead, CD81 knockdown significantly reduced the total vesicle number to about 50%. Tetraspanin composition did not change by the knockdown of CD81. Thus, this approach could not be used to investigate further the association of miR-574-5p function with the presence of tetraspanins. Therefore, a different approach was established and used.

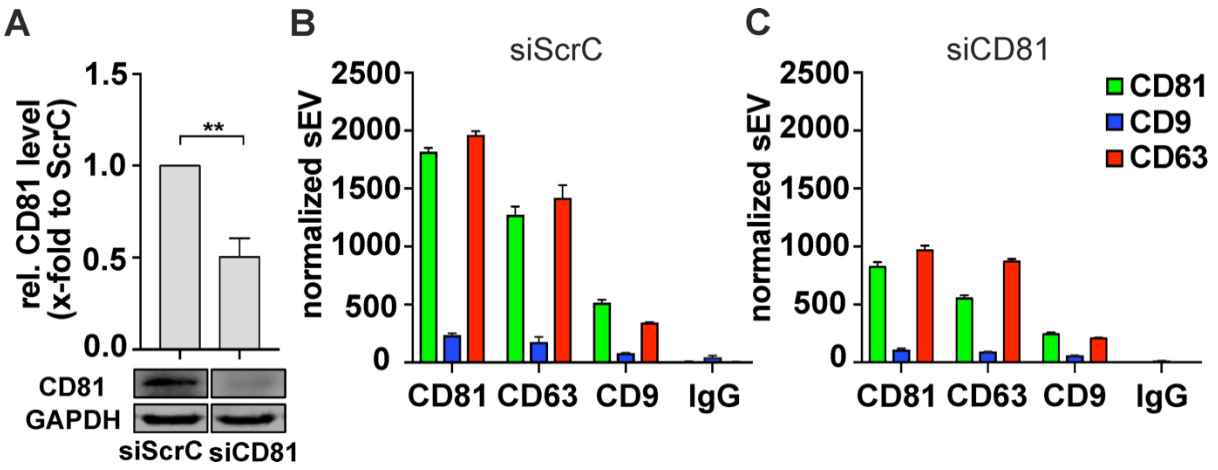

Figure 29: SiRNA mediated CD81 knockdown in SK-N-AS cells.

Cells were transfected with siCD81 or siScrC RNAs. (A) Knockdown validation of CD81 on Western blot. A representative Western blot of 4 independent experiments is shown. (B) ExoView R100 analysis of supernatants derived from siScrC transfected cells or (C) siCD81 transfected cells. Unpurified sEV were captured at antibody-coated spots against the tetraspanins CD9, CD63, and CD81, and sEV were further stained with antibodies against CD9, CD63, and CD81 to analyze the tetraspanin composition on the surface. Results are shown as mean +SEM and experiments were performed in two biological replicates with each of 3 technical replicates.

3.3.3. Antibody blocking of CD63 and CD81 alters sEV functionality

The use of neutralizing antibodies is a well-established method in the treatment of viral diseases. Treatment with neutralizing antibodies against tetraspanins on the cell surface blocks the uptake mechanisms and prevents viruses from being taken up by the cells [104,108,306]. SEV were treated with neutralizing antibodies against CD9, CD63 and CD81 or an IgG control, and the function of miR-574-5p oe sEV was analyzed (Figure 30). SK-N-AS-derived miR-574-5p oe sEV were treated with antibodies and the α-SMA level of treated HFL1 cells was analyzed on Western blot. In the previous experiments, miR-574-5p oe sEV derived from SK-N-AS cells significantly induced the α-SMA level of fibroblasts (Figure 24A). Here, treatment of the sEV with antibodies against CD63 and CD81 significantly decreased the α-SMA level (Figure 30A). To exclude an influence of the antibodies on the HFL1 cells, the cells were also treated exclusively with antibodies without miR-574-5p sEV. No effect on the α-SMA level could be observed. To apply these results to the function of sEV-miR-574-5p of

A549 cells, these experiments were also performed with miR-574-5p oe sEV of A549 cells. For this purpose, miR-574-5p oe sEV from A549 cells were treated with the same amounts of antibodies against CD9, CD63, or CD81, and the mPGES-1 level of treated cells was detected by Western blot analysis. In previous experiments, the mPGES-1 level was decreased by adding sEV-miR-574-5p [52]. Treatment of sEV with CD63 antibody lowered the mPGES-1 level even more to 0.7-fold (Figure 30B). Addition of antibodies without sEV did not significantly affect the mPGES-1 level.

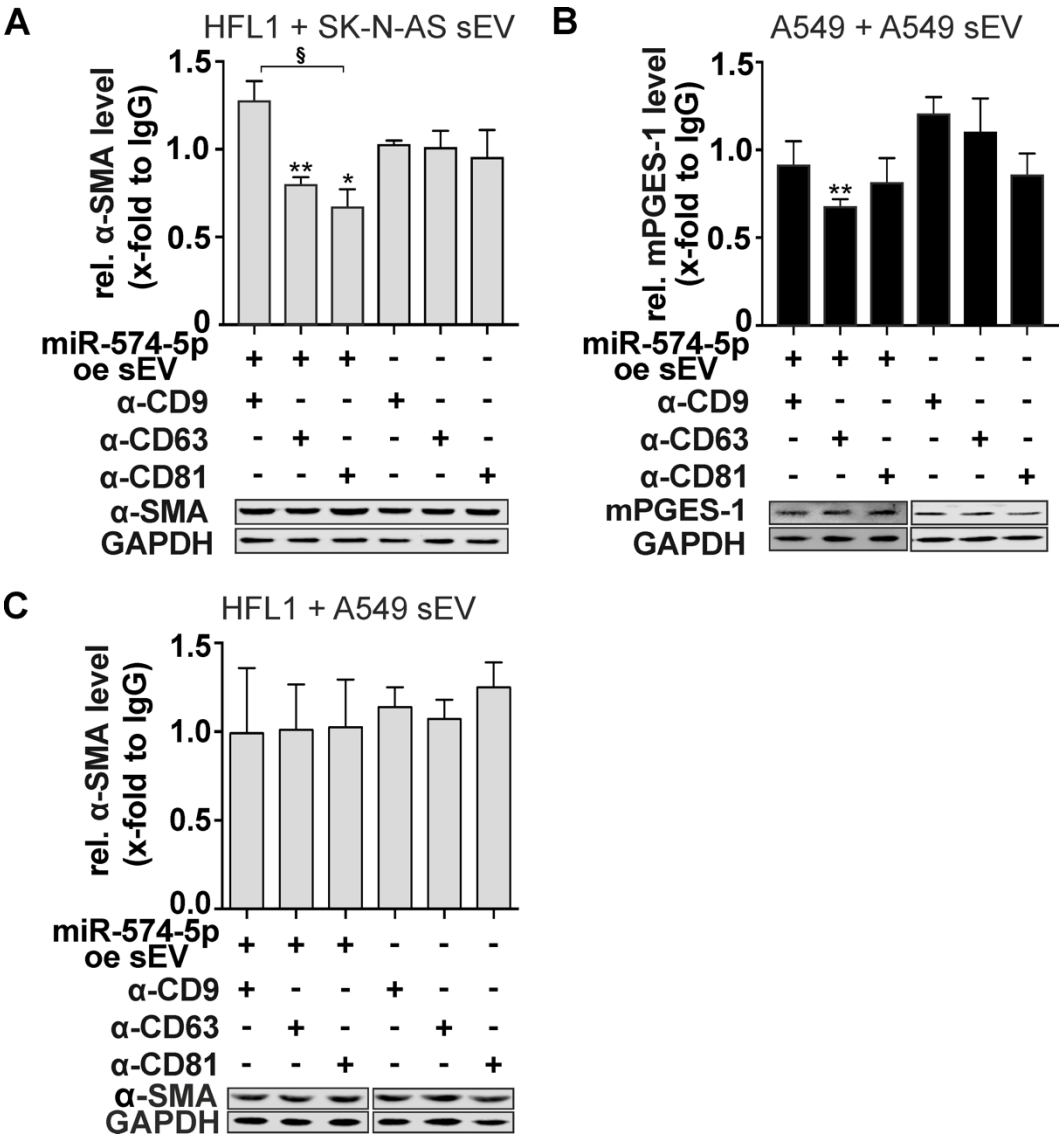

Figure 30: Treatment of sEV with antibodies against tetraspanins alters the function of sEV-miR-574-5p.

A) Western blot analysis of α-SMA levels of HFL1 cells treated with SK-N-AS-derived miR-574-5p oe sEV blocked with α-CD9, α-CD63, α-CD81 or mouse IgG antibodies or antibodies without sEV for 21 h (N=4). (B) Western blot analysis of mPGES-1 levels of A549 cells treated with antibody-treated A549-derived miR-574-5p oe sEV (N=3). (C) Western blot analysis of α-SMA levels of HFL1 cells treated with antibody-treated A549-derived miR-574-5p oe sEV (N=3). α-SMA and mPGES-1-levels were normalized to GAPDH and folded to IgG control samples. Results are shown as mean +SEM, unpaired t-test to untreated control or IgG control, * $p \leq 0.05$, ** $p \leq 0.01$. Unpaired t-test to other samples, §$p \leq 0.05$.

To verify whether the effect was specific to the sEV-miR-574-5p and their elicited function, HFL1 cells were also stimulated with the antibody-treated A549-derived miR-574-5p oe sEV (Figure 30C). Here, however, we did not detect a significant effect. Therefore, the effect seems specific for sEV-miR-574-5p with a physiological function on their target cells.

In addition, experiments were performed using a combination of antibodies to block SK-N-AS-derived sEV. It was expected that the addition of CD63 and CD81 would enhance the effect on HFL1 cells. This expectation was not confirmed (Figure 31). The addition of the combination of CD63 and CD81 antibodies triggered no effect on the α-SMA level. After the addition of the combination of CD9 and CD81 antibodies, a slight but significant decrease in α-SMA level was observed. The combination of CD9 and CD63 antibodies also showed no effect. Strikingly, the controls of cells treated without sEV and only with antibodies showed strongly fluctuating α-SMA levels.

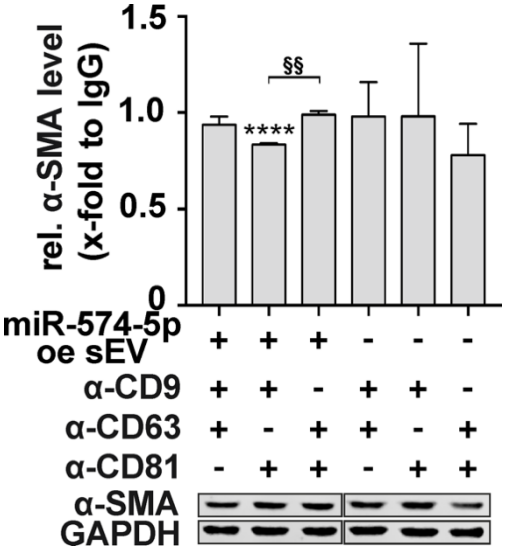

Figure 31: A combination of antibodies does not enhance the effect of tetraspanin antibody treatment of miR-574-5p oe sEV.

Western blot analysis of α-SMA levels of HFL1 cells treated with SK-N-AS-derived miR-574-5p oe sEV blocked with combinations of α-CD9, α-CD63, α-CD81 or mouse IgG antibodies or antibodies without sEV for 21 h. α-SMA-levels were normalized to GAPDH and folded to IgG control samples. Results are shown as mean +SEM (N=3). Unpaired t-test to IgG control, **** p≤0.001. Unpaired t-test to other samples, §§p≤0.01.

Overall, in the context of both NB and NSCLC, an effect of blocking tetraspanins on the physiological function of sEV-miR-574-5p was observed. Whereas SK-N-AS-derived sEV significantly lowered α-SMA levels in HFL1 cells by treatment with CD63 or CD81 antibodies, thereby inhibiting miR-574-5p function, treatment with CD63 antibodies enhanced the lowering effect on mPGES-1 that A549-derived sEV-miR-574-5p has. The combination of antibodies used to treat sEV showed no enhancing effect. Since protein levels were lowered in both models, it is reasonable to assume that the uptake of sEV plays a role in this effect. This hypothesis is proved in the following chapters.

3.4. The role of tetraspanins in sEV uptake

3.4.1. Qualitative observations of sEV internalization

To determine whether the effects of antibody treatment against tetraspanins were due to a change in sEV uptake, live cell imaging experiments were first performed. For this purpose, cells were seeded in microscopy-suitable chambers and stained with an endocytosis-labeling dye pHrodo™ shortly before the addition of sEV treated with antibodies and stained with DiO. The pHrodo™ dye allowed us to observe the sEV that were actually internalized by the cells by colocalizing pHrodo with DiO. The experiment was first performed with SK-N-AS-derived sEV and HFL1 cells (Figure 32).

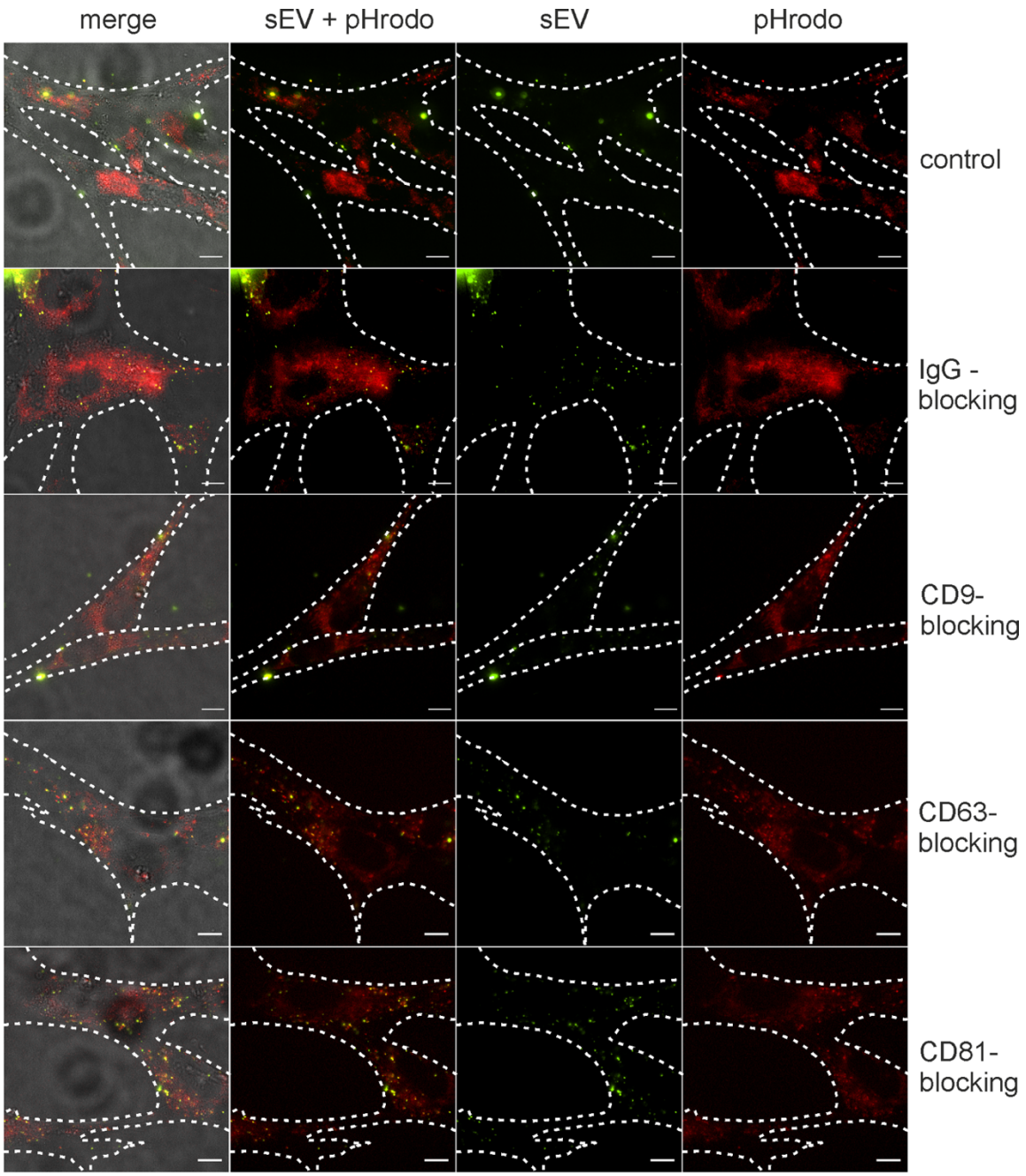

Figure 32: Live cell microscopy of HFL1 cells and SK-N-AS-derived sEV treated with tetraspanin antibodies.

SEV from SK-N-AS were treated with α-CD9, α-CD63, α-CD81, or mouse IgG antibodies for 21 h. Then, sEV were stained with DiO for 15 min. HFL1 cells were incubated with 20 µg/mL pHrodoTM Red Dextran and DiO-labeled sEV. After 30 min - 1 h, cells were washed briefly and were imaged within 15 min. The experiment was performed using protocol B described in 2.2.7. Representative images of 3 independent biological replicates with at least 5 technical replicates are shown. Scale bars = 10 µm.

The size of the HFL1 cells varied greatly, making it difficult to compare the uptake of sEV. In addition, the cells could not be separated very well. However, it can be speculated that the sEV treated with IgG, CD63, and CD81 are more internalized by the cells. The control sEV and the CD9-treated sEV are less present in the cells. These experiments were also performed for A549 cells and their sEV (Figure 33). Overall, the cells were more comparable and the sEV appeared more uniform in size. There were no visible differences observed. Therefore, it can

be assumed that there are no quantitative differences in the internalization rate of sEV as a result of antibody treatment.

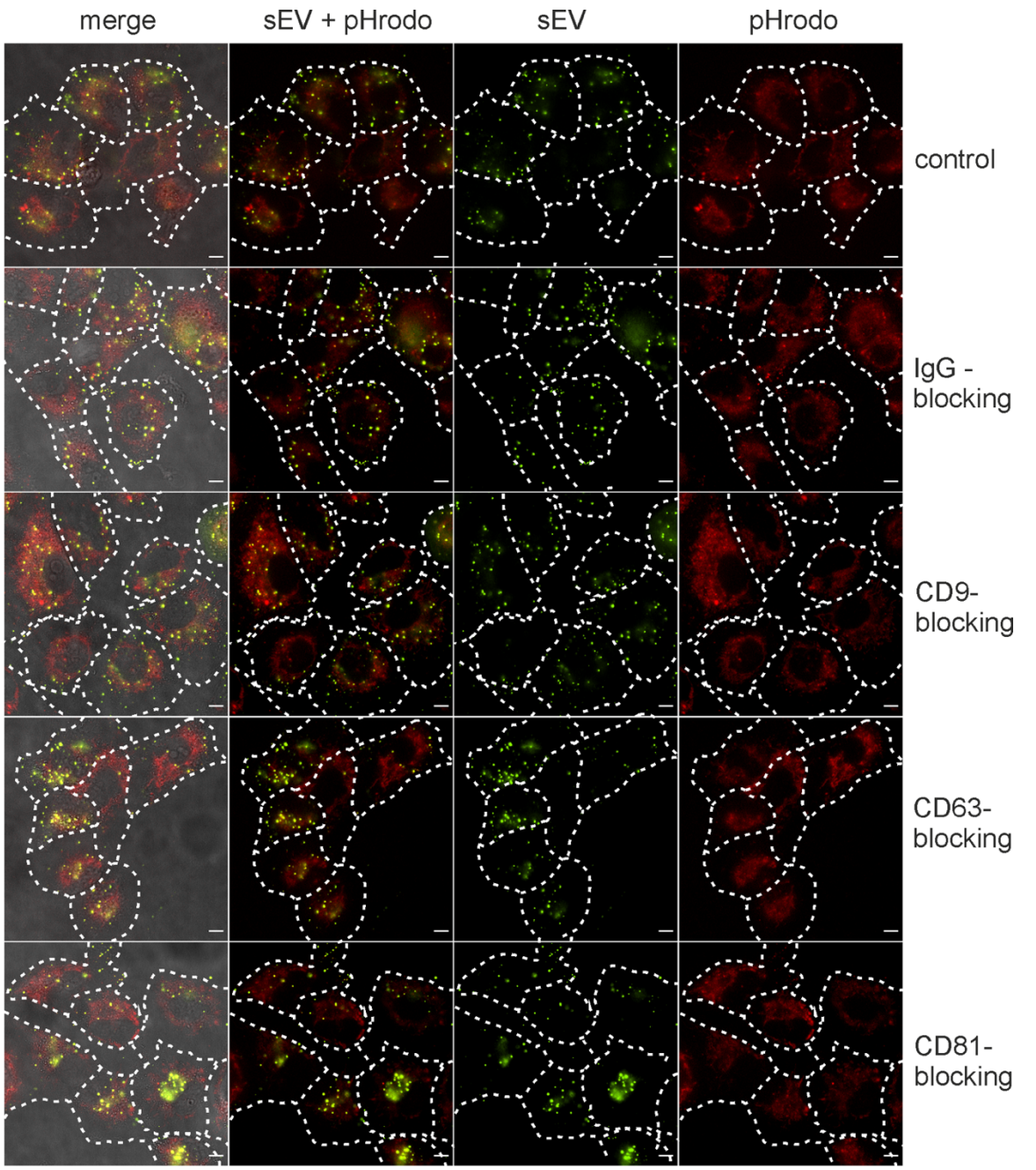

Figure 33: Live cell microscopy of A549 cells and A549-derived sEV treated with tetraspanin antibodies.

SEV were treated with α-CD9, α-CD63, α-CD81, or mouse IgG antibodies for 21 h. Then, sEV were stained with DiO for 15 min. Cells were incubated with 20 µg/mL pHrodoTM Red Dextran together with DiO-labeled sEV. After 30 min - 1 h, cells were washed briefly and were imaged within 15 min. The experiment was performed using protocol B, described in 2.2.7. Representative images of 3 independent biological replicates with at least 5 technical replicates are shown. Scale bars = 10 µm.

3.4.2. Microscopy-based uptake quantification

Further imaging experiments with antibody-treated sEV were performed because these initial live cell microscopy experiments showed promising results but were not well quantifiable. In this case, the sEV were also treated with DiO and stained. The cells were fixed and stained after 4 h of sEV uptake. The cytoskeleton was visualized with phalloidin. The nuclei were stained with DAPI. This allowed the determination of the total cell area and quantitative assessment of sEV uptake. The number of sEV was normalized to cell area and untreated control. Three experiments were performed for HFL1 and A549 cells, and at least 30 cells were analyzed per condition. Microscopy and evaluation were performed by Kai Breitwieser.

In general, antibody-treated SK-N-AS-derived sEV were less internalized by HFL1 cells compared to untreated sEV (Figure 34). The sEV were taken up at least 40% less than the control sEV. There were no significant differences in relative uptake between antibody-treated sEV.

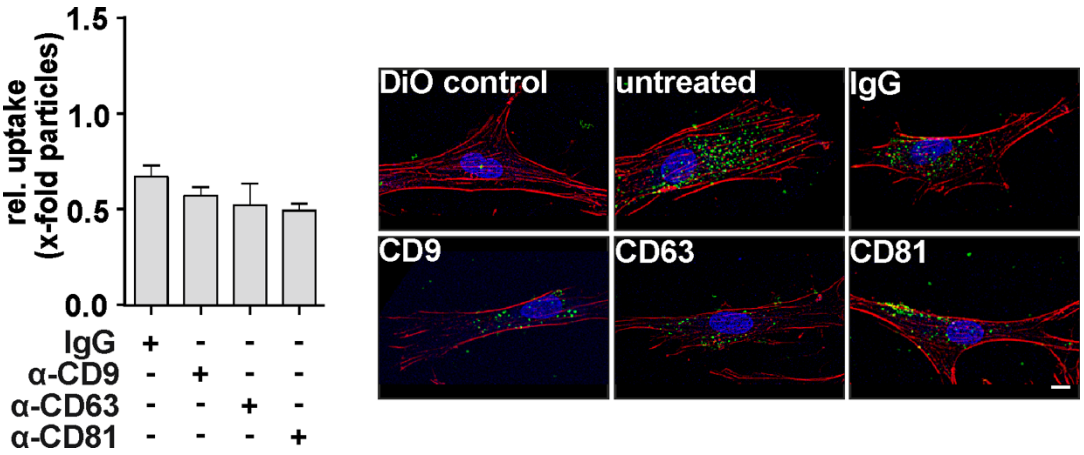

Figure 34: Microscopy-based uptake quantification of HFL1 cells taking up SK-N-AS-derived sEV.

1 µg sEV were treated with 100 ng α-CD9, α-CD63, α-CD81, or mouse IgG antibodies for 21 h. SEV were labeled with DiO and incubated with the cells for 4 h. Then, cells were fixed and stained with phalloidin and DAPI. Taken-up sEV were counted, and relative uptake is shown as x-fold to untreated sEV. Relative changes are shown as mean +SEM (N=3). Representative HFL1 micrographs were shown after 4 h of SK-N-AS sEV uptake. Scale bars = 10 µm. Kai Breitwieser performed microscopy and evaluation.

The uptake of A549-derived sEV was not reduced by antibody treatment (Figure 35). Neither the IgG control nor antibodies against CD9, CD63, or CD81 resulted in significant changes in the relative uptake rate. Thus, this experiment does not confirm the assumption from the previous live cell microscopy experiments that the overall uptake rate of sEV is specifically altered by antibody treatment of the tetraspanins. To confirm this, further non microscopy-based experiments were performed.

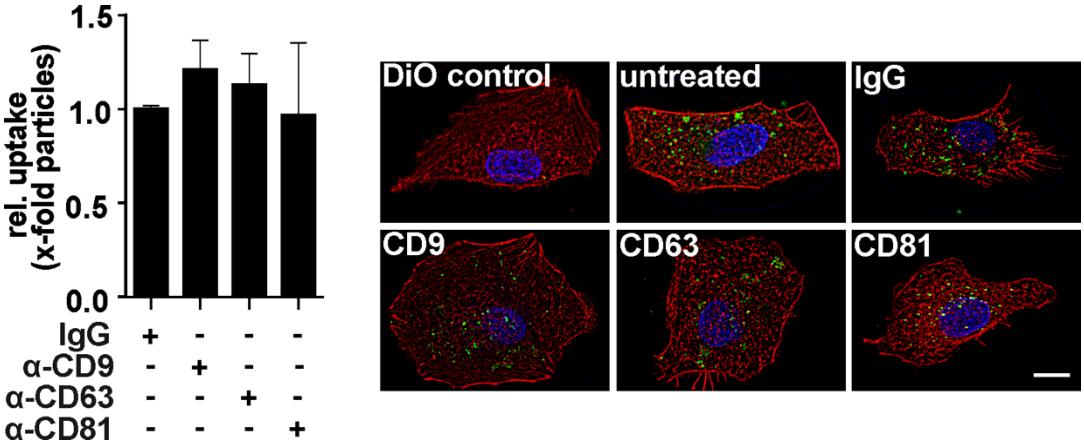

Figure 35: Microscopy-based uptake quantification of A549 cells taking up A549-derived sEV.

1 µg sEV were incubated with 100 ng α-CD9, α-CD63, α-CD81, or mouse IgG antibodies for 21 h. SEV were labeled with DiO and incubated with the cells for 4 h. Then, cells were fixed and stained with phalloidin and DAPI. Taken-up sEV were counted, and relative uptake is shown as x-fold to untreated sEV. Relative changes are shown as mean +SEM (N=3). Representative A549 micrographs were shown after 4 h of sEV uptake. Scale bars = 10 µm. Kai Breitwieser performed microscopy and evaluation.

3.4.3. Uptake quantification by luciferase-assay

Microscopy-based uptake quantification showed no significant effects on the relative uptake rate between sEV treated with different antibodies. Therefore, another luciferase assay-based approach was used. For this, an NLuc-Hsp70 plasmid and the protocol for the luciferase-based uptake assay were kindly provided by Dr. Gregory Lavieu [298]. The donor sEV cells are transfected with the NLuc-Hsp70 plasmid to produce sEV containing NLuc. These sEV can be used to treat the sEV recipient cells with the NLuc-containing sEV. When the sEV are taken up, the NLuc is taken up as well, and a luciferase assay can be performed with the recipient cells. Luciferase activity can be measured and normalized to the untreated control. This allows the relative uptake of sEV to be indicated. Here, the sEV were again additionally treated with antibodies against the tetraspanins CD9, CD63, and CD81 or an IgG control antibody. The cells were incubated with the sEV for 4 h to observe the uptake.

No significant differences occurred in the luciferase assay of HFL1 cells treated with SK-N-AS-derived sEV (Figure 36A). There were also no significant differences in the luciferase assay of A549 cells treated with A549-derived sEV (Figure 36B). However, it can be suggested here that there are slight differences between the individual antibody-treated sEV. The uptake rate looks slightly increased with CD63 and CD81 treatment compared with CD9-treated sEV. However, since no significant effects are seen, it can be assumed that tetraspanin treatment does not affect the uptake rate of sEV.

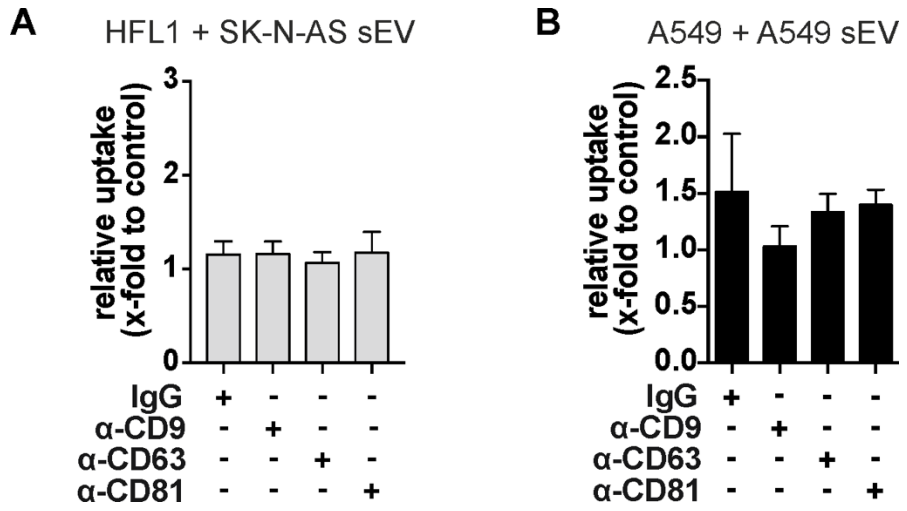

Figure 36: Luciferase-based uptake quantification of antibody-treated sEV.

SEV-donor cells were transfected with NLuc-Hsp70 plasmid 21 h before sEV-harvesting. Isolated sEV were blocked with 50 ng α-CD9, α-CD63, α-CD81, or mouse IgG antibodies for 21 h. (A) HFL1-cells were treated with sEV from SK-N-AS cells, and (B) A549-cells were treated with sEV from A549-cells for 4 h. Afterward, a luciferase assay was performed. Results are shown as mean +SEM (HFL1: N=4; A549: N=5).

4. Discussion

4.1. The function of miR-574-5p in the PGE_2 biosynthesis of neuroblastoma

Dysregulation of the PGE_2 biosynthesis promotes tumor progression by increasing cell proliferation, angiogenesis, and metastasis, as well as by suppressing the immune response [185,191]. In 2019, Saul et al. revealed the regulation of PGE_2 by the interaction of miR-574-5p and CUGBP1 in A549 cells [264]. In an inflammatory environment, increased miR-574-5p leads to the binding of miR-574-5p to CUGBP1 as a decoy, preventing the binding of CUGBP1 and mPGES-1 RNA. This allows the mPGES-1 mRNA to be alternatively spliced, resulting in a shorter 3'UTR isoform that has a higher translation rate than the mPGES-1 WT form. This results in increased mPGES-1 and PGE_2 levels. The decoy function of miR-574-5p appears to be specific for CUGBP1 and unique in A549 cells, whereas it is unlikely to be present in the SCC cell line 2106T [52,264,265].

To address the transferability of the miR functions to other tumor models, NB was chosen as a physiological contrasting model to NSCLC. Both tumor types are PGE_2-dependent, but unlike in NSCLC, mPGES-1 is usually not present in the cancer cells of NB [52,264,295,296]. However, CAFs appear to be the major producers of mPGES-1-dependent PGE_2 in the tumor microenvironment [295,296]. It is known that CAFs can promote tumor progression via different pathways [231,241]. Proliferation and metastasis can be increased via the secretion of growth factors [228]. Likewise, favored angiogenesis may provide nutrients to tumor cells, and CAFs may promote chemoresistance [241]. Therefore, a better understanding of the communication between tumor cells and CAFs is a step toward new therapeutic options in the treatment of cancers.

In this work, tissue staining confirmed that in tumors with 11q deletion, the surrounding fibroblasts have high levels of mPGES-1. This is in line with the findings of Larsson et al., published in 2015, that CAFs in the NB have a crucial influence on PGE_2 synthesis and are the primary source of mPGES-1 [295]. They showed that in 11q deleted NBs, the mPGES-1 level is significantly higher than in low-risk or *MYCN*-amplified tumors, which correlates with the PGE_2 levels and survival rate. Furthermore, Kock et al. showed that inhibition of mPGES-1 in CAFs leads to the suppression of tumor growth, further highlighting the unique role of CAFs in NB [296]. In line with these observations, Elwakeel et al. showed that the disruption of PGE_2 signaling in CAFs leads to the inhibition of tumor growth, while metastasis is increased in breast cancer [193]. However, up to now, the role of PGE_2 in CAFs is not well understood because, although PGE_2 contributes to CAF formation, it has been shown to be a negative regulator of fibrosis-promoting fibroblasts [193]. The diverse effects of PGE_2 inhibition on CAFs

are also reflected in the literature, possibly due to the fact that fibroblasts are generally highly heterogeneous in the tumor environment [307,308].

Unexpectedly, we found that the expression of mPGES-1 in differentiated NB cells, presumably ganglion cells, correlated with the expression of miR-574-5p and CUGBP1 [273,274]. This suggests that the miR-574-5p-CUGBP1 decoy may occur in cancer cells in both tumor entities. NB is the least differentiated and most malignant neuroblastic tumor, but can spontaneously differentiate into ganglioneuroblastoma or ganglioneuroma [269]. This observation is therefore of great interest and raises the question of whether this differentiation process is influenced by miR-574-5p-regulated PGE_2 biosynthesis. In order to establish a link between differentiation and intercellular communication via PGE_2, this question should be further addressed.

The findings obtained by the tissue stainings are supported by the performed spheroid experiments with the NB cell line SK-N-AS and the NSCLC cell line A549 [304]. Consistent with tissue staining, SK-N-AS cells expressed significantly lower basal levels of the key enzymes in the PGE_2 biosynthesis mPGES-1 and COX-2 compared to A549 cells. SK-N-AS spheroids also showed lower levels of miR-574-5p and NOXP20, but higher levels of CUGBP1. Together with the upregulation of all mPGES-1 isoforms after IL-1β treatment, this supports the hypothesis of the presence of the miR-574-5p-CUGBP1 decoy, but to a lesser extent compared to A549 [304]. It is plausible that SK-N-AS cells generally produce less PGE_2 than A549 cells. To prove this PGE_2 could be measured in supernatants of the cells by ELISA or mass spectrometry. RIPs of SK-N-AS cells confirmed that miR-574-5p and mPGES-1 bind to CUGBP1. All experiments supported the hypothesis that the interaction between miR-574-5p and CUGBP1 regulates mPGES-1-dependent PGE_2 biosynthesis in NB cancer cells and that the intracellular function of miR-574-5p can thus be transferred from NSCLC to NB.

4.2. The role of sEV-miR-574-5p in neuroblastoma

MiRs are key players in intracellular communication in the tumor environment [109,309]. They can be exchanged between cells via sEV and thus be transferred from the donor cell to the recipient cell, triggering physiological functions in the recipient cells [58,91,140].

There has been increasing interest in sEV and the identification of their functions in recent years [13]. Initially, these were mistakenly seen as waste disposal [53,54]. However, it is now known that sEV can perform physiological functions, mediated by their contents, as miRs [27,232,310]. At the same time, the physiological processes of miRs are discussed controversially because the calculated miR content with about 0.00825 +- 0.02 miR molecules per exosome is very low [311,312]. Other publications confirm that sEV are poorly internalized by target cells, with about 1% of the total sEV amount [91]. Nevertheless, physiological

functions of sEV have been observed in various studies [27,310,313]. This suggests very specific effects triggered even by small amounts of sEV and their transported miRs resulting in amplifying signal cascades. It has been previously shown that by the trigger PGE_2, NSCLC cells secrete miR-574-5p specifically into their sEV, even compared to other miRs [52].

In this work, it was shown that NB cells also secrete miR-574-5p into the sEV upon PGE_2 stimulation. By measuring the particles after PGE_2 stimulation, it was confirmed that more miRs are packed into the sEV, and not just the sEV number was increased by the stimulus. No significant effect was observed on the total particle number. Since the intracellular level of miR-574-5p was also not significantly affected, this supports a targeted secretion of miR-574-5p into the sEV. Levels of other miRs commonly found in NSCLC were also determined in A549 cells and were not increased after PGE_2 stimulation, further supporting the hypothesis of a specific secretion and increasing the attractiveness of miR-574-5p as a potential biomarker [52,314–316]. To determine the specificity of the secretion of miR-574-5p in NB, other miRs frequently found and discussed as biomarkers, such as miR-375, miR-21-5p, or miR-199a-3p, could be measured [27,310,317]. The very fast secretion process occurs only after 30 min in SK-N-AS cells. In general, sEV seem to be involved in very fast processes. It is also described that both secretion and uptake are rapid, energy-dependent processes [65–67]. In 2020, Matsumoto et al. described that sEV, when injected into mice, have a half-life of only 7 min and that one cell secretes an average of 100 sEV per hour [318]. Internalization of sEV was also observed after 20 min in the live cell experiments of SK-N-AS and SK-N-SH cells and their sEV. Thus, it is plausible that the secretion of miR-574-5p is significantly higher after 30 min than after 60 min because the cells internalize sEV rapidly after the secretion. In the NB cell line SK-N-SH, the secretion of miR-574-5p was triggered after 2 h. These cell-dependent differences could arise either within the signaling cascade involving PGE_2 receptors and translation to the cell or within the executing pathway that mediates the packaging and secretion of sEV. Another explanation for the cell-dependent differences would be differences in the abundance of the EP receptors. Rasmuson et al. showed that both NB cell lines, SK-N-AS and SK-N-SH, express all EP receptors and that the levels of the receptors differ between 7 different analyzed NB cell lines [294]. By treatment with the EP1/3 agonist sulprostone, it was shown that in the cell types SK-N-AS and A549, the secretion of miR-574-5p is mediated via EP1/3 [52]. Sulprostone triggered the same secretory effects as PGE_2, whereas the EP2 agonist butaprost and EP4 agonist L-902,688 did not. EP1 increases PLC and the cytosolic Ca^{2+} level, which triggers PKC activation [193]. This can lead to downstream processes and induce various gene expressions. These include the activation of NFκB and the MAPK pathway, which can lead to further downstream processes [186]. EP3 has no apparent function but may also trigger Ca^{2+} levels by coupling to different G proteins [198].

These downstream processes could activate different miR sorting pathways. First, post-translational modifications of hnRNPs such as SUMOylation have been shown to control miR sorting into sEV [149]. These post-translational modifications could be affected by PGE_2 stimulation, allowing hnRNPs to bind to miR-574-5p and subsequently sort into sEV. Other miR sorting mechanisms may also be affected by downstream processes. In 2022, Garcia-Martin et al. showed that specific motifs in the sequence of miRs encode the sorting of miRs into sEV [319]. These EXO-motifs are cell type specific and distinct from the sEV populations present in the cell of origin. Several RBPs can bind these specific EXO-motifs and are involved in the sorting of miRs into sEV. Alyref and Fus are two RBPs that can bind the EXO-motif CGGGAG and are involved in the sorting process [319]. Targeted secretion of miR-574-5p into sEV appears to be present in all NSCLC and NB cell lines tested, suggesting one EXO-motif occurring in all these cell lines and being present in miR-574-5p. A possible EXO-motif in miR-574-5p would be UGUGUG, which was first identified in the mouse myoblast cell line C2C12, but is also present in the sEV of a number of other cell lines, such as primary hepatocytes [319]. It is possible that PGE_2 triggers the transport of miRs into sEV by affecting the specific binding of RBPs to this EXO-motif. Another sorting mechanism that may be affected is that components of the RISC complex, as AGO2 may be upregulated, leading to increased binding of miRs and sorting in sEV [151,152]. Another possibility would be the translocation of nSMase2 to the site of sEV biogenesis, where increased production of ceramides could enhance sEV formation and secretion [29]. It would be interesting to further investigate the sorting processes of miR-574-5p. For this purpose, for example, after PGE_2 stimulation, RIPs of the different proteins involved in the miR sorting process could be performed, followed by analysis of miR-574-5p bound to the proteins. Another possibility would be to perform a cell-free *in vitro* sorting assay as described by Shurtleff et al. in 2016 [153]. Here, the influence of a specific protein on the sorting of miR-574-5p could be shown.

It was hypothesized that sEV-derived miR-574-5p would have the same function as in A549 cells, since the intracellular function of miR-574-5p remains the same in SK-N-AS cells and PGE_2 also induces miR-574-5p secretion. In order to investigate the autocrine function of sEV-miR-574-5p in NB cells, miR-574-5p oe sEV of SK-N-AS and SK-N-SH cells were established. This is physiologically plausible because the subtype-specific composition of the sEV envelope and content may have an impact on the internalization and physiological function of miR-574-5p [18]. For example, the donor cell-specific proteins in the sEV membrane may interact with receptors on target cells and thereby influence the functional mediation of miR-574-5p [320].

Contrary to expectations, no autocrine effect of sEV-miR-574-5p on mPGES-1 levels of SK-N-AS cells was observed. The TLR7/8 ligand showed a slight downregulating effect on the

mPGES-1 mRNA level of SK-N-AS cells. Although the literature shows that SK-N-AS cells do not respond significantly to the TLR7/8 agonists Imiquimod and SSRNA40 compared to other agonists as for TLR1/2 or TLR 3, the slight downregulating effect suggests that the cells do not lack TLR7/8 receptors [321]. Therefore, SK-N-AS cells would be able to respond to sEV-derived miRs as ligands. Immunostaining or Western blot analyses could be performed to determine whether SK-N-AS cells express TLR7/8 receptors, The TLR1/2, -3, -4 and -6-dependent immune response is cell line-dependent and correlates with the differentiation status of NB cells [321,322]. To the adrenergic state differentiated NB cell lines, such as SK-N-SH, lack TLR-mediated responses [323]. Undifferentiated NB cells in the mesenchymal state, such as SK-N-AS have higher basal levels of inflammation [321]. However, as this correlation with differentiation status does not hold for TLR7/8, it is likely that these receptors have other regulatory roles, such as PGE_2 regulation [131]. In conclusion, miR-574-5p regulates PGE_2 synthesis intracellularly, but sEV-miR-574-5p has no significant autocrine effect on PGE_2 synthesis in NB.

To further investigate the function of sEV-miR-574-5p in NB, CAFs were included in the experiments. Tumor cells can induce a CAF phenotype of fibroblasts in the TME [231]. Identifying suitable markers for CAFs is challenging due to their heterogeneity [236]. The best known markers are α-SMA and other cytoskeletal markers such as vimentin, desmin, or smooth muscle myosin, which are increased during fibroblast activation [234–236]. In the experiments, α-SMA was used as a commonly-used and representative marker for fibroblast differentiation [324]. TGFβ was added to mimic an inflammatory tumor environment and to further induce the fibroblast activation of CAFs [222]. SEV-derived miR-574-5p from SK-N-AS cells showed a specific induction of α-SMA levels of the fibroblasts, which was not induced by sEV-miR-574-5p derived from A549, 2106T, or SK-N-SH cells. A toxic or anti-proliferative effect on cell viability with or without TGFβ was excluded.

Further characterization showed that the effect was not mediated by the miR-574-5p-CUGBP1 decoy in HFL1. We hypothesized that the binding of miR-574-5p and CUGBP1 would be could displace CUGBP1 binding to α-SMA and thus increase α-SMA levels. A connection between α-SMA and CUGBP1 has already been established, as CUGBP1 can bind to α-SMA, and in mouse stem cells and liver fibrosis models, the knockdown of CUGBP1 leads to altered α-SMA levels [325,326]. In general, the miR-574-5p-CUGBP1 decoy is not present in HFL1 cells because neither mPGES-1 nor miR-574-5p binds to CUGBP1. In addition, no staining for miR-574-5p or CUGBP1 was detected in fibroblasts in the TME, which would be a criterion for the presence of the miR-574-5p-CUGBP1 decoy.

Since it is already known that miR-574-5p can bind to TLR7/8 as a ligand and thereby trigger downstream signaling [52,144,268], it was likely that the effect on α-SMA was also mediated

via TLR7/8. Stimulation of the cells with the TLR7/8 ligand R848 elicited the effect on α-SMA levels, which was inhibited by the TLR7/8 inhibitor ODN 2088. To bind TLR7/8, miR-574-5p has to reach the endosomal compartment where TLR7/8 is located [144]. Therefore, the sEV would have to be taken up by endocytosis, as fusion with the plasma membrane would release the sEV content directly into the cytoplasm of the cell, where it would be loaded into RISC [80].

Based on live cell experiments showing that sEV are taken up by HFL1 cells via long membrane protrusions, endocytotic internalization via filopodia would be plausible [327,328]. Filopodia are structural elements of the cell membrane that protrude from the lamellipodial actin network and consist of tightly packed actin filaments [329]. They are involved in cell motility, which contributes to wound healing, adhesion to the ECM, embryonic development, and guidance to chemoattractants [327]. They were first identified in the context of virus uptake, but it has already been shown that filopodia also contribute to sEV uptake [2,328]. As observed in the live cell experiments, the filopodia “grab the sEV and pull them into the cells” as described by Heusermann et al. in 2016, where they are presumably sorted to the endosome or lysosome [328]. When miR-574-5p interacts with TLR7/8, it can trigger downstream signaling via the NFκB pathway, which might lead to transcriptional activation of target genes like α-SMA [144,330]. The α-SMA mRNA levels of the fibroblasts are not affected by sEV-miR-574-5p, but there are several ways in which α-SMA could be regulated post-transcriptionally. For example, α-SMA might be activated by extracellular signal-regulated kinases 1/2 (ERK1/2, also known as MAPK1), activated via the NFκB regulatory pathway [331]. ERK1/2 is also known to regulate α-SMA [332]. This hypothesis could be tested using an ERK1/2 inhibitor for example Ulixertinib [333]. In 2020, Cui et al. showed that miR-574-5p plays a role in CAF activation of cardiac fibroblasts, which is mediated by AT-rich interaction domain 3A (ARID3A) [334]. They also showed that miR-574-5p is upregulated after TGFβ stimulation, which may explain the enhanced effect of sEV-miR-574-5p on α-SMA. As TLR ligands have been shown to induce ARID3A, this provides a possible link between miR-574-5p as a TLR7/8 ligand and α-SMA upregulation [335].

SEV-miR-574-5p derived from NSCLC cell lines did not show an up-regulating effect on α-SMA levels in fibroblasts. This supports the hypothesis that fibroblasts play a special role in NB. Larsson et al. and Kock et al. showed that CAFs are the primary source of PGE_2 in the TME and that the inhibition of mPGES-1 in the fibroblasts resulted in the suppression of PGE_2 levels and tumor growth [295,296]. In NSCLC, however, tumor cells are the primary source of mPGES-1, while surrounding fibroblasts play a minor role [262]. In addition, sEV-miR-574-5p from the NB cell line SK-N-SH showed a significant upregulating effect, but not with additional stimulation with TGFβ. As live cell imaging of NB cells indicated some differences in the uptake pattern, the sEV-derived from SK-N-SH might be taken up via other internalization

mechanisms than SK-N-AS-derived sEV. Proposed mechanisms for sEV internalization include fusion with the plasma membrane, receptor-mediated endocytosis, phagocytosis, and macropinocytosis [336]. The accumulation of sEV at the cell membrane after 20 min suggests a receptor-mediated function of sEV [91]. The function of sEV-derived miRs is likely to depend on the mode of internalization into the target cell, and this mode of internalization is cell-dependent [52]. SEV-miR-574-5p derived from 2106T squamous cell carcinoma cells had an opposite effect on the α-SMA level of HFL1 cells additionally stimulated with TGFβ. A possible explanation here is also that the 2106T-derived-sEV-miR-574-5p is internalized by fibroblasts via a different pathway. Further, ScrC sEV of 2106T cells have a slight inhibitory effect on the α-SMA level. This is probably due to the fact that the ScrC sEV of the 2106T sEV also contain miR-574-5p, although to a lesser extent than the miR-574-5p oe sEV. However, it is noteworthy that the additional stimulation with TGFβ is crucial for this, which may amplify the stimulatory effects of sEV-miR-574-5p by additionally promoting fibroblast differentiation [334,337,338].

In conclusion, the intracellular function of miR-574-5p in NSCLC was shown to be transferable to NB, whereas the function mediated by sEV-derived miR-574-5p was not. In NB, sEV-miR-574-5p exerts a newly discovered paracrine function by specifically inducing the α-SMA level of fibroblasts via TLR7/8. Also in NSCLC, the function of sEV-miR-574-5p has previously been shown to be specific for AC cells, whereas SCC-derived sEV-miR-574-5p has no effect [52]. One possible explanation is that specific sEV are more likely to be taken up by specific target cells, as has been shown for other cell types [32,339]. Another possible explanation is that in the absence of miR-574-5p function, sEV are not endosomally internalized and thus sEV-miR-574-5p is unable to function as a ligand for TLR7/8 [140,144]. Overall, it is likely that the cell-specific composition of sEV is critical for mediating sEV-miR-574-5p function. Furthermore, the results suggest that miR-574-5p may be a suitable therapeutic gene for to regulate PGE_2 biosynthesis in NSCLC and NB. Inhibition of miR-574-5p has a distinct advantage over conventional PGE_2 inhibitors in cancer therapy due to its diverse effects as a TLR7/8 ligand. It has the potential to inhibit tumor progression at multiple levels.

4.3. Tetraspanins and their role in the function of sEV-miR-574-5p

As differences between sEV subtypes were also observed in the ScrC conditions, it is likely that sEV-specific differences, for example in the sEV envelope, affect the functionality of sEV-derived cargo. Tetraspanins are membrane proteins commonly used as markers for sEV and have many different roles in sEV formation, cargo sorting, and uptake [93,94,97]. Tetraspanin clusters are known to occur in the membrane of sEV and contribute to target cell selection [305]. It is therefore likely that they also play a role in transmitting the functions of miRs transported by sEV to target cells. The tetraspanin composition is characteristic for each sEV population and may be used to determine the origin of sEV [101]. The most commonly used

markers for sEV are CD9, CD63, and CD81 [93,98,101]. The sEV from the two NB cell lines were characterized using the ExoView R100, which is one of the best methods for characterizing surface markers within an sEV population without purification [340]. A disadvantage is that only the tetraspanin-positive sEV are bound by the tetraspanin antibodies coated on the chips. Therefore, sEV that are negative for the specific tetraspanins cannot be immobilized and characterized using this method.

ExoView R100 analysis revealed that NB-derived sEV, had high proportions of CD81-positive sEV, whereas A549- and 2106T-derived sEV had low proportions of sEV positive for CD81 [52]. Breitwieser et al. showed that the NB cell line SK-SY5Y also had increased levels of CD81-positive sEV, whereas the sEV derived from other cancer cell lines had a low proportion of CD81-positive sEV [101]. This suggests a cancer type-specific distribution of tetraspanins. In addition, CD81 may play a more important role in NB than the other tetraspanins due to its increased presence.

The details of how tetraspanins are involved in the uptake of sEV by target cells are not well understood [93]. However, there are some studies showing that tetraspanins influence the target cell selection [102,305]. In addition, CD9- and CD81-deficient mice have been shown to impair sperm-egg fusion and other fusion events [105]. It has also been suggested that some tetraspanins, including CD9, CD63, CD151, or CD81, influence the internalization process of viruses [64,104,108]. Therefore, it is plausible that the tetraspanin composition affects the internalization and uptake pathway of sEV. To determine whether the tetraspanins play a role in mediating the function of miR-574-5p, we aimed to inhibit them by siRNA-mediated knockdown and then examine the function of miR-574-5p. Since siRNA-mediated knockdown of CD81 significantly reduced the total number of sEV, CD81 appears to be involved in sEV biogenesis. This is plausible, as CD63 is also known to be involved in endosomal sorting through ESCRT-dependent and -independent pathways [45].

Therefore, antibodies were used to block tetraspanin function in sEV uptake. To date, neutralization antibodies have been mainly used to treat viruses [108]. In the treatment of viruses, antibodies against different tetraspanins are used to inhibit viral uptake into cells [106,107]. Here, blocking CD63 and CD81 of SK-N-AS-derived miR-574-5p oe sEV had an inhibitory effect on α-SMA levels in HFL1 cells, in contrast to the upregulation by the miR-574-5p oe sEV. Blocking tetraspanins on A549-derived sEV also had no significant effect on α-SMA levels in HFL1 cells. This suggests a sEV subtype-specific effect. Since A549-derived miR-574-5p oe sEV generally had no effect on α-SMA levels in HFL1 cells, this is presumably not affected by the tetraspanin treatment. In A549 cells, blocking CD63 on A549-derived miR-574-5p oe sEV also had a significant inhibitory effect on mPGES-1 levels, but

rather than opposing, it enhanced the decrease induced by sEV-miR-574-5p. CD9- and CD81-blocked sEV showed slightly inhibitory but not significant effects.

While CD63 has also been shown to be located in the late endosome and lysosome, CD9 and CD81 are mainly found in the plasma membrane [91,341]. In 2021, Mathieu et al. provided evidence that sEV with higher levels of CD63 are presumably exosomes derived from the late endosome, whereas sEV bearing higher levels of other tetraspanins, especially CD9 and CD81, mainly bud from the plasma membrane, thus qualifying them rather as microvesicles [342]. CD63-positive sEV did not colocalize with other tetraspanins to a large extent in the ExoView R100 analyses. This may suggest that CD63- and CD9/CD81-bearing sEV are distinct subgroups mediating different functions and may explain the differential effects of CD63 versus CD9 and CD81 blocking.

To test whether the differences in the physiological function of miR-574-5p oe sEV of the two cell lines were due to differences in internalization, live cell experiments were performed. Minor differences were observed in the internalization of the SK-N-AS-derived sEV by the HFL1 cells but indicated an altered internalization. Therefore, two assays were performed to quantify the uptake rate of the sEV. However, neither the microscopy-based assay nor the luciferase-based assay showed a significant effect between the individual tetraspanin antibody-treated sEV conditions. Interestingly, at least 40% less treated sEV were taken up by the HFL1 cells compared to the control without antibodies. It is possible that steric hindrance occurs due to the enlargement of the sEV by the combination with antibodies, resulting in fewer sEV taken up via the filopodia. At approximately 10 nm, an IgG antibody is only 1/5 the size of one of the smaller sEV [343]. Nevertheless, no tetraspanin-mediated effect on the relative sEV uptake number was detected in either A549 or HFL1 cells.

However, it is also possible that the visual and non-quantifiable differences in microscopy are due to differences in cell size and the plane of microscopy. If the internalization of sEV does not result in the differences, there may be other downstream processes that alter the physiological function of sEV by blocking the tetraspanins. One possible explanation could be the influence of ERK1/2 signaling, since the overexpression of CD81 leads to increased ERK1/2 signaling, which also positively influences proliferation in HepG2 liver tumor cells [344]. Inhibition of CD81 could also lead to a decrease in ERK1/2 activity, which would result in a downstream downregulation of α-SMA levels. It has also been shown that the inhibition of CD9 in the cells decreases ERK1/2 activity [345]. It is therefore possible that tetraspanins in general are associated with the ERK1/2 pathway. Inhibition of CD63 on sEV may down-regulate ERK1/2 and trigger downstream processes in the respective cell type, such as the reduction of mPGES-1 [346,347]. So far, only opposite effects have been found, showing an increase in MAPK/ERK signaling as a result of a CD63 knockout [348]. To find out whether the

effects are also mediated in the absence of miR-574-5p oe, the tetraspanin-blocking experiments would have to be performed with sEV without miR-574-5p oe. It would also be interesting to use an ERK1/2 inhibitor to determine whether the regulation is mediated via this pathway.

In conclusion, it has been shown that the tetraspanins on the surface of sEV influence the functionality of the sEV-derived miR-574-5p. The novel approach of blocking sEV membrane proteins with antibodies is promising and has so far only been used as a therapy for viruses [106,107]. However, the results should also be verified by overexpressing the tetraspanins in sEV. In the future, blocking tetraspanins could be used to specifically inhibit the mediation of sEV-miR-574-5p functions and its various roles as a TLR7/8 ligand, which would in turn inhibit tumour progression.

4.4. Outlook

This study provided a better understanding of the different functions of miR-574-5p in the regulation of PGE_2 biosynthesis in cancer. It was shown that the transferability of regulatory mechanisms is present in some cases, but not always. In NB, the interaction of intracellular miR-574-5p and CUGBP1 also regulates mPGES-1 and PGE_2, whereas sEV-miR-574-5p has no autocrine regulatory function in PGE_2 synthesis. In addition, a novel subtype-specific paracrine function of sEV-miR-574-5p was discovered in NB, which is not transferable to NSCLC. Therefore, the transferability to other tumor types should be further investigated in order to expand the therapeutic approaches with the least effort and the greatest effect.

Due to the specific secretion of miR-574-5p by two NSCLC cell lines and two NB cell lines, miR-574-5p may be a potential biomarker in several cancer types [52]. MiRs are perfect candidates as biomarkers because their small size makes them very stable compared to other RNAs, and they are present in many body fluids [117]. This makes them easy to detect minimally invasively, for example in saliva, urine, or blood [117,154]. Particularly in NSCLC, miR-574-5p has been considered and investigated as a diagnostic and prognostic biomarker [161,162]. Other cancers where miR-574-5p could be used as a potential marker include breast cancer, squamous cell carcinoma of the esophagus, or SCLC [164–166]. MiR-574-5p has not been previously associated with NB, although there have been several studies of changes in miR expression patterns in different NB subtypes [317,349]. In the spheroid experiments, the NB cell line SK-N-AS was shown to have low intracellular levels of miR-574-5p compared to the adenocarcinoma cell line A549, even after stimulation with the inflammatory mediator IL-1β [304]. This confirms that even low levels of miRs can mediate important physiological functions and contribute to tumor progression. However, due to the low levels it may be difficult to use miR-574-5p as a single prognostic biomarker in NB. A potential use as a prognostic biomarker

would be in combination with the tetraspanin CD81, which is, as shown in the characterization studies of NB sEV, particularly abundant in NB-derived sEV compared to sEV from other cancer cells [52,101]. Thus, CD81- and miR-574-5p-positive sEV may represent a new promising tool for early detection of NB-related diseases.

This work identified a novel function of miR-574-5p. It was shown that sEV-miR-574-5p has a paracrine function on fibroblast differentiation and not an autocrine function as in NSCLC [52]. To investigate the global effect of sEV-miR-574-5p on CAF activation, further studies could use other differentiation markers. Other markers that could be analyzed include cytoskeletal markers, ECM components or growth factors and cytokines [229,237–241]. Further research in this field could also help to use the understanding of intracellular communication to develop new therapeutic approaches against tumor progression. It has also been shown that blocking tetraspanins on the sEV surface can alter the function of sEV-derived miR-miR-574-5p, which in turn is due to intracellular communication in the TME. Further investigation of the influence of the tetraspanins is an interesting aspect that should be included in future studies.

5. References

[1] Neijssen J, Herberts C, Drijfhout JW, Reits E, Janssen L, Neefjes J. Cross-presentation by intercellular peptide transfer through gap junctions. Nature 2005;434:83–8. https://doi.org/10.1038/nature03290.

[2] Sherer NM, Lehmann MJ, Jimenez-Soto LF, Horensavitz C, Pypaert M, Mothes W. Retroviruses can establish filopodial bridges for efficient cell-to-cell transmission. Nat Cell Biol 2007;9:310–5. https://doi.org/10.1038/ncb1544.

[3] Pierelli L, Marone M, Bonanno G, Mozzetti S, Rutella S, Morosetti R, et al. Modulation of bcl-2 and p27 in human primitive proliferating hematopoietic progenitors by autocrine TGF-beta1 is a cell cycle-independent effect and influences their hematopoietic potential. Blood 2000;95:3001–9.

[4] Gao Y, Qin Y, Wan C, Sun Y, Meng J, Huang J, et al. Small Extracellular Vesicles: A Novel Avenue for Cancer Management. Front Oncol 2021;11:638357. https://doi.org/10.3389/fonc.2021.638357.

[5] Caby M-P, Lankar D, Vincendeau-Scherrer C, Raposo G, Bonnerot C. Exosomal-like vesicles are present in human blood plasma. Int Immunol 2005;17:879–87. https://doi.org/10.1093/intimm/dxh267.

[6] Ogawa Y, Kanai-Azuma M, Akimoto Y, Kawakami H, Yanoshita R. Exosome-Like Vesicles with Dipeptidyl Peptidase IV in Human Saliva. Biol Pharm Bull 2008;31:1059–62. https://doi.org/10.1248/bpb.31.1059.

[7] Théry C, Zitvogel L, Amigorena S. Exosomes: composition, biogenesis and function. Nat Rev Immunol 2002;2:569–79. https://doi.org/10.1038/nri855.

[8] Thakur A, Parra DC, Motallebnejad P, Brocchi M, Chen HJ. Exosomes: Small vesicles with big roles in cancer, vaccine development, and therapeutics. Bioact Mater 2022;10:281–94. https://doi.org/10.1016/j.bioactmat.2021.08.029.

[9] Di Vizio D, Morello M, Dudley AC, Schow PW, Adam RM, Morley S, et al. Large Oncosomes in Human Prostate Cancer Tissues and in the Circulation of Mice with Metastatic Disease. Am J Pathol 2012;181:1573–84. https://doi.org/10.1016/j.ajpath.2012.07.030.

[10] Ciardiello C, Migliorino R, Leone A, Budillon A. Large extracellular vesicles: Size matters in tumor progression. Cytokine Growth Factor Rev 2020;51:69–74. https://doi.org/10.1016/j.cytogfr.2019.12.007.

[11] Kakarla R, Hur J, Kim YJ, Kim J, Chwae Y-J. Apoptotic cell-derived exosomes: messages from dying cells. Exp Mol Med 2020;52:1–6. https://doi.org/10.1038/s12276-019-0362-8.

[12] Kang T, Atukorala I, Mathivanan S. Biogenesis of Extracellular Vesicles. In: Mathivanan S, Fonseka P, Nedeva C, Atukorala I, editors. New Front. Extracell. Vesicles, vol. 97, Cham: Springer International Publishing; 2021, p. 19–43. https://doi.org/10.1007/978-3-030-67171-6_2.

[13] Raposo G, Stoorvogel W. Extracellular vesicles: Exosomes, microvesicles, and friends. J Cell Biol 2013;200:373–83. https://doi.org/10.1083/jcb.201211138.

[14] Cocucci E, Meldolesi J. Ectosomes and exosomes: shedding the confusion between extracellular vesicles. Trends Cell Biol 2015;25:364–72. https://doi.org/10.1016/j.tcb.2015.01.004.

[15] Zhang H, Freitas D, Kim HS, Fabijanic K, Li Z, Chen H, et al. Identification of distinct

nanoparticles and subsets of extracellular vesicles by asymmetric flow field-flow fractionation. Nat Cell Biol 2018;20:332–43. https://doi.org/10.1038/s41556-018-0040-4.

[16] Zhang Q, Higginbotham JN, Jeppesen DK, Yang Y-P, Li W, McKinley ET, et al. Transfer of Functional Cargo in Exomeres. Cell Rep 2019;27:940-954.e6. https://doi.org/10.1016/j.celrep.2019.01.009.

[17] Witwer KW, Théry C. Extracellular vesicles or exosomes? On primacy, precision, and popularity influencing a choice of nomenclature. J Extracell Vesicles 2019;8:1648167. https://doi.org/10.1080/20013078.2019.1648167.

[18] Théry C, Witwer KW, Aikawa E, Alcaraz MJ, Anderson JD, Andriantsitohaina R, et al. Minimal information for studies of extracellular vesicles 2018 (MISEV2018): a position statement of the International Society for Extracellular Vesicles and update of the MISEV2014 guidelines. J Extracell Vesicles 2018;7:1535750. https://doi.org/10.1080/20013078.2018.1535750.

[19] Mathivanan S, Fahner CJ, Reid GE, Simpson RJ. ExoCarta 2012: database of exosomal proteins, RNA and lipids. Nucleic Acids Res 2012;40:D1241–4. https://doi.org/10.1093/nar/gkr828.

[20] Vlassov AV, Magdaleno S, Setterquist R, Conrad R. Exosomes: Current knowledge of their composition, biological functions, and diagnostic and therapeutic potentials. Biochim Biophys Acta BBA - Gen Subj 2012;1820:940–8. https://doi.org/10.1016/j.bbagen.2012.03.017.

[21] Llorente A, Skotland T, Sylvänne T, Kauhanen D, Róg T, Orłowski A, et al. Molecular lipidomics of exosomes released by PC-3 prostate cancer cells. Biochim Biophys Acta BBA - Mol Cell Biol Lipids 2013;1831:1302–9. https://doi.org/10.1016/j.bbalip.2013.04.011.

[22] Skotland T, Ekroos K, Kauhanen D, Simolin H, Seierstad T, Berge V, et al. Molecular lipid species in urinary exosomes as potential prostate cancer biomarkers. Eur J Cancer 2017;70:122–32. https://doi.org/10.1016/j.ejca.2016.10.011.

[23] Wang D, DuBois RN. Eicosanoids and cancer. Nat Rev Cancer 2010;10:181–93. https://doi.org/10.1038/nrc2809.

[24] Kim J, Hong S-W, Kim S, Kim D, Hur D, Jin D-H, et al. Cyclooxygenase-2 expression is induced by celecoxib treatment in lung cancer cells and is transferred to neighbor cells via exosomes. Int J Oncol 2017. https://doi.org/10.3892/ijo.2017.4227.

[25] Esser J, Gehrmann U, D'Alexandri FL, Hidalgo-Estévez AM, Wheelock CE, Scheynius A, et al. Exosomes from human macrophages and dendritic cells contain enzymes for leukotriene biosynthesis and promote granulocyte migration. J Allergy Clin Immunol 2010;126:1032-1040.e4. https://doi.org/10.1016/j.jaci.2010.06.039.

[26] Huang X, Yuan T, Tschannen M, Sun Z, Jacob H, Du M, et al. Characterization of human plasma-derived exosomal RNAs by deep sequencing. BMC Genomics 2013;14:319. https://doi.org/10.1186/1471-2164-14-319.

[27] Ma J, Xu M, Yin M, Hong J, Chen H, Gao Y, et al. Exosomal hsa-miR199a-3p Promotes Proliferation and Migration in Neuroblastoma. Front Oncol 2019;9:459. https://doi.org/10.3389/fonc.2019.00459.

[28] Alexander M, Hu R, Runtsch MC, Kagele DA, Mosbruger TL, Tolmachova T, et al. Exosome-delivered microRNAs modulate the inflammatory response to endotoxin. Nat Commun 2015;6:7321. https://doi.org/10.1038/ncomms8321.

[29] Kosaka N, Iguchi H, Hagiwara K, Yoshioka Y, Takeshita F, Ochiya T. Neutral

Sphingomyelinase 2 (nSMase2)-dependent Exosomal Transfer of Angiogenic MicroRNAs Regulate Cancer Cell Metastasis. J Biol Chem 2013;288:10849–59. https://doi.org/10.1074/jbc.M112.446831.

[30] Zhang Y, Liu Y, Liu H, Tang WH. Exosomes: biogenesis, biologic function and clinical potential. Cell Biosci 2019;9:19. https://doi.org/10.1186/s13578-019-0282-2.

[31] Stahl PD, Barbieri MA. Multivesicular Bodies and Multivesicular Endosomes: The “Ins and Outs” of Endosomal Traffic. Sci STKE 2002;2002. https://doi.org/10.1126/stke.2002.141.pe32.

[32] Denzer K, Kleijmeer MJ, Heijnen HF, Stoorvogel W, Geuze HJ. Exosome: from internal vesicle of the multivesicular body to intercellular signaling device. J Cell Sci 2000;113:3365–74. https://doi.org/10.1242/jcs.113.19.3365.

[33] Doyle L, Wang M. Overview of Extracellular Vesicles, Their Origin, Composition, Purpose, and Methods for Exosome Isolation and Analysis. Cells 2019;8:727. https://doi.org/10.3390/cells8070727.

[34] Colombo M, Moita C, van Niel G, Kowal J, Vigneron J, Benaroch P, et al. Analysis of ESCRT functions in exosome biogenesis, composition and secretion highlights the heterogeneity of extracellular vesicles. J Cell Sci 2013:jcs.128868. https://doi.org/10.1242/jcs.128868.

[35] Raiborg C, Stenmark H. The ESCRT machinery in endosomal sorting of ubiquitylated membrane proteins. Nature 2009;458:445–52. https://doi.org/10.1038/nature07961.

[36] Baietti MF, Zhang Z, Mortier E, Melchior A, Degeest G, Geeraerts A, et al. Syndecan–syntenin–ALIX regulates the biogenesis of exosomes. Nat Cell Biol 2012;14:677–85. https://doi.org/10.1038/ncb2502.

[37] Huotari J, Helenius A. Endosome maturation: Endosome maturation. EMBO J 2011;30:3481–500. https://doi.org/10.1038/emboj.2011.286.

[38] Hoshino D, Kirkbride KC, Costello K, Clark ES, Sinha S, Grega-Larson N, et al. Exosome Secretion Is Enhanced by Invadopodia and Drives Invasive Behavior. Cell Rep 2013;5:1159–68. https://doi.org/10.1016/j.celrep.2013.10.050.

[39] Villarroya-Beltri C, Baixauli F, Gutiérrez-Vázquez C, Sánchez-Madrid F, Mittelbrunn M. Sorting it out: Regulation of exosome loading. Semin Cancer Biol 2014;28:3–13. https://doi.org/10.1016/j.semcancer.2014.04.009.

[40] Savina A, Fader CM, Damiani MT, Colombo MI. Rab11 Promotes Docking and Fusion of Multivesicular Bodies in a Calcium-Dependent Manner: Ca2+-Dependent Multivesicular Body Fusion. Traffic 2005;6:131–43. https://doi.org/10.1111/j.1600-0854.2004.00257.x.

[41] Ostrowski M, Carmo NB, Krumeich S, Fanget I, Raposo G, Savina A, et al. Rab27a and Rab27b control different steps of the exosome secretion pathway. Nat Cell Biol 2010;12:19–30. https://doi.org/10.1038/ncb2000.

[42] Hessvik NP, Llorente A. Current knowledge on exosome biogenesis and release. Cell Mol Life Sci 2018;75:193–208. https://doi.org/10.1007/s00018-017-2595-9.

[43] Han J, Pluhackova K, Böckmann RA. The Multifaceted Role of SNARE Proteins in Membrane Fusion. Front Physiol 2017;8. https://doi.org/10.3389/fphys.2017.00005.

[44] Escola J-M, Kleijmeer MJ, Stoorvogel W, Griffith JM, Yoshie O, Geuze HJ. Selective Enrichment of Tetraspan Proteins on the Internal Vesicles of Multivesicular Endosomes and on Exosomes Secreted by Human B-lymphocytes. J Biol Chem 1998;273:20121–7. https://doi.org/10.1074/jbc.273.32.20121.

[45] van Niel G, Charrin S, Simoes S, Romao M, Rochin L, Saftig P, et al. The Tetraspanin CD63 Regulates ESCRT-Independent and -Dependent Endosomal Sorting during Melanogenesis. Dev Cell 2011;21:708–21. https://doi.org/10.1016/j.devcel.2011.08.019.

[46] Hurwitz SN, Conlon MM, Rider MA, Brownstein NC, Meckes DG. Nanoparticle analysis sheds budding insights into genetic drivers of extracellular vesicle biogenesis. J Extracell Vesicles 2016;5:31295. https://doi.org/10.3402/jev.v5.31295.

[47] Trajkovic K, Hsu C, Chiantia S, Rajendran L, Wenzel D, Wieland F, et al. Ceramide Triggers Budding of Exosome Vesicles into Multivesicular Endosomes. Science 2008;319:1244–7. https://doi.org/10.1126/science.1153124.

[48] Phuyal S, Hessvik NP, Skotland T, Sandvig K, Llorente A. Regulation of exosome release by glycosphingolipids and flotillins. FEBS J 2014;281:2214–27. https://doi.org/10.1111/febs.12775.

[49] Lehmann BD, Paine MS, Brooks AM, McCubrey JA, Renegar RH, Wang R, et al. Senescence-Associated Exosome Release from Human Prostate Cancer Cells. Cancer Res 2008;68:7864–71. https://doi.org/10.1158/0008-5472.CAN-07-6538.

[50] King HW, Michael MZ, Gleadle JM. Hypoxic enhancement of exosome release by breast cancer cells. BMC Cancer 2012;12:421. https://doi.org/10.1186/1471-2407-12-421.

[51] Salomon C, Kobayashi M, Ashman K, Sobrevia L, Mitchell MD, Rice GE. Hypoxia-Induced Changes in the Bioactivity of Cytotrophoblast-Derived Exosomes. PLoS ONE 2013;8:e79636. https://doi.org/10.1371/journal.pone.0079636.

[52] Donzelli J, Proestler E, Riedel A, Nevermann S, Hertel B, Guenther A, et al. Small extracellular vesicle-derived miR-574-5p regulates PGE2-biosynthesis via TLR7/8 in lung cancer. J Extracell Vesicles 2021;10:12143. https://doi.org/10.1002/jev2.12143.

[53] Harding C, Heuser J, Stahl P. Receptor-mediated endocytosis of transferrin and recycling of the transferrin receptor in rat reticulocytes. J Cell Biol 1983;97:329–39. https://doi.org/10.1083/jcb.97.2.329.

[54] Pan BT, Teng K, Wu C, Adam M, Johnstone RM. Electron microscopic evidence for externalization of the transferrin receptor in vesicular form in sheep reticulocytes. J Cell Biol 1985;101:942–8. https://doi.org/10.1083/jcb.101.3.942.

[55] Raposo G, Nijman HW, Stoorvogel W, Liejendekker R, Harding CV, Melief CJ, et al. B lymphocytes secrete antigen-presenting vesicles. J Exp Med 1996;183:1161–72. https://doi.org/10.1084/jem.183.3.1161.

[56] Ratajczak J, Wysoczynski M, Hayek F, Janowska-Wieczorek A, Ratajczak MZ. Membrane-derived microvesicles: important and underappreciated mediators of cell-to-cell communication. Leukemia 2006;20:1487–95. https://doi.org/10.1038/sj.leu.2404296.

[57] Penfornis P, Vallabhaneni KC, Whitt J, Pochampally R. Extracellular vesicles as carriers of microRNA, proteins and lipids in tumor microenvironment: Extracellular Vesicles as Carriers of mRNA, Proteins and Lipids. Int J Cancer 2016;138:14–21. https://doi.org/10.1002/ijc.29417.

[58] Mulcahy LA, Pink RC, Carter DRF. Routes and mechanisms of extracellular vesicle uptake. J Extracell Vesicles 2014;3:24641. https://doi.org/10.3402/jev.v3.24641.

[59] McKelvey KJ, Powell KL, Ashton AW, Morris JM, McCracken SA. Exosomes: Mechanisms of Uptake. J Circ Biomark 2015;4:7. https://doi.org/10.5772/61186.

[60] Tkach M, Kowal J, Zucchetti AE, Enserink L, Jouve M, Lankar D, et al. Qualitative differences in T-cell activation by dendritic cell-derived extracellular vesicle subtypes. EMBO

J 2017;36:3012–28. https://doi.org/10.15252/embj.201696003.

[61] Munich S, Sobo-Vujanovic A, Buchser WJ, Beer-Stolz D, Vujanovic NL. Dendritic cell exosomes directly kill tumor cells and activate natural killer cells via TNF superfamily ligands. OncoImmunology 2012;1:1074–83. https://doi.org/10.4161/onci.20897.

[62] Gurung S, Perocheau D, Touramanidou L, Baruteau J. The exosome journey: from biogenesis to uptake and intracellular signalling. Cell Commun Signal 2021;19:47. https://doi.org/10.1186/s12964-021-00730-1.

[63] Gordón-Alonso M, Yañez-Mó M, Barreiro O, Álvarez S, Muñoz-Fernández MÁ, Valenzuela-Fernández A, et al. Tetraspanins CD9 and CD81 Modulate HIV-1-Induced Membrane Fusion. J Immunol 2006;177:5129–37. https://doi.org/10.4049/jimmunol.177.8.5129.

[64] Symeonides M, Lambelé M, Roy N, Thali M. Evidence Showing that Tetraspanins Inhibit HIV-1-Induced Cell-Cell Fusion at a Post-Hemifusion Stage. Viruses 2014;6:1078–90. https://doi.org/10.3390/v6031078.

[65] Escrevente C, Keller S, Altevogt P, Costa J. Interaction and uptake of exosomes by ovarian cancer cells. BMC Cancer 2011;11:108. https://doi.org/10.1186/1471-2407-11-108.

[66] Feng D, Zhao W-L, Ye Y-Y, Bai X-C, Liu R-Q, Chang L-F, et al. Cellular Internalization of Exosomes Occurs Through Phagocytosis. Traffic 2010;11:675–87. https://doi.org/10.1111/j.1600-0854.2010.01041.x.

[67] Sung BH, von Lersner A, Guerrero J, Krystofiak ES, Inman D, Pelletier R, et al. A live cell reporter of exosome secretion and uptake reveals pathfinding behavior of migrating cells. Nat Commun 2020;11:2092. https://doi.org/10.1038/s41467-020-15747-2.

[68] Mettlen M, Chen P-H, Srinivasan S, Danuser G, Schmid SL. Regulation of Clathrin-Mediated Endocytosis. Annu Rev Biochem 2018;87:871–96. https://doi.org/10.1146/annurev-biochem-062917-012644.

[69] Sweitzer SM, Hinshaw JE. Dynamin Undergoes a GTP-Dependent Conformational Change Causing Vesiculation. Cell 1998;93:1021–9. https://doi.org/10.1016/S0092-8674(00)81207-6.

[70] Takei K, Haucke V, Slepnev V, Farsad K, Salazar M, Chen H, et al. Generation of Coated Intermediates of Clathrin-Mediated Endocytosis on Protein-Free Liposomes. Cell 1998;94:131–41. https://doi.org/10.1016/S0092-8674(00)81228-3.

[71] Kurzchalia TV, Partan RG. Membrane microdomains and caveolae. Curr Opin Cell Biol 1999;11:424–31. https://doi.org/10.1016/S0955-0674(99)80061-1.

[72] Harder T, Simons K. Caveolae, DIGs, and the dynamics of sphingolipid—cholesterol microdomains. Curr Opin Cell Biol 1997;9:534–42. https://doi.org/10.1016/S0955-0674(97)80030-0.

[73] Drab M, Verkade P, Elger M, Kasper M, Lohn M, Lauterbach B, et al. Loss of Caveolae, Vascular Dysfunction, and Pulmonary Defects in Caveolin-1 Gene-Disrupted Mice. Science 2001;293:2449–52. https://doi.org/10.1126/science.1062688.

[74] Monier S, Dietzen DJ, Hastings WR, Lublin DM, Kurzchalia TV. Oligomerization of VIP21-caveolin in vitro is stabilized by long chain fatty acylation or cholesterol. FEBS Lett 1996;388:143–9. https://doi.org/10.1016/0014-5793(96)00519-4.

[75] Rothberg KG, Heuser JE, Donzell WC, Ying Y-S, Glenney JR, Anderson RGW. Caveolin, a protein component of caveolae membrane coats. Cell 1992;68:673–82. https://doi.org/10.1016/0092-8674(92)90143-Z.

[76] Orth JD, Krueger EW, Cao H, McNiven MA. The large GTPase dynamin regulates actin comet formation and movement in living cells. Proc Natl Acad Sci 2002;99:167–72. https://doi.org/10.1073/pnas.012607899.

[77] Swanson JA. Shaping cups into phagosomes and macropinosomes. Nat Rev Mol Cell Biol 2008;9:639–49. https://doi.org/10.1038/nrm2447.

[78] Barrès C, Blanc L, Bette-Bobillo P, André S, Mamoun R, Gabius H-J, et al. Galectin-5 is bound onto the surface of rat reticulocyte exosomes and modulates vesicle uptake by macrophages. Blood 2010;115:696–705. https://doi.org/10.1182/blood-2009-07-231449.

[79] Christianson HC, Svensson KJ, van Kuppevelt TH, Li J-P, Belting M. Cancer cell exosomes depend on cell-surface heparan sulfate proteoglycans for their internalization and functional activity. Proc Natl Acad Sci 2013;110:17380–5. https://doi.org/10.1073/pnas.1304266110.

[80] Tian T, Wang Y, Wang H, Zhu Z, Xiao Z. Visualizing of the cellular uptake and intracellular trafficking of exosomes by live-cell microscopy. J Cell Biochem 2010;111:488–96. https://doi.org/10.1002/jcb.22733.

[81] Massol P, Montcourrier P, Guillemot J-C, Chavrier P. Fc receptor-mediated phagocytosis requires CDC42 and Rac1. EMBO J 1998;17:6219–29. https://doi.org/10.1093/emboj/17.21.6219.

[82] Rudt S, Müller RH. In vitro phagocytosis assay of nano- and microparticles by chemiluminescence. III. Uptake of differently sized surface-modified particles, and its correlation to particle properties and in vivo distribution. Eur J Pharm Sci 1993;1:31–9. https://doi.org/10.1016/0928-0987(93)90015-3.

[83] Doherty GJ, McMahon HT. Mechanisms of Endocytosis. Annu Rev Biochem 2009;78:857–902. https://doi.org/10.1146/annurev.biochem.78.081307.110540.

[84] Hoppe AD, Swanson JA. Cdc42, Rac1, and Rac2 Display Distinct Patterns of Activation during Phagocytosis. Mol Biol Cell 2004;15:3509–19. https://doi.org/10.1091/mbc.e03-11-0847.

[85] Olazabal IM, Caron E, May RC, Schilling K, Knecht DA, Machesky LM. Rho-Kinase and Myosin-II Control Phagocytic Cup Formation during CR, but Not FcγR, Phagocytosis. Curr Biol 2002;12:1413–8. https://doi.org/10.1016/S0960-9822(02)01069-2.

[86] Caron E, Hall A. Identification of Two Distinct Mechanisms of Phagocytosis Controlled by Different Rho GTPases. Science 1998;282:1717–21. https://doi.org/10.1126/science.282.5394.1717.

[87] Simons K, Ehehalt R. Cholesterol, lipid rafts, and disease. J Clin Invest 2002;110:597–603. https://doi.org/10.1172/JCI0216390.

[88] Glebov OO, Bright NA, Nichols BJ. Flotillin-1 defines a clathrin-independent endocytic pathway in mammalian cells. Nat Cell Biol 2006;8:46–54. https://doi.org/10.1038/ncb1342.

[89] Plebanek MP, Mutharasan RK, Volpert O, Matov A, Gatlin JC, Thaxton CS. Nanoparticle Targeting and Cholesterol Flux Through Scavenger Receptor Type B-1 Inhibits Cellular Exosome Uptake. Sci Rep 2015;5:15724. https://doi.org/10.1038/srep15724.

[90] Emam SE, Ando H, Lila ASA, Shimizu T, Okuhira K, Ishima Y, et al. Liposome co-incubation with cancer cells secreted exosomes (extracellular vesicles) with different proteins expressions and different uptake pathways. Sci Rep 2018;8:14493. https://doi.org/10.1038/s41598-018-32861-w.

[91] Mathieu M, Martin-Jaular L, Lavieu G, Théry C. Specificities of secretion and uptake of

exosomes and other extracellular vesicles for cell-to-cell communication. Nat Cell Biol 2019;21:9–17. https://doi.org/10.1038/s41556-018-0250-9.

[92] Luga V, Zhang L, Viloria-Petit AM, Ogunjimi AA, Inanlou MR, Chiu E, et al. Exosomes Mediate Stromal Mobilization of Autocrine Wnt-PCP Signaling in Breast Cancer Cell Migration. Cell 2012;151:1542–56. https://doi.org/10.1016/j.cell.2012.11.024.

[93] Andreu Z, Yáñez-Mó* M. Tetraspanins in Extracellular Vesicle Formation and Function. Front Immunol 2014;5. https://doi.org/10.3389/fimmu.2014.00442.

[94] Rana S, Zöller M. Exosome target cell selection and the importance of exosomal tetraspanins: a hypothesis. Biochem Soc Trans 2011;39:559–62. https://doi.org/10.1042/BST0390559.

[95] Charrin S, Manié S, Thiele C, Billard M, Gerlier D, Boucheix C, et al. A physical and functional link between cholesterol and tetraspanins. Eur J Immunol 2003;33:2479–89. https://doi.org/10.1002/eji.200323884.

[96] Regina Todeschini A, Hakomori S. Functional role of glycosphingolipids and gangliosides in control of cell adhesion, motility, and growth, through glycosynaptic microdomains. Biochim Biophys Acta BBA - Gen Subj 2008;1780:421–33. https://doi.org/10.1016/j.bbagen.2007.10.008.

[97] Hemler ME. Tetraspanin functions and associated microdomains. Nat Rev Mol Cell Biol 2005;6:801–11. https://doi.org/10.1038/nrm1736.

[98] Jankovičová J, Sečová P, Michalková K, Antalíková J. Tetraspanins, More than Markers of Extracellular Vesicles in Reproduction. Int J Mol Sci 2020;21:7568. https://doi.org/10.3390/ijms21207568.

[99] Berditchevski F, Odintsova E, Sawada S, Gilbert E. Expression of the Palmitoylation-deficient CD151 Weakens the Association of α3β1 Integrin with the Tetraspanin-enriched Microdomains and Affects Integrin-dependent Signaling. J Biol Chem 2002;277:36991–7000. https://doi.org/10.1074/jbc.M205265200.

[100] Hemler ME. Tetraspanin proteins promote multiple cancer stages. Nat Rev Cancer 2014;14:49–60. https://doi.org/10.1038/nrc3640.

[101] Breitwieser K, Koch LF, Tertel T, Proestler E, Burgers LD, Lipps C, et al. Detailed Characterization of Small Extracellular Vesicles from Different Cell Types Based on Tetraspanin Composition by ExoView R100 Platform. Int J Mol Sci 2022;23:8544. https://doi.org/10.3390/ijms23158544.

[102] Rana S, Claas C, Kretz CC, Nazarenko I, Zoeller M. Activation-induced internalization differs for the tetraspanins CD9 and Tspan8: Impact on tumor cell motility. Int J Biochem Cell Biol 2011;43:106–19. https://doi.org/10.1016/j.biocel.2010.10.002.

[103] Wang T, Wang X, Wang H, Li L, Zhang C, Xiang R, et al. High TSPAN8 expression in epithelial cancer cell-derived small extracellular vesicles promote confined diffusion and pronounced uptake. J Extracell Vesicles 2021;10. https://doi.org/10.1002/jev2.12167.

[104] Scheffer KD, Gawlitza A, Spoden GA, Zhang XA, Lambert C, Berditchevski F, et al. Tetraspanin CD151 Mediates Papillomavirus Type 16 Endocytosis. J Virol 2013;87:3435–46. https://doi.org/10.1128/JVI.02906-12.

[105] Hemler ME. Tetraspanin proteins mediate cellular penetration, invasion, and fusion events and define a novel type of membrane microdomain. Annu Rev Cell Dev Biol 2003;19:397–422. https://doi.org/10.1146/annurev.cellbio.19.111301.153609.

[106] Neumann AU, Phillips S, Levine I, Ijaz S, Dahari H, Eren R, et al. Novel mechanism of

antibodies to hepatitis B virus in blocking viral particle release from cells. Hepatology 2010;52:875–85. https://doi.org/10.1002/hep.23778.

[107] Hemler ME. Targeting of tetraspanin proteins — potential benefits and strategies. Nat Rev Drug Discov 2008;7:747–58. https://doi.org/10.1038/nrd2659.

[108] Fénéant L, Levy S, Cocquerel L. CD81 and Hepatitis C Virus (HCV) Infection. Viruses 2014;6:535–72. https://doi.org/10.3390/v6020535.

[109] O'Brien J, Hayder H, Zayed Y, Peng C. Overview of MicroRNA Biogenesis, Mechanisms of Actions, and Circulation. Front Endocrinol 2018;9:402. https://doi.org/10.3389/fendo.2018.00402.

[110] Huntzinger E, Izaurralde E. Gene silencing by microRNAs: contributions of translational repression and mRNA decay. Nat Rev Genet 2011;12:99–110. https://doi.org/10.1038/nrg2936.

[111] Lee RC, Feinbaum RL, Ambros V. The C. elegans heterochronic gene lin-4 encodes small RNAs with antisense complementarity to lin-14. Cell 1993;75:843–54. https://doi.org/10.1016/0092-8674(93)90529-y.

[112] Lau NC, Lim LP, Weinstein EG, Bartel DP. An Abundant Class of Tiny RNAs with Probable Regulatory Roles in *Caenorhabditis elegans*. Science 2001;294:858–62. https://doi.org/10.1126/science.1065062.

[113] Lee RC, Ambros V. An Extensive Class of Small RNAs in *Caenorhabditis elegans*. Science 2001;294:862–4. https://doi.org/10.1126/science.1065329.

[114] Lagos-Quintana M, Rauhut R, Lendeckel W, Tuschl T. Identification of Novel Genes Coding for Small Expressed RNAs. Science 2001;294:853–8. https://doi.org/10.1126/science.1064921.

[115] Li S-C, Chan W-C, Hu L-Y, Lai C-H, Hsu C-N, Lin W. Identification of homologous microRNAs in 56 animal genomes. Genomics 2010;96:1–9. https://doi.org/10.1016/j.ygeno.2010.03.009.

[116] http://www.mirbase.org 2023.

[117] Condrat CE, Thompson DC, Barbu MG, Bugnar OL, Boboc A, Cretoiu D, et al. miRNAs as Biomarkers in Disease: Latest Findings Regarding Their Role in Diagnosis and Prognosis. Cells 2020;9:276. https://doi.org/10.3390/cells9020276.

[118] Denli AM, Tops BBJ, Plasterk RHA, Ketting RF, Hannon GJ. Processing of primary microRNAs by the Microprocessor complex. Nature 2004;432:231–5. https://doi.org/10.1038/nature03049.

[119] Han J, Lee Y, Yeom K-H, Kim Y-K, Jin H, Kim VN. The Drosha-DGCR8 complex in primary microRNA processing. Genes Dev 2004;18:3016–27. https://doi.org/10.1101/gad.1262504.

[120] Okada C, Yamashita E, Lee SJ, Shibata S, Katahira J, Nakagawa A, et al. A High-Resolution Structure of the Pre-microRNA Nuclear Export Machinery. Science 2009;326:1275–9. https://doi.org/10.1126/science.1178705.

[121] Zhang H, Kolb FA, Jaskiewicz L, Westhof E, Filipowicz W. Single Processing Center Models for Human Dicer and Bacterial RNase III. Cell 2004;118:57–68. https://doi.org/10.1016/j.cell.2004.06.017.

[122] Shukla GC, Singh J, Barik S. MicroRNAs: Processing, Maturation, Target Recognition and Regulatory Functions. Mol Cell Pharmacol 2011;3:83–92.

[123] Meijer HA, Smith EM, Bushell M. Regulation of miRNA strand selection: follow the leader? Biochem Soc Trans 2014;42:1135–40. https://doi.org/10.1042/BST20140142.

[124] Medley JC, Panzade G, Zinovyeva AY. microRNA strand selection: Unwinding the rules. WIREs RNA 2021;12. https://doi.org/10.1002/wrna.1627.

[125] Xie M, Li M, Vilborg A, Lee N, Shu M-D, Yartseva V, et al. Mammalian 5′-Capped MicroRNA Precursors that Generate a Single MicroRNA. Cell 2013;155:1568–80. https://doi.org/10.1016/j.cell.2013.11.027.

[126] Kim Y-K, Kim VN. Processing of intronic microRNAs. EMBO J 2007;26:775–83. https://doi.org/10.1038/sj.emboj.7601512.

[127] The FANTOM Consortium, de Rie D, Abugessaisa I, Alam T, Arner E, Arner P, et al. An integrated expression atlas of miRNAs and their promoters in human and mouse. Nat Biotechnol 2017;35:872–8. https://doi.org/10.1038/nbt.3947.

[128] Rorbach G, Unold O, Konopka BM. Distinguishing mirtrons from canonical miRNAs with data exploration and machine learning methods. Sci Rep 2018;8:7560. https://doi.org/10.1038/s41598-018-25578-3.

[129] Gao Z, Dou Y, Chen Y, Zheng Y. MicroRNA Roles in the NF- κ B Signaling Pathway during Viral Infections. BioMed Res Int 2014;2014:1–8. https://doi.org/10.1155/2014/436097.

[130] Winter J, Jung S, Keller S, Gregory RI, Diederichs S. Many roads to maturity: microRNA biogenesis pathways and their regulation. Nat Cell Biol 2009;11:228–34. https://doi.org/10.1038/ncb0309-228.

[131] Saul MJ, Emmerich AC, Steinhilber D, Suess B. Regulation of Eicosanoid Pathways by MicroRNAs. Front Pharmacol 2019;10:824. https://doi.org/10.3389/fphar.2019.00824.

[132] Jo MH, Shin S, Jung S-R, Kim E, Song J-J, Hohng S. Human Argonaute 2 Has Diverse Reaction Pathways on Target RNAs. Mol Cell 2015;59:117–24. https://doi.org/10.1016/j.molcel.2015.04.027.

[133] Jonas S, Izaurralde E. Towards a molecular understanding of microRNA-mediated gene silencing. Nat Rev Genet 2015;16:421–33. https://doi.org/10.1038/nrg3965.

[134] Dharap A, Pokrzywa C, Murali S, Pandi G, Vemuganti R. MicroRNA miR-324-3p Induces Promoter-Mediated Expression of RelA Gene. PLoS ONE 2013;8:e79467. https://doi.org/10.1371/journal.pone.0079467.

[135] Place RF, Li L-C, Pookot D, Noonan EJ, Dahiya R. MicroRNA-373 induces expression of genes with complementary promoter sequences. Proc Natl Acad Sci 2008;105:1608–13. https://doi.org/10.1073/pnas.0707594105.

[136] Zisoulis DG, Kai ZS, Chang RK, Pasquinelli AE. Autoregulation of microRNA biogenesis by let-7 and Argonaute. Nature 2012;486:541–4. https://doi.org/10.1038/nature11134.

[137] Eiring AM, Harb JG, Neviani P, Garton C, Oaks JJ, Spizzo R, et al. miR-328 Functions as an RNA Decoy to Modulate hnRNP E2 Regulation of mRNA Translation in Leukemic Blasts. Cell 2010;140:652–65. https://doi.org/10.1016/j.cell.2010.01.007.

[138] Saul MJ, Stein S, Grez M, Jakobsson P-J, Steinhilber D, Suess B. UPF1 regulates myeloid cell functions and S100A9 expression by the hnRNP E2/miRNA-328 balance. Sci Rep 2016;6:31995. https://doi.org/10.1038/srep31995.

[139] Saul MJ, Hegewald AB, Emmerich AC, Ossipova E, Vogel M, Baumann I, et al. Mass Spectrometry-Based Proteomics Approach Characterizes the Dual Functionality of miR-328 in

Monocytes. Front Pharmacol 2019;10:640. https://doi.org/10.3389/fphar.2019.00640.

[140] Liang H, Kidder K, Liu Y. Extracellular microRNAs initiate immunostimulation via activating toll-like receptor signaling pathways. ExRNA 2019;1:9. https://doi.org/10.1186/s41544-019-0009-x.

[141] Karikó K, Bhuyan P, Capodici J, Weissman D. Small Interfering RNAs Mediate Sequence-Independent Gene Suppression and Induce Immune Activation by Signaling through Toll-Like Receptor 3. J Immunol 2004;172:6545–9. https://doi.org/10.4049/jimmunol.172.11.6545.

[142] Blasius AL, Arnold CN, Georgel P, Rutschmann S, Xia Y, Lin P, et al. Slc15a4, AP-3, and Hermansky-Pudlak syndrome proteins are required for Toll-like receptor signaling in plasmacytoid dendritic cells. Proc Natl Acad Sci 2010;107:19973–8. https://doi.org/10.1073/pnas.1014051107.

[143] de Marcken M, Dhaliwal K, Danielsen AC, Gautron AS, Dominguez-Villar M. TLR7 and TLR8 activate distinct pathways in monocytes during RNA virus infection. Sci Signal 2019;12:eaaw1347. https://doi.org/10.1126/scisignal.aaw1347.

[144] Fabbri M, Paone A, Calore F, Galli R, Gaudio E, Santhanam R, et al. MicroRNAs bind to Toll-like receptors to induce prometastatic inflammatory response. Proc Natl Acad Sci 2012;109. https://doi.org/10.1073/pnas.1209414109.

[145] Lehmann SM, Krüger C, Park B, Derkow K, Rosenberger K, Baumgart J, et al. An unconventional role for miRNA: let-7 activates Toll-like receptor 7 and causes neurodegeneration. Nat Neurosci 2012;15:827–35. https://doi.org/10.1038/nn.3113.

[146] Challagundla KB, Wise PM, Neviani P, Chava H, Murtadha M, Xu T, et al. Exosome-Mediated Transfer of microRNAs Within the Tumor Microenvironment and Neuroblastoma Resistance to Chemotherapy. JNCI J Natl Cancer Inst 2015;107. https://doi.org/10.1093/jnci/djv135.

[147] Goldie BJ, Dun MD, Lin M, Smith ND, Verrills NM, Dayas CV, et al. Activity-associated miRNA are packaged in Map1b-enriched exosomes released from depolarized neurons. Nucleic Acids Res 2014;42:9195–208. https://doi.org/10.1093/nar/gku594.

[148] Garcia-Martin R, Wang G, Brandão BB, Zanotto TM, Shah S, Kumar Patel S, et al. MicroRNA sequence codes for small extracellular vesicle release and cellular retention. Nature 2022;601:446–51. https://doi.org/10.1038/s41586-021-04234-3.

[149] Villarroya-Beltri C, Gutiérrez-Vázquez C, Sánchez-Cabo F, Pérez-Hernández D, Vázquez J, Martin-Cofreces N, et al. Sumoylated hnRNPA2B1 controls the sorting of miRNAs into exosomes through binding to specific motifs. Nat Commun 2013;4:2980. https://doi.org/10.1038/ncomms3980.

[150] Bolukbasi MF, Mizrak A, Ozdener GB, Madlener S, Ströbel T, Erkan EP, et al. miR-1289 and “Zipcode”-like Sequence Enrich mRNAs in Microvesicles. Mol Ther - Nucleic Acids 2012;1:e10. https://doi.org/10.1038/mtna.2011.2.

[151] Frank F, Sonenberg N, Nagar B. Structural basis for 5′-nucleotide base-specific recognition of guide RNA by human AGO2. Nature 2010;465:818–22. https://doi.org/10.1038/nature09039.

[152] McKenzie AJ, Hoshino D, Hong NH, Cha DJ, Franklin JL, Coffey RJ, et al. KRAS-MEK Signaling Controls Ago2 Sorting into Exosomes. Cell Rep 2016;15:978–87. https://doi.org/10.1016/j.celrep.2016.03.085.

[153] Shurtleff MJ, Temoche-Diaz MM, Karfilis KV, Ri S, Schekman R. Y-box protein 1 is

required to sort microRNAs into exosomes in cells and in a cell-free reaction. ELife 2016;5:e19276. https://doi.org/10.7554/eLife.19276.

[154] Berindan-Neagoe I, Monroig P del C, Pasculli B, Calin GA. MicroRNAome genome: A treasure for cancer diagnosis and therapy: miRNA Knowledge for Clinicians. CA Cancer J Clin 2014;64:311–36. https://doi.org/10.3322/caac.21244.

[155] Mitchell PS, Parkin RK, Kroh EM, Fritz BR, Wyman SK, Pogosova-Agadjanyan EL, et al. Circulating microRNAs as stable blood-based markers for cancer detection. Proc Natl Acad Sci 2008;105:10513–8. https://doi.org/10.1073/pnas.0804549105.

[156] Lawrie CH, Gal S, Dunlop HM, Pushkaran B, Liggins AP, Pulford K, et al. Detection of elevated levels of tumour-associated microRNAs in serum of patients with diffuse large B-cell lymphoma. Br J Haematol 2008;141:672–5. https://doi.org/10.1111/j.1365-2141.2008.07077.x.

[157] Gyoba J, Shan S, Roa W, Bédard E. Diagnosing Lung Cancers through Examination of Micro-RNA Biomarkers in Blood, Plasma, Serum and Sputum: A Review and Summary of Current Literature. Int J Mol Sci 2016;17:494. https://doi.org/10.3390/ijms17040494.

[158] Xiong D-D, Lv J, Wei K-L, Feng Z-B, Chen J-T, Liu K-C, et al. A nine-miRNA signature as a potential diagnostic marker for breast carcinoma: An integrated study of 1,110 cases. Oncol Rep 2017;37:3297–304. https://doi.org/10.3892/or.2017.5600.

[159] Macha M, Seshacharyulu P, Krishn S, Pai P, Rachagani S, Jain M, et al. MicroRNAs (miRNAs) as Biomarker(s) for Prognosis and Diagnosis of Gastrointestinal (GI) Cancers. Curr Pharm Des 2014;20:5287–97. https://doi.org/10.2174/1381612820666140128213117.

[160] Quirico L, Orso F. The power of microRNAs as diagnostic and prognostic biomarkers in liquid biopsies. Cancer Drug Resist 2020. https://doi.org/10.20517/cdr.2019.103.

[161] Han Z, Li Y, Zhang J, Guo C, Li Q, Zhang X, et al. Tumor-derived circulating exosomal miR-342-5p and miR-574-5p as promising diagnostic biomarkers for early-stage Lung Adenocarcinoma. Int J Med Sci 2020;17:1428–38. https://doi.org/10.7150/ijms.43500.

[162] Foss KM, Sima C, Ugolini D, Neri M, Allen KE, Weiss GJ. miR-1254 and miR-574-5p: Serum-Based microRNA Biomarkers for Early-Stage Non-small Cell Lung Cancer. J Thorac Oncol 2011;6:482–8. https://doi.org/10.1097/JTO.0b013e318208c785.

[163] Peng H, Wang J, Li J, Zhao M, Huang S, Gu Y, et al. A circulating non-coding RNA panel as an early detection predictor of non-small cell lung cancer. Life Sci 2016;151:235–42. https://doi.org/10.1016/j.lfs.2016.03.002.

[164] Wang P-S, Chou C-H, Lin C-H, Yao Y-C, Cheng H-C, Li H-Y, et al. A novel long non-coding RNA linc-ZNF469-3 promotes lung metastasis through miR-574-5p-ZEB1 axis in triple negative breast cancer. Oncogene 2018;37:4662–78. https://doi.org/10.1038/s41388-018-0293-1.

[165] Huang S, Luo Q, Peng H, Li J, Zhao M, Wang J, et al. A Panel of Serum Noncoding RNAs for the Diagnosis and Monitoring of Response to Therapy in Patients with Breast Cancer. Med Sci Monit 2018;24:2476–88. https://doi.org/10.12659/MSM.909453.

[166] Zheng D, Ding Y, Ma Q, Zhao L, Guo X, Shen Y, et al. Identification of Serum MicroRNAs as Novel Biomarkers in Esophageal Squamous Cell Carcinoma Using Feature Selection Algorithms. Front Oncol 2019;8:674. https://doi.org/10.3389/fonc.2018.00674.

[167] Huang W, Zhao Y, Xu Z, Wu X, Qiao M, Zhu Z, et al. The Regulatory Mechanism of miR-574-5p Expression in Cancer. Biomolecules 2022;13:40. https://doi.org/10.3390/biom13010040.

[168] Zerbino DR, Achuthan P, Akanni W, Amode MR, Barrell D, Bhai J, et al. Ensembl 2018. Nucleic Acids Res 2018;46:D754–61. https://doi.org/10.1093/nar/gkx1098.

[169] Boucquey M, De Plaen E, Locker M, Poliard A, Mouillet-Richard S, Boon T, et al. Noxp20 and Noxp70, two new markers of early neuronal differentiation, detected in teratocarcinoma-derived neuroectodermic precursor cells. J Neurochem 2006;99:657–69. https://doi.org/10.1111/j.1471-4159.2006.04093.x.

[170] D'Angelo MA, Gomez-Cavazos JS, Mei A, Lackner DH, Hetzer MW. A Change in Nuclear Pore Complex Composition Regulates Cell Differentiation. Dev Cell 2012;22:446–58. https://doi.org/10.1016/j.devcel.2011.11.021.

[171] Zhang Z, Pi J, Zou D, Wang X, Xu J, Yu S, et al. microRNA arm-imbalance in part from complementary targets mediated decay promotes gastric cancer progression. Nat Commun 2019;10:4397. https://doi.org/10.1038/s41467-019-12292-5.

[172] Yao P, Wu J, Lindner D, Fox PL. Interplay between miR-574-3p and hnRNP L regulates VEGFA mRNA translation and tumorigenesis. Nucleic Acids Res 2017;45:7950–64. https://doi.org/10.1093/nar/gkx440.

[173] Li S-C, Liao Y-L, Ho M-R, Tsai K-W, Lai C-H, Lin W. miRNA arm selection and isomiR distribution in gastric cancer. BMC Genomics 2012;13:S13. https://doi.org/10.1186/1471-2164-13-S1-S13.

[174] Tsai K-W, Leung C-M, Lo Y-H, Chen T-W, Chan W-C, Yu S-Y, et al. Arm Selection Preference of MicroRNA-193a Varies in Breast Cancer. Sci Rep 2016;6:28176. https://doi.org/10.1038/srep28176.

[175] Zhang K, Hu Y, Luo N, Li X, Chen F, Yuan J, et al. miR-574-5p attenuates proliferation, migration and EMT in triple-negative breast cancer cells by targeting BCL11A and SOX2 to inhibit the SKIL/TAZ/CTGF axis. Int J Oncol 2020. https://doi.org/10.3892/ijo.2020.4995.

[176] Bruick RK, McKnight SL. A Conserved Family of Prolyl-4-Hydroxylases That Modify HIF. Science 2001;294:1337–40. https://doi.org/10.1126/science.1066373.

[177] Zhang S, Zhang R, Xu R, Shang J, He H, Yang Q. MicroRNA-574-5p in gastric cancer cells promotes angiogenesis by targeting protein tyrosine phosphatase non-receptor type 3 (PTPN3). Gene 2020;733:144383. https://doi.org/10.1016/j.gene.2020.144383.

[178] Lin Z, Chen M, Wan Y, Lei L, Ruan H. miR-574-5p Targets FOXN3 to Regulate the Invasion of Nasopharyngeal Carcinoma Cells via Wnt/β-Catenin Pathway. Technol Cancer Res Treat 2020;19:153303382097165. https://doi.org/10.1177/1533033820971659.

[179] Ji S, Ye G, Zhang J, Wang L, Wang T, Wang Z, et al. miR-574-5p negatively regulates *Qki6/7* to impact *β-catenin* /Wnt signalling and the development of colorectal cancer. Gut 2013;62:716–26. https://doi.org/10.1136/gutjnl-2011-301083.

[180] Tong R, Zhang J, Wang C, Li X, Yu T, Wang L. LncRNA PTCSC3 inhibits the proliferation, invasion and migration of cervical cancer cells via sponging miR-574-5p. Clin Exp Pharmacol Physiol 2020;47:439–48. https://doi.org/10.1111/1440-1681.13186.

[181] Li Q, Li X, Guo Z, Xu F, Xia J, Liu Z, et al. MicroRNA-574-5p Was Pivotal for TLR9 Signaling Enhanced Tumor Progression via Down-Regulating Checkpoint Suppressor 1 in Human Lung Cancer. PLoS ONE 2012;7:e48278. https://doi.org/10.1371/journal.pone.0048278.

[182] McLemore TL, Hubbard WC, Litterst CL, Liu MC, Miller S, McMahon NA, et al. Profiles of prostaglandin biosynthesis in normal lung and tumor tissue from lung cancer patients. Cancer Res 1988;48:3140–7.

[183] Wang D, Dubois RN. Cyclooxygenase-2: a potential target in breast cancer. Semin Oncol 2004;31:64–73. https://doi.org/10.1053/j.seminoncol.2004.01.008.

[184] Rigas B, Goldman IS, Levine L. Altered eicosanoid levels in human colon cancer. J Lab Clin Med 1993;122:518–23.

[185] Finetti F, Travelli C, Ercoli J, Colombo G, Buoso E, Trabalzini L. Prostaglandin E2 and Cancer: Insight into Tumor Progression and Immunity. Biology 2020;9:434. https://doi.org/10.3390/biology9120434.

[186] Kawahara K, Hohjoh H, Inazumi T, Tsuchiya S, Sugimoto Y. Prostaglandin E2-induced inflammation: Relevance of prostaglandin E receptors. Biochim Biophys Acta BBA - Mol Cell Biol Lipids 2015;1851:414–21. https://doi.org/10.1016/j.bbalip.2014.07.008.

[187] Dubois RN, Abramson SB, Crofford L, Gupta RA, Simon LS, Van De Putte LB, et al. Cyclooxygenase in biology and disease. FASEB J Off Publ Fed Am Soc Exp Biol 1998;12:1063–73.

[188] Simmons DL, Botting RM, Hla T. Cyclooxygenase Isozymes: The Biology of Prostaglandin Synthesis and Inhibition. Pharmacol Rev 2004;56:387–437. https://doi.org/10.1124/pr.56.3.3.

[189] Adelizzi RA. COX-1 and COX-2 in health and disease. J Am Osteopath Assoc 1999;99:S7-12.

[190] Murakami M, Nakatani Y, Tanioka T, Kudo I. Prostaglandin E synthase. Prostaglandins Other Lipid Mediat 2002;68–69:383–99. https://doi.org/10.1016/S0090-6980(02)00043-6.

[191] Samuelsson B, Morgenstern R, Jakobsson P-J. Membrane Prostaglandin E Synthase-1: A Novel Therapeutic Target. Pharmacol Rev 2007;59:207–24. https://doi.org/10.1124/pr.59.3.1.

[192] Wu Y-C, Su L-J, Wang H-W, Jeff Lin C-F, Hsu W-H, Chou T-Y, et al. Co-Overexpression of Cyclooxygenase-2 and Microsomal Prostaglandin E Synthase-1 Adversely Affects the Postoperative Survival in Non-small Cell Lung Cancer. J Thorac Oncol 2010;5:1167–74. https://doi.org/10.1097/JTO.0b013e3181e2f4f5.

[193] Elwakeel E, Brüne B, Weigert A. PGE2 in fibrosis and cancer: Insights into fibroblast activation. Prostaglandins Other Lipid Mediat 2019;143:106339. https://doi.org/10.1016/j.prostaglandins.2019.106339.

[194] O'Callaghan G, Houston A. Prostaglandin E2 and the EP receptors in malignancy: possible therapeutic targets?: PGE $_2$ receptors as targets in cancer therapy. Br J Pharmacol 2015;172:5239–50. https://doi.org/10.1111/bph.13331.

[195] Markovič T, Jakopin Ž, Dolenc MS, Mlinarič-Raščan I. Structural features of subtype-selective EP receptor modulators. Drug Discov Today 2017;22:57–71. https://doi.org/10.1016/j.drudis.2016.08.003.

[196] Watabe A, Sugimoto Y, Honda A, Irie A, Namba T, Negishi M, et al. Cloning and expression of cDNA for a mouse EP1 subtype of prostaglandin E receptor. J Biol Chem 1993;268:20175–8. https://doi.org/10.1016/S0021-9258(20)80710-8.

[197] Honda A, Sugimoto Y, Namba T, Watabe A, Irie A, Negishi M, et al. Cloning and expression of a cDNA for mouse prostaglandin E receptor EP2 subtype. J Biol Chem 1993;268:7759–62. https://doi.org/10.1016/S0021-9258(18)53022-2.

[198] Amano H, Ito Y, Suzuki T, Kato S, Matsui Y, Ogawa F, et al. Roles of a prostaglandin E-type receptor, EP3, in upregulation of matrix metalloproteinase-9 and vascular endothelial growth factor during enhancement of tumor metastasis. Cancer Sci 2009;100:2318–24.

https://doi.org/10.1111/j.1349-7006.2009.01322.x.

[199] Israel DD, Regan JW. EP3 prostanoid receptor isoforms utilize distinct mechanisms to regulate ERK 1/2 activation. Biochim Biophys Acta BBA - Mol Cell Biol Lipids 2009;1791:238–45. https://doi.org/10.1016/j.bbalip.2009.01.021.

[200] Bindu S, Mazumder S, Bandyopadhyay U. Non-steroidal anti-inflammatory drugs (NSAIDs) and organ damage: A current perspective. Biochem Pharmacol 2020;180:114147. https://doi.org/10.1016/j.bcp.2020.114147.

[201] Harirforoosh S, Asghar W, Jamali F. Adverse Effects of Nonsteroidal Antiinflammatory Drugs: An Update of Gastrointestinal, Cardiovascular and Renal Complications. J Pharm Pharm Sci 2014;16:821. https://doi.org/10.18433/J3VW2F.

[202] Hanaka H, Pawelzik S-C, Johnsen JI, Rakonjac M, Terawaki K, Rasmuson A, et al. Microsomal prostaglandin E synthase 1 determines tumor growth in vivo of prostate and lung cancer cells. Proc Natl Acad Sci 2009;106:18757–62. https://doi.org/10.1073/pnas.0910218106.

[203] Siljehav V, Olsson Hofstetter A, Jakobsson P-J, Herlenius E. mPGES-1 and prostaglandin E2: vital role in inflammation, hypoxic response, and survival. Pediatr Res 2012;72:460–7. https://doi.org/10.1038/pr.2012.119.

[204] Kamei D, Yamakawa K, Takegoshi Y, Mikami-Nakanishi M, Nakatani Y, Oh-ishi S, et al. Reduced Pain Hypersensitivity and Inflammation in Mice Lacking Microsomal Prostaglandin E Synthase-1. J Biol Chem 2004;279:33684–95. https://doi.org/10.1074/jbc.M400199200.

[205] Coceani F, Akarsu ES. Prostaglandin E $_2$ in the Pathogenesis of Fever: An Update [a]. Ann N Y Acad Sci 1998;856:76–82. https://doi.org/10.1111/j.1749-6632.1998.tb08315.x.

[206] Bergqvist F, Morgenstern R, Jakobsson P-J. A review on mPGES-1 inhibitors: From preclinical studies to clinical applications. Prostaglandins Other Lipid Mediat 2020;147:106383. https://doi.org/10.1016/j.prostaglandins.2019.106383.

[207] Hanahan D, Coussens LM. Accessories to the Crime: Functions of Cells Recruited to the Tumor Microenvironment. Cancer Cell 2012;21:309–22. https://doi.org/10.1016/j.ccr.2012.02.022.

[208] Hanahan D, Weinberg RA. The Hallmarks of Cancer. Cell 2000;100:57–70. https://doi.org/10.1016/S0092-8674(00)81683-9.

[209] Hanahan D, Weinberg RA. Hallmarks of Cancer: The Next Generation. Cell 2011;144:646–74. https://doi.org/10.1016/j.cell.2011.02.013.

[210] Baghban R, Roshangar L, Jahanban-Esfahlan R, Seidi K, Ebrahimi-Kalan A, Jaymand M, et al. Tumor microenvironment complexity and therapeutic implications at a glance. Cell Commun Signal 2020;18:59. https://doi.org/10.1186/s12964-020-0530-4.

[211] Junttila MR, de Sauvage FJ. Influence of tumour micro-environment heterogeneity on therapeutic response. Nature 2013;501:346–54. https://doi.org/10.1038/nature12626.

[212] Lu P, Takai K, Weaver VM, Werb Z. Extracellular Matrix Degradation and Remodeling in Development and Disease. Cold Spring Harb Perspect Biol 2011;3:a005058–a005058. https://doi.org/10.1101/cshperspect.a005058.

[213] Bagher M, Rosmark O, Elowsson Rendin L, Nybom A, Wasserstrom S, Müller C, et al. Crosstalk between Mast Cells and Lung Fibroblasts Is Modified by Alveolar Extracellular Matrix and Influences Epithelial Migration. Int J Mol Sci 2021;22:506. https://doi.org/10.3390/ijms22020506.

[214] Winkler J, Abisoye-Ogunniyan A, Metcalf KJ, Werb Z. Concepts of extracellular matrix remodelling in tumour progression and metastasis. Nat Commun 2020;11:5120. https://doi.org/10.1038/s41467-020-18794-x.

[215] Shrihari T. Dual role of inflammatory mediators in cancer. Ecancermedicalscience 2017;11. https://doi.org/10.3332/ecancer.2017.721.

[216] Bang C, Thum T. Exosomes: New players in cell–cell communication. Int J Biochem Cell Biol 2012;44:2060–4. https://doi.org/10.1016/j.biocel.2012.08.007.

[217] Nawaz M, Shah N, Zanetti B, Maugeri M, Silvestre R, Fatima F, et al. Extracellular Vesicles and Matrix Remodeling Enzymes: The Emerging Roles in Extracellular Matrix Remodeling, Progression of Diseases and Tissue Repair. Cells 2018;7:167. https://doi.org/10.3390/cells7100167.

[218] Peela N, Truong D, Saini H, Chu H, Mashaghi S, Ham SL, et al. Advanced biomaterials and microengineering technologies to recapitulate the stepwise process of cancer metastasis. Biomaterials 2017;133:176–207. https://doi.org/10.1016/j.biomaterials.2017.04.017.

[219] Sounni NE, Noel A. Targeting the Tumor Microenvironment for Cancer Therapy. Clin Chem 2013;59:85–93. https://doi.org/10.1373/clinchem.2012.185363.

[220] Karagiannis GS, Poutahidis T, Erdman SE, Kirsch R, Riddell RH, Diamandis EP. Cancer-Associated Fibroblasts Drive the Progression of Metastasis through both Paracrine and Mechanical Pressure on Cancer Tissue. Mol Cancer Res 2012;10:1403–18. https://doi.org/10.1158/1541-7786.MCR-12-0307.

[221] LeBleu VS, Kalluri R. A peek into cancer-associated fibroblasts: origins, functions and translational impact. Dis Model Mech 2018;11:dmm029447. https://doi.org/10.1242/dmm.029447.

[222] Calon A, Tauriello DVF, Batlle E. TGF-beta in CAF-mediated tumor growth and metastasis. Semin Cancer Biol 2014;25:15–22. https://doi.org/10.1016/j.semcancer.2013.12.008.

[223] David CJ, Huang Y-H, Chen M, Su J, Zou Y, Bardeesy N, et al. TGF-β Tumor Suppression through a Lethal EMT. Cell 2016;164:1015–30. https://doi.org/10.1016/j.cell.2016.01.009.

[224] Bonneaud TL, Lefebvre CC, Nocquet L, Basseville A, Roul J, Weber H, et al. Targeting of MCL-1 in breast cancer-associated fibroblasts reverses their myofibroblastic phenotype and pro-invasive properties. Cell Death Dis 2022;13:787. https://doi.org/10.1038/s41419-022-05214-9.

[225] Olive KP, Jacobetz MA, Davidson CJ, Gopinathan A, McIntyre D, Honess D, et al. Inhibition of Hedgehog Signaling Enhances Delivery of Chemotherapy in a Mouse Model of Pancreatic Cancer. Science 2009;324:1457–61. https://doi.org/10.1126/science.1171362.

[226] Liu L, Liu L, Yao HH, Zhu ZQ, Ning ZL, Huang Q. Stromal Myofibroblasts Are Associated with Poor Prognosis in Solid Cancers: A Meta-Analysis of Published Studies. PLOS ONE 2016;11:e0159947. https://doi.org/10.1371/journal.pone.0159947.

[227] Elwakeel, Brüggemann, Fink, Schulz, Schmid, Savai, et al. Phenotypic Plasticity of Fibroblasts during Mammary Carcinoma Development. Int J Mol Sci 2019;20:4438. https://doi.org/10.3390/ijms20184438.

[228] Grugan KD, Miller CG, Yao Y, Michaylira CZ, Ohashi S, Klein-Szanto AJ, et al. Fibroblast-secreted hepatocyte growth factor plays a functional role in esophageal squamous cell carcinoma invasion. Proc Natl Acad Sci 2010;107:11026–31.

https://doi.org/10.1073/pnas.0914295107.

[229] Erez N, Truitt M, Olson P, Hanahan D. Cancer-Associated Fibroblasts Are Activated in Incipient Neoplasia to Orchestrate Tumor-Promoting Inflammation in an NF-κB-Dependent Manner. Cancer Cell 2010;17:135–47. https://doi.org/10.1016/j.ccr.2009.12.041.

[230] Pankova D, Chen Y, Terajima M, Schliekelman MJ, Baird BN, Fahrenholtz M, et al. Cancer-Associated Fibroblasts Induce a Collagen Cross-link Switch in Tumor Stroma. Mol Cancer Res 2016;14:287–95. https://doi.org/10.1158/1541-7786.MCR-15-0307.

[231] Monteran L, Erez N. The Dark Side of Fibroblasts: Cancer-Associated Fibroblasts as Mediators of Immunosuppression in the Tumor Microenvironment. Front Immunol 2019;10:1835. https://doi.org/10.3389/fimmu.2019.01835.

[232] Yang F, Ning Z, Ma L, Liu W, Shao C, Shu Y, et al. Exosomal miRNAs and miRNA dysregulation in cancer-associated fibroblasts. Mol Cancer 2017;16:148. https://doi.org/10.1186/s12943-017-0718-4.

[233] Schoepp M, Ströse A, Haier J. Dysregulation of miRNA Expression in Cancer Associated Fibroblasts (CAFs) and Its Consequences on the Tumor Microenvironment. Cancers 2017;9:54. https://doi.org/10.3390/cancers9060054.

[234] Kunz-Schughart LA, Knuechel R. Tumor-associated fibroblasts (part I): Active stromal participants in tumor development and progression? Histol Histopathol 2002;17:599–621. https://doi.org/10.14670/HH-17.599.

[235] Tuxhorn JA, Ayala GE, Rowley DR. Reactive stroma in prostate cancer progression. J Urol 2001;166:2472–83.

[236] Sugimoto H, Mundel TM, Kieran MW, Kalluri R. Identification of fibroblast heterogeneity in the tumor microenvironment. Cancer Biol Ther 2006;5:1640–6. https://doi.org/10.4161/cbt.5.12.3354.

[237] O'Connell JT, Sugimoto H, Cooke VG, MacDonald BA, Mehta AI, LeBleu VS, et al. VEGF-A and Tenascin-C produced by S100A4 $^{+}$ stromal cells are important for metastatic colonization. Proc Natl Acad Sci 2011;108:16002–7. https://doi.org/10.1073/pnas.1109493108.

[238] Louka ML, Ramzy MM. Involvement of fibroblast-specific protein 1 (S100A4) and matrix metalloproteinase-13 (MMP-13) in CCl4-induced reversible liver fibrosis. Gene 2016;579:29–33. https://doi.org/10.1016/j.gene.2015.12.042.

[239] Sotgia F, Del Galdo F, Casimiro MC, Bonuccelli G, Mercier I, Whitaker-Menezes D, et al. Caveolin-1−/− Null Mammary Stromal Fibroblasts Share Characteristics with Human Breast Cancer-Associated Fibroblasts. Am J Pathol 2009;174:746–61. https://doi.org/10.2353/ajpath.2009.080658.

[240] Wang L, Yang D, Tian J, Gao A, Shen Y, Ren X, et al. Tumor necrosis factor receptor 2/AKT and ERK signaling pathways contribute to the switch from fibroblasts to CAFs by progranulin in microenvironment of colorectal cancer. Oncotarget 2017;8:26323–33. https://doi.org/10.18632/oncotarget.15461.

[241] Franco OE, Shaw AK, Strand DW, Hayward SW. Cancer associated fibroblasts in cancer pathogenesis. Semin Cell Dev Biol 2010;21:33–9. https://doi.org/10.1016/j.semcdb.2009.10.010.

[242] Linares J, Marín-Jiménez JA, Badia-Ramentol J, Calon A. Determinants and Functions of CAFs Secretome During Cancer Progression and Therapy. Front Cell Dev Biol 2021;8:621070. https://doi.org/10.3389/fcell.2020.621070.

[243] Ferlay J, Colombet M, Soerjomataram I, Mathers C, Parkin DM, Piñeros M, et al. Estimating the global cancer incidence and mortality in 2018: GLOBOCAN sources and methods. Int J Cancer 2019;144:1941–53. https://doi.org/10.1002/ijc.31937.

[244] Walser T, Cui X, Yanagawa J, Lee JM, Heinrich E, Lee G, et al. Smoking and Lung Cancer: The Role of Inflammation. Proc Am Thorac Soc 2008;5:811–5. https://doi.org/10.1513/pats.200809-100TH.

[245] Bodner SM, Minna JD, Jensen SM, D'Amico D, Carbone D, Mitsudomi T, et al. Expression of mutant p53 proteins in lung cancer correlates with the class of p53 gene mutation. Oncogene 1992;7:743–9.

[246] Boffetta P. Human cancer from environmental pollutants: the epidemiological evidence. Mutat Res 2006;608:157–62. https://doi.org/10.1016/j.mrgentox.2006.02.015.

[247] Molina JR, Yang P, Cassivi SD, Schild SE, Adjei AA. Non-Small Cell Lung Cancer: Epidemiology, Risk Factors, Treatment, and Survivorship. Mayo Clin Proc 2008;83:584–94. https://doi.org/10.4065/83.5.584.

[248] Novaes FT, Cataneo DC, Ruiz Junior RL, Defaveri J, Michelin OC, Cataneo AJM. Lung cancer: histology, staging, treatment and survival. J Bras Pneumol 2008;34:595–600. https://doi.org/10.1590/S1806-37132008000800009.

[249] Kenfield SA, Wei EK, Stampfer MJ, Rosner BA, Colditz GA. Comparison of aspects of smoking among the four histological types of lung cancer. Tob Control 2008;17:198–204. https://doi.org/10.1136/tc.2007.022582.

[250] Raffei H, El-Bahesh E, Finianos A, Nasseredine S, Tabbara I. Immune-based Therapies for Non-small Cell Lung Cancer. Anticancer Res 2017;37:377–88. https://doi.org/10.21873/anticanres.11330.

[251] Weir BA, Woo MS, Getz G, Perner S, Ding L, Beroukhim R, et al. Characterizing the cancer genome in lung adenocarcinoma. Nature 2007;450:893–8. https://doi.org/10.1038/nature06358.

[252] The Cancer Genome Atlas Research Network. Comprehensive molecular profiling of lung adenocarcinoma. Nature 2014;511:543–50. https://doi.org/10.1038/nature13385.

[253] The Cancer Genome Atlas Research Network. Comprehensive genomic characterization of squamous cell lung cancers. Nature 2012;489:519–25. https://doi.org/10.1038/nature11404.

[254] Peifer M, Fernández-Cuesta L, Sos ML, George J, Seidel D, Kasper LH, et al. Integrative genome analyses identify key somatic driver mutations of small-cell lung cancer. Nat Genet 2012;44:1104–10. https://doi.org/10.1038/ng.2396.

[255] Sheppard K-A, Fitz LJ, Lee JM, Benander C, George JA, Wooters J, et al. PD-1 inhibits T-cell receptor induced phosphorylation of the ZAP70/CD3ζ signalosome and downstream signaling to PKCθ. FEBS Lett 2004;574:37–41. https://doi.org/10.1016/j.febslet.2004.07.083.

[256] Prima V, Kaliberova LN, Kaliberov S, Curiel DT, Kusmartsev S. COX2/mPGES1/PGE$_2$ pathway regulates PD-L1 expression in tumor-associated macrophages and myeloid-derived suppressor cells. Proc Natl Acad Sci 2017;114:1117–22. https://doi.org/10.1073/pnas.1612920114.

[257] Santos AM, Jung J, Aziz N, Kissil JL, Puré E. Targeting fibroblast activation protein inhibits tumor stromagenesis and growth in mice. J Clin Invest 2009;119:3613–25. https://doi.org/10.1172/JCI38988.

[258] Gaud G, Iochmann S, Guillon-Munos A, Brillet B, Petiot S, Seigneuret F, et al. TFPI-2

silencing increases tumour progression and promotes metalloproteinase 1 and 3 induction through tumour-stromal cell interactions. J Cell Mol Med 2011;15:196–208. https://doi.org/10.1111/j.1582-4934.2009.00989.x.

[259] Bremnes RM, Dønnem T, Al-Saad S, Al-Shibli K, Andersen S, Sirera R, et al. The Role of Tumor Stroma in Cancer Progression and Prognosis: Emphasis on Carcinoma-Associated Fibroblasts and Non-small Cell Lung Cancer. J Thorac Oncol 2011;6:209–17. https://doi.org/10.1097/JTO.0b013e3181f8a1bd.

[260] Fromigué O, Louis K, Dayem M, Milanini J, Pages G, Tartare-Deckert S, et al. Gene expression profiling of normal human pulmonary fibroblasts following coculture with non-small-cell lung cancer cells reveals alterations related to matrix degradation, angiogenesis, cell growth and survival. Oncogene 2003;22:8487–97. https://doi.org/10.1038/sj.onc.1206918.

[261] Tokunou M, Niki T, Eguchi K, Iba S, Tsuda H, Yamada T, et al. c-MET Expression in Myofibroblasts. Am J Pathol 2001;158:1451–63. https://doi.org/10.1016/S0002-9440(10)64096-5.

[262] Yoshimatsu K, Altorki NK, Golijanin D, Zhang F, Jakobsson PJ, Dannenberg AJ, et al. Inducible prostaglandin E synthase is overexpressed in non-small cell lung cancer. Clin Cancer Res Off J Am Assoc Cancer Res 2001;7:2669–74.

[263] Bergqvist F, Ossipova E, Idborg H, Raouf J, Checa A, Englund K, et al. Inhibition of mPGES-1 or COX-2 Results in Different Proteomic and Lipidomic Profiles in A549 Lung Cancer Cells. Front Pharmacol 2019;10:636. https://doi.org/10.3389/fphar.2019.00636.

[264] Saul MJ, Baumann I, Bruno A, Emmerich AC, Wellstein J, Ottinger SM, et al. miR-574-5p as RNA decoy for CUGBP1 stimulates human lung tumor growth by mPGES-1 induction. FASEB J 2019;33:6933–47. https://doi.org/10.1096/fj.201802547R.

[265] Emmerich AC, Wellstein J, Ossipova E, Baumann I, Lengqvist J, Kultima K, et al. Proteomics-Based Characterization of miR-574-5p Decoy to CUGBP1 Suggests Specificity for mPGES-1 Regulation in Human Lung Cancer Cells 2020. https://doi.org/10.25534/TUPRINTS-00011599.

[266] Zhou R, Zhou X, Yin Z, Guo J, Hu T, Jiang S, et al. MicroRNA-574-5p promotes metastasis of non-small cell lung cancer by targeting PTPRU. Sci Rep 2016;6:35714. https://doi.org/10.1038/srep35714.

[267] Jiang W, He Y, Ma Z, Zhang Y, Zhang C, Zheng N, et al. hsa_circ_0008234 inhibits the progression of lung adenocarcinoma by sponging miR-574-5p. Cell Death Discov 2021;7:123. https://doi.org/10.1038/s41420-021-00512-1.

[268] Hegewald AB, Breitwieser K, Ottinger SM, Mobarrez F, Korotkova M, Rethi B, et al. Extracellular miR-574-5p Induces Osteoclast Differentiation via TLR 7/8 in Rheumatoid Arthritis. Front Immunol 2020;11:585282. https://doi.org/10.3389/fimmu.2020.585282.

[269] Johnsen JI, Dyberg C, Wickström M. Neuroblastoma—A Neural Crest Derived Embryonal Malignancy. Front Mol Neurosci 2019;12:9. https://doi.org/10.3389/fnmol.2019.00009.

[270] Louis CU, Shohet JM. Neuroblastoma: Molecular Pathogenesis and Therapy. Annu Rev Med 2015;66:49–63. https://doi.org/10.1146/annurev-med-011514-023121.

[271] Park JR, Eggert A, Caron H. Neuroblastoma: Biology, Prognosis, and Treatment. Hematol Oncol Clin North Am 2010;24:65–86. https://doi.org/10.1016/j.hoc.2009.11.011.

[272] Brodeur GM. Neuroblastoma: biological insights into a clinical enigma. Nat Rev Cancer 2003;3:203–16. https://doi.org/10.1038/nrc1014.

[273] Kushner BH. Neuroblastoma: a disease requiring a multitude of imaging studies. J Nucl Med Off Publ Soc Nucl Med 2004;45:1172–88.

[274] L'Abbate A, Macchia G, D'Addabbo P, Lonoce A, Tolomeo D, Trombetta D, et al. Genomic organization and evolution of double minutes/homogeneously staining regions with *MYC* amplification in human cancer. Nucleic Acids Res 2014;42:9131–45. https://doi.org/10.1093/nar/gku590.

[275] PDQ Pediatric Treatment Editorial Board. Neuroblastoma Treatment (PDQ®). National Cancer Institute (US); 2002.

[276] Brodeur GM. Spontaneous regression of neuroblastoma. Cell Tissue Res 2018;372:277–86. https://doi.org/10.1007/s00441-017-2761-2.

[277] Cohn SL, Pearson ADJ, London WB, Monclair T, Ambros PF, Brodeur GM, et al. The International Neuroblastoma Risk Group (INRG) Classification System: An INRG Task Force Report. J Clin Oncol 2009;27:289–97. https://doi.org/10.1200/JCO.2008.16.6785.

[278] Matthay KK, Reynolds CP, Seeger RC, Shimada H, Adkins ES, Haas-Kogan D, et al. Long-Term Results for Children With High-Risk Neuroblastoma Treated on a Randomized Trial of Myeloablative Therapy Followed by 13- *cis* -Retinoic Acid: A Children's Oncology Group Study. J Clin Oncol 2009;27:1007–13. https://doi.org/10.1200/JCO.2007.13.8925.

[279] Brodeur GM, Nakagawara A, Yamashiro DJ, Ikegaki N, Liu X-G, Azar CG, et al. Expression of TrkA, TrkB and TrkC in human neuroblastomas. J Neurooncol 1997;31:49–56. https://doi.org/10.1023/A:1005729329526.

[280] Lammie G, Cheung N, Gerald W, Rosenblum M, Cordoncardo C. GANGLIOSIDE GD(2) EXPRESSION IN THE HUMAN NERVOUS-SYSTEM AND IN NEUROBLASTOMAS - AN IMMUNOHISTOCHEMICAL STUDY. Int J Oncol 1993. https://doi.org/10.3892/ijo.3.5.909.

[281] Ambros PF, Ambros IM, Brodeur GM, Haber M, Khan J, Nakagawara A, et al. International consensus for neuroblastoma molecular diagnostics: report from the International Neuroblastoma Risk Group (INRG) Biology Committee. Br J Cancer 2009;100:1471–82. https://doi.org/10.1038/sj.bjc.6605014.

[282] Maris JM, Matthay KK. Molecular Biology of Neuroblastoma. J Clin Oncol 1999;17:2264–2264. https://doi.org/10.1200/JCO.1999.17.7.2264.

[283] Hansford LM, Thomas WD, Keating JM, Burkhart CA, Peaston AE, Norris MD, et al. Mechanisms of embryonal tumor initiation: Distinct roles for MycN expression and *MYCN* amplification. Proc Natl Acad Sci 2004;101:12664–9. https://doi.org/10.1073/pnas.0401083101.

[284] Zimmerman KA, Yancopoulos GD, Collum RG, Smith RK, Kohl NE, Denis KA, et al. Differential expression of myc family genes during murine development. Nature 1986;319:780–3. https://doi.org/10.1038/319780a0.

[285] Fischer M, Bauer T, Oberthür A, Hero B, Theissen J, Ehrich M, et al. Integrated genomic profiling identifies two distinct molecular subtypes with divergent outcome in neuroblastoma with loss of chromosome 11q. Oncogene 2010;29:865–75. https://doi.org/10.1038/onc.2009.390.

[286] Plantaz D, Vandesompele J, Van Roy N, Łastowska M, Bown N, Combaret V, et al. Comparative genomic hybridization (CGH) analysis of stage 4 neuroblastoma reveals high frequency of 11q deletion in tumors lackingMYCN amplification. Int J Cancer 2001;91:680–6. https://doi.org/10.1002/1097-0215(200002)9999:9999<::AID-IJC1114>3.0.CO;2-R.

[287] Buckley PG, Alcock L, Bryan K, Bray I, Schulte JH, Schramm A, et al. Chromosomal

and MicroRNA Expression Patterns Reveal Biologically Distinct Subgroups of 11q− Neuroblastoma. Clin Cancer Res 2010;16:2971–8. https://doi.org/10.1158/1078-0432.CCR-09-3215.

[288] Carén H, Kryh H, Nethander M, Sjöberg R-M, Träger C, Nilsson S, et al. High-risk neuroblastoma tumors with 11q-deletion display a poor prognostic, chromosome instability phenotype with later onset. Proc Natl Acad Sci 2010;107:4323–8. https://doi.org/10.1073/pnas.0910684107.

[289] Mehrotra S, Morimiya A, Agarwal B, Konger R, Badve S. Microsomal prostaglandin E2 synthase-1 in breast cancer: a potential target for therapy. J Pathol 2006;208:356–63. https://doi.org/10.1002/path.1907.

[290] Yoshimatsu K, Golijanin D, Paty PB, Soslow RA, Jakobsson PJ, DeLellis RA, et al. Inducible microsomal prostaglandin E synthase is overexpressed in colorectal adenomas and cancer. Clin Cancer Res Off J Am Assoc Cancer Res 2001;7:3971–6.

[291] Sano H, Kawahito Y, Wilder RL, Hashiramoto A, Mukai S, Asai K, et al. Expression of cyclooxygenase-1 and -2 in human colorectal cancer. Cancer Res 1995;55:3785–9.

[292] Khor L-Y, Bae K, Pollack A, Hammond MEH, Grignon DJ, Venkatesan VM, et al. COX-2 expression predicts prostate-cancer outcome: analysis of data from the RTOG 92-02 trial. Lancet Oncol 2007;8:912–20. https://doi.org/10.1016/S1470-2045(07)70280-2.

[293] Johnsen JI, Lindskog M, Ponthan F, Pettersen I, Elfman L, Orrego A, et al. Cyclooxygenase-2 Is Expressed in Neuroblastoma, and Nonsteroidal Anti-Inflammatory Drugs Induce Apoptosis and Inhibit Tumor Growth ***In vivo*** . Cancer Res 2004;64:7210–5. https://doi.org/10.1158/0008-5472.CAN-04-1795.

[294] Rasmuson A, Kock A, Fuskevåg OM, Kruspig B, Simón-Santamaría J, Gogvadze V, et al. Autocrine prostaglandin E2 signaling promotes tumor cell survival and proliferation in childhood neuroblastoma. PloS One 2012;7:e29331. https://doi.org/10.1371/journal.pone.0029331.

[295] Larsson K, Kock A, Idborg H, Arsenian Henriksson M, Martinsson T, Johnsen JI, et al. COX/mPGES-1/PGE $_2$ pathway depicts an inflammatory-dependent high-risk neuroblastoma subset. Proc Natl Acad Sci 2015;112:8070–5. https://doi.org/10.1073/pnas.1424355112.

[296] Kock A, Larsson K, Bergqvist F, Eissler N, Elfman LHM, Raouf J, et al. Inhibition of Microsomal Prostaglandin E Synthase-1 in Cancer-Associated Fibroblasts Suppresses Neuroblastoma Tumor Growth. EBioMedicine 2018;32:84–92. https://doi.org/10.1016/j.ebiom.2018.05.008.

[297] ExoView, Unchainedlabs. https://www.unchainedlabs.com/exoview n.d.

[298] Bonsergent E, Grisard E, Buchrieser J, Schwartz O, Théry C, Lavieu G. Quantitative characterization of extracellular vesicle uptake and content delivery within mammalian cells. Nat Commun 2021;12:1864. https://doi.org/10.1038/s41467-021-22126-y.

[299] Mayerhöfer TG, Popp J. Beer's Law - Why Absorbance Depends (Almost) Linearly on Concentration. ChemPhysChem 2019;20:511–5. https://doi.org/10.1002/cphc.201801073.

[300] Korotkova M, Jakobsson P-J. Microsomal Prostaglandin E Synthase-1 in Rheumatic Diseases. Front Pharmacol 2011;1. https://doi.org/10.3389/fphar.2010.00146.

[301] Timchenko LT, Miller JW, Timchenko NA, DeVore DR, Datar KV, Lin L, et al. Identification of a (CUG)n Triplet Repeat RNA-Binding Protein and Its Expression in Myotonic Dystrophy. Nucleic Acids Res 1996;24:4407–14. https://doi.org/10.1093/nar/24.22.4407.

[302] Fujimura K, Kano F, Murata M. Dual localization of the RNA binding protein CUGBP-1

to stress granule and perinucleolar compartment. Exp Cell Res 2008;314:543–53. https://doi.org/10.1016/j.yexcr.2007.10.024.

[303] Hicks MJ, Mackay B. Comparison of Ultrastructural Features Among Neuroblastic Tumors: Maturation from Neuroblastoma to Ganglioneuroma. Ultrastruct Pathol 1995;19:311–22. https://doi.org/10.3109/01913129509064236.

[304] Wolf E. The role of miR-574-5p in the microenvironment of prostaglandin E2-dependent tumors. Masterthesis. TU Darmstadt, 2019.

[305] Rana S, Yue S, Stadel D, Zöller M. Toward tailored exosomes: The exosomal tetraspanin web contributes to target cell selection. Int J Biochem Cell Biol 2012;44:1574–84. https://doi.org/10.1016/j.biocel.2012.06.018.

[306] Spenlehauer C, Kirn A, Aubertin A-M, Moog C. Antibody-Mediated Neutralization of Primary Human Immunodeficiency Virus Type 1 Isolates: Investigation of the Mechanism of Inhibition. J Virol 2001;75:2235–45. https://doi.org/10.1128/JVI.75.5.2235-2245.2001.

[307] Ishii G, Ochiai A, Neri S. Phenotypic and functional heterogeneity of cancer-associated fibroblast within the tumor microenvironment. Adv Drug Deliv Rev 2016;99:186–96. https://doi.org/10.1016/j.addr.2015.07.007.

[308] Elwakeel E, Brüne B, Weigert A. PGE2 in fibrosis and cancer: Insights into fibroblast activation. Prostaglandins Other Lipid Mediat 2019;143:106339. https://doi.org/10.1016/j.prostaglandins.2019.106339.

[309] O'Brien K, Breyne K, Ughetto S, Laurent LC, Breakefield XO. RNA delivery by extracellular vesicles in mammalian cells and its applications. Nat Rev Mol Cell Biol 2020;21:585–606. https://doi.org/10.1038/s41580-020-0251-y.

[310] Colletti M, Tomao L, Galardi A, Paolini A, Di Paolo V, De Stefanis C, et al. Neuroblastoma-secreted exosomes carrying miR-375 promote osteogenic differentiation of bone-marrow mesenchymal stromal cells. J Extracell Vesicles 2020;9:1774144. https://doi.org/10.1080/20013078.2020.1774144.

[311] Albanese M, Chen Y-FA, Hüls C, Gärtner K, Tagawa T, Mejias-Perez E, et al. MicroRNAs are minor constituents of extracellular vesicles that are rarely delivered to target cells. PLOS Genet 2021;17:e1009951. https://doi.org/10.1371/journal.pgen.1009951.

[312] Chevillet JR, Kang Q, Ruf IK, Briggs HA, Vojtech LN, Hughes SM, et al. Quantitative and stoichiometric analysis of the microRNA content of exosomes. Proc Natl Acad Sci 2014;111:14888–93. https://doi.org/10.1073/pnas.1408301111.

[313] McDonald MK, Tian Y, Qureshi RA, Gormley M, Ertel A, Gao R, et al. Functional significance of macrophage-derived exosomes in inflammation and pain. Pain 2014;155:1527–39. https://doi.org/10.1016/j.pain.2014.04.029.

[314] Reis PP, Drigo SA, Carvalho RF, Lopez Lapa RM, Felix TF, Patel D, et al. Circulating miR-16-5p, miR-92a-3p, and miR-451a in Plasma from Lung Cancer Patients: Potential Application in Early Detection and a Regulatory Role in Tumorigenesis Pathways. Cancers 2020;12:2071. https://doi.org/10.3390/cancers12082071.

[315] Rabinowits G, Gerçel-Taylor C, Day JM, Taylor DD, Kloecker GH. Exosomal MicroRNA: A Diagnostic Marker for Lung Cancer. Clin Lung Cancer 2009;10:42–6. https://doi.org/10.3816/CLC.2009.n.006.

[316] Jin X, Chen Y, Chen H, Fei S, Chen D, Cai X, et al. Evaluation of Tumor-Derived Exosomal miRNA as Potential Diagnostic Biomarkers for Early-Stage Non–Small Cell Lung Cancer Using Next-Generation Sequencing. Clin Cancer Res 2017;23:5311–9.

https://doi.org/10.1158/1078-0432.CCR-17-0577.

[317] Mohammadi M, Goodarzi M, Jaafari MR, Mirzaei HR, Mirzaei H. Circulating microRNA: a new candidate for diagnostic biomarker in neuroblastoma. Cancer Gene Ther 2016;23:371–2. https://doi.org/10.1038/cgt.2016.45.

[318] Matsumoto A, Takahashi Y, Chang H, Wu Y, Yamamoto A, Ishihama Y, et al. Blood concentrations of small extracellular vesicles are determined by a balance between abundant secretion and rapid clearance. J Extracell Vesicles 2020;9:1696517. https://doi.org/10.1080/20013078.2019.1696517.

[319] Garcia-Martin R, Brandao BB, Thomou T, Altindis E, Kahn CR. Tissue differences in the exosomal/small extracellular vesicle proteome and their potential as indicators of altered tissue metabolism. Cell Rep 2022;38:110277. https://doi.org/10.1016/j.celrep.2021.110277.

[320] Yáñez-Mó M, Siljander PR-M, Andreu Z, Bedina Zavec A, Borràs FE, Buzas EI, et al. Biological properties of extracellular vesicles and their physiological functions. J Extracell Vesicles 2015;4:27066. https://doi.org/10.3402/jev.v4.27066.

[321] Wolpaw AJ, Grossmann LD, Dessau JL, Dong MM, Aaron BJ, Brafford PA, et al. Epigenetic state determines inflammatory sensing in neuroblastoma. Proc Natl Acad Sci 2022;119:e2102358119. https://doi.org/10.1073/pnas.2102358119.

[322] Chuang J-H, Chuang H-C, Huang C-C, Wu C-L, Du Y-Y, Kung M-L, et al. Differential toll-like receptor 3 (TLR3) expression and apoptotic response to TLR3 agonist in human neuroblastoma cells. J Biomed Sci 2011;18:65. https://doi.org/10.1186/1423-0127-18-65.

[323] Hassan F, Islam S, Tumurkhuu G, Naiki Y, Koide N, Mori I, et al. Intracellular expression of toll-like receptor 4 in neuroblastoma cells and their unresponsiveness to lipopolysaccharide. BMC Cancer 2006;6:281. https://doi.org/10.1186/1471-2407-6-281.

[324] Nurmik M, Ullmann P, Rodriguez F, Haan S, Letellier E. In search of definitions: Cancer-associated fibroblasts and their markers. Int J Cancer 2020;146:895–905. https://doi.org/10.1002/ijc.32193.

[325] Wu X, Wu X, Ma Y, Shao F, Tan Y, Tan T, et al. CUG-binding protein 1 regulates HSC activation and liver fibrogenesis. Nat Commun 2016;7:13498. https://doi.org/10.1038/ncomms13498.

[326] Cast A, Kumbaji M, D'Souza A, Rodriguez K, Gupta A, Karns R, et al. Liver Proliferation Is an Essential Driver of Fibrosis in Mouse Models of Nonalcoholic Fatty Liver Disease. Hepatol Commun 2019;3:1036–49. https://doi.org/10.1002/hep4.1381.

[327] Chang K, Baginski J, Hassan SF, Volin M, Shukla D, Tiwari V. Filopodia and Viruses: An Analysis of Membrane Processes in Entry Mechanisms. Front Microbiol 2016;7. https://doi.org/10.3389/fmicb.2016.00300.

[328] Heusermann W, Hean J, Trojer D, Steib E, von Bueren S, Graff-Meyer A, et al. Exosomes surf on filopodia to enter cells at endocytic hot spots, traffic within endosomes, and are targeted to the ER. J Cell Biol 2016;213:173–84. https://doi.org/10.1083/jcb.201506084.

[329] Mattila PK, Lappalainen P. Filopodia: molecular architecture and cellular functions. Nat Rev Mol Cell Biol 2008;9:446–54. https://doi.org/10.1038/nrm2406.

[330] Karin M, Greten FR. NF-κB: linking inflammation and immunity to cancer development and progression. Nat Rev Immunol 2005;5:749–59. https://doi.org/10.1038/nri1703.

[331] Kawai T, Akira S. The role of pattern-recognition receptors in innate immunity: update on Toll-like receptors. Nat Immunol 2010;11:373–84. https://doi.org/10.1038/ni.1863.

[332] Zhang A, Liu X, Cogan JG, Fuerst MD, Polikandriotis JA, Kelm RJ, et al. YB-1 Coordinates Vascular Smooth Muscle α-Actin Gene Activation by Transforming Growth Factor β1 and Thrombin during Differentiation of Human Pulmonary Myofibroblasts. Mol Biol Cell 2005;16:4931–40. https://doi.org/10.1091/mbc.e05-03-0216.

[333] Germann UA, Furey BF, Markland W, Hoover RR, Aronov AM, Roix JJ, et al. Targeting the MAPK Signaling Pathway in Cancer: Promising Preclinical Activity with the Novel Selective ERK1/2 Inhibitor BVD-523 (Ulixertinib). Mol Cancer Ther 2017;16:2351–63. https://doi.org/10.1158/1535-7163.MCT-17-0456.

[334] Cui J, Qi S, Liao R, Su D, Wang Y, Xue S. MiR-574–5p promotes the differentiation of human cardiac fibroblasts via regulating ARID3A. Biochem Biophys Res Commun 2020;521:427–33. https://doi.org/10.1016/j.bbrc.2019.09.107.

[335] Ratliff ML, Shankar M, Guthridge JM, James JA, Webb CF. TLR engagement induces ARID3a in human blood hematopoietic progenitors and modulates IFNα production. Cell Immunol 2020;357:104201. https://doi.org/10.1016/j.cellimm.2020.104201.

[336] Horibe S, Tanahashi T, Kawauchi S, Murakami Y, Rikitake Y. Mechanism of recipient cell-dependent differences in exosome uptake. BMC Cancer 2018;18:47. https://doi.org/10.1186/s12885-017-3958-1.

[337] Borges FT, Melo SA, Özdemir BC, Kato N, Revuelta I, Miller CA, et al. TGF- β 1–Containing Exosomes from Injured Epithelial Cells Activate Fibroblasts to Initiate Tissue Regenerative Responses and Fibrosis. J Am Soc Nephrol 2013;24:385–92. https://doi.org/10.1681/ASN.2012101031.

[338] Biernacka A, Dobaczewski M, Frangogiannis NG. TGF-β signaling in fibrosis. Growth Factors 2011;29:196–202. https://doi.org/10.3109/08977194.2011.595714.

[339] Mallegol J, Van Niel G, Lebreton C, Lepelletier Y, Candalh C, Dugave C, et al. T84-Intestinal Epithelial Exosomes Bear MHC Class II/Peptide Complexes Potentiating Antigen Presentation by Dendritic Cells. Gastroenterology 2007;132:1866–76. https://doi.org/10.1053/j.gastro.2007.02.043.

[340] Arab T, Mallick ER, Huang Y, Dong L, Liao Z, Zhao Z, et al. Characterization of extracellular vesicles and synthetic nanoparticles with four orthogonal single-particle analysis platforms. J Extracell Vesicles 2021;10. https://doi.org/10.1002/jev2.12079.

[341] Pols MS, Klumperman J. Trafficking and function of the tetraspanin CD63. Exp Cell Res 2009;315:1584–92. https://doi.org/10.1016/j.yexcr.2008.09.020.

[342] Mathieu M, Névo N, Jouve M, Valenzuela JI, Maurin M, Verweij FJ, et al. Specificities of exosome versus small ectosome secretion revealed by live intracellular tracking of CD63 and CD9. Nat Commun 2021;12:4389. https://doi.org/10.1038/s41467-021-24384-2.

[343] Tan YH, Liu M, Nolting B, Go JG, Gervay-Hague J, Liu G. A Nanoengineering Approach for Investigation and Regulation of Protein Immobilization. ACS Nano 2008;2:2374–84. https://doi.org/10.1021/nn800508f.

[344] Carloni V, Mazzocca A, Ravichandran KS. Tetraspanin CD81 is linked to ERK/MAPKinase signaling by Shc in liver tumor cells. Oncogene 2004;23:1566–74. https://doi.org/10.1038/sj.onc.1207287.

[345] Murayama Y, Miyagawa J, Oritani K, Yoshida H, Yamamoto K, Kishida O, et al. CD9-mediated activation of the p46 Shc isoform leads to apoptosis in cancer cells. J Cell Sci 2004;117:3379–88. https://doi.org/10.1242/jcs.01201.

[346] Galán M, Miguel M, Beltrán AE, Rodríguez C, García-Redondo AB, Rodríguez-Calvo

R, et al. Angiotensin II differentially modulates cyclooxygenase-2, microsomal prostaglandin E2 synthase-1 and prostaglandin I2 synthase expression in adventitial fibroblasts exposed to inflammatory stimuli. J Hypertens 2011;29:529–36. https://doi.org/10.1097/HJH.0b013e328342b271.

[347] Nah S-S, Won H-J, Ha E, Kang I, Cho HY, Hur S-J, et al. Epidermal growth factor increases prostaglandin E2 production via ERK1/2 MAPK and NF-κB pathway in fibroblast like synoviocytes from patients with rheumatoid arthritis. Rheumatol Int 2010;30:443–9. https://doi.org/10.1007/s00296-009-0976-6.

[348] Hurwitz SN, Nkosi D, Conlon MM, York SB, Liu X, Tremblay DC, et al. CD63 Regulates Epstein-Barr Virus LMP1 Exosomal Packaging, Enhancement of Vesicle Production, and Noncanonical NF-κB Signaling. J Virol 2017;91:e02251-16. https://doi.org/10.1128/JVI.02251-16.

[349] Yamagata T, Yoshizawa J, Ohashi S, Yanaga K, Ohki T. Expression patterns of microRNAs are altered in hypoxic human neuroblastoma cells. Pediatr Surg Int 2010;26:1179–84. https://doi.org/10.1007/s00383-010-2700-8.

6. Appendix

6.1. Abbreviations

AC	Adenocarcinoma of the Lung
AGO2	Argonaute 2
ALIX	Apoptosis-linked gene 2 interacting protein X
Alyref	Aly/REF export factor
AP	Alkaline phosphatase
ARID3A	AT-Rich Interaction Domain 3A
ath	*Arabidopsis thaliana*
BSA	Bovine serum albumin
Ca^{2+}	Calcium
CAF	Cancer associated fibroblast
cAMP	Cyclic adenosine monophosphate
cDNA	Complementary DNA
CEBPA	CCAAT/enhancer-binding protein alpha
cel	*Caenorhabditis elegans*
COX	Cyclooxygenase
cPGES	Cytosolic PGE synthase
ct	Cycle threshold
CUGBP1	CUG-RNA binding protein 1
DAB	3,3′-Diaminobenzidine
DAPI	4',6-Diamidino-2-phenylindol
DIG	Digoxygenin
DiO	3,3′- dioctadecyloxacarbocyanine perchlorate
DMEM	Dulbecco's modified Eagle medium
DMSO	Dimethyl sulfoxide
DNA	Desoxyribonucleic acid
ECM	Extracellular matrix
EDTA	Ethylenediaminetetraacetic acid
EGFR	Epidermal growth factor receptor
EP1-4	E-type prostanoids receptors 1-4
ERK1/2	extracellular signal-regulated kinases 1/2
ESCRT	Endosomal sorting complexes required for transport
EtOH	Ethanol
EV	Extracellular vesicle
F12K	Ham's F-12 medium
FA	Formaldehyde
FAP	Fibroblast activation protein
FasL	Fas ligand

FCS	Fetal calf serum
FSP	Fibroblast specific protein
Fus	Fused in sarcoma
GAPDH	Glycerinaldehyd-3-phosphate-dehydrogenase
GD2	Disialoganglioside
GFP	Green fluorescent protein
GTC	Guanidinium thiocyanate
GTP	Guanosine-5'-triphosphate
$G\alpha_s$	Stimulatory G-protein coupled receptor subunit
HIV	Human immunodeficiency virus
HMGB1	high-mobility group protein B1
hnRNPs	Heterogeneous nuclear ribonucleoproteins
HPDG	15-prostaglandin dehydrogenase
HPGD	15-PG dehydrogenase
HRS	Hepatocyte growth factor-regulated tyrosine kinase substrate
HSP	Heat Shock Protein
IHC	Immunohistochemistry
IL	Interleukin
ILV	Intraluminal vesicle
ISH	*In-situ* hybridization
KRAS	Kirsten rat sarcoma viral oncogene homologue
LC	Lung cancer
LNA	Locked nucleic acid
MAPK	Mitogen-activated protein kinases
miR	MicroRNA
MISEV	Minimal information for studies of extracellular vesicles
mPGES-1, or PTGES	Microsomal Prostaglandin E2 Synthase 1
MQ	Milli Q water
mRNA	Messenger RNA
MRP	Multidrug resistance protein
MTT	3-(4,5-dimethylthiazol-2-yl)-2,5-diphenyltetrazoliumbromide
MVB	Multivesicular body
MVE	Multivesicular endosomes
MYCN	*MYCN* proto-oncogene
NB	Neuroblastoma
NBT/BCIP	Nitro blue tetrazolium/ 5-Bromo-4-chloro-3-indolyl-phosphate
NF1	Neurofibromatosis type 1 gene
NFκB	Nuclear factor-kappaB
NLuc	Nano-Luciferase
NOXP20	Nervous system overexpressed protein 20
NSAIDs	Non-steroidal anti-inflammatory drugs

NSCLC	Non-small cell lung cancer
nSMase2	Neutral sphingomyelinase 2
Nts	Nucleotides
Oe	Overexpression
PBS	Phosphate Buffered Saline
PD-L1	Programmed cell death protein ligand 1
PDGFR	Platelet-derived growth factor receptor
PEI	Polyethyleneimine
PG	Prostaglandin
PGE_2	Prostaglandin E_2
PKA	Protein kinase A
PKC	Protein kinase C
PLC	Phospholipase C
PTPRU	Protein typrosine phosphatase receptor type U
Rab proteins	Rat sarcoma viral oncogene homologue associated binding protein
RBP	RNA-binding protein
RIP	RNA-Immunoprecipitation
RISC	RNA-induces silencing complex
RNA	Ribonucleic acid
RND3	Rho family GTPase 3
RT	Room temperature
RT-qPCR	Reverse transcription polymerase chain reaction
SCC	Squamous cell carcinoma
SCLC	Small-cell lung cancer
ScrC sEV	Scrambled control
SDS	Sodium dodecyl sulfate
SDS-PAGE	Sodium dodecyl sulfate-polyacrylamide gel electrophoresis
SEM	Standard error of mean
sEV	Small extracellular vesicle (s)
siRNA	Small interfering RNA
SNAP-25	Synaptosomal-associated protein of 25 kDa
SNARE	Soluble N-ethylmaleimide-sensitive-factor attachment receptor
SSC	Saline-sodium citrate
SYNCRIP	Synaptotagmin-binding cytoplasmic RNA-interacting protein
TE	Trypsin-EDTA
TEM	Transmission electron microscopy
TGFβ	Transforming growth factor-β
TLR	Toll-Like receptor
TME	Tumor microenvironment
TNF	Tumor necrosis factor
Trk	Tropomysin receptor kinase

Tspan8	Tetraspanin 8
TXA2	Thromboxane A2
UTR	Untranslated region
VCAM-1	vascular cell adhesion molecule 1
VPS4A	Vacuolar protein sorting-associated protein 4A
VTA1	Vesicle trafficking 1
WT	Wildtype
α-SMA	α-smooth muscle actin

6.2. Supplementary data

Table S1: Buffer compositions of self-made buffers and solutions

Buffer	Composition
B1 (RIP)	20 mM Tris-HCl pH 7.5 (Carl Roth, Karlsruhe, GER) 150 mM NaCl 2 mM EDTA 0.1% SDS 1% Triton X-100 1x Protease Inhibitor Cocktail (Roche) Ad 10 mL MQ
B2 (RIP)	20 mM Tris-HCl pH 7.5 (Carl Roth, Karlsruhe, GER) 500 mM NaCl 2 mM EDTA 0.1% SDS 1% Triton X-100 1x Protease Inhibitor Cocktail (Roche) Ad 10 mL MQ
B3 (RIP)	10 mM Tris-HCl pH 7.5 (Carl Roth, Karlsruhe, GER) 250 mM LiCl 1 mM EDTA (Roche) 1% NaDeoxycholate (Sigma-Aldrich) 1% NP-40 (Igepal) (Sigma-Aldrich) 1x Protease Inhibitor Cocktail (Roche) Ad 10 mL MQ
Citrate Buffer	10 mM trisodium citrate (Carl Roth, Karlsruhe, GER), pH 6
Extraction buffer	10 mM sodium acetate (Carl Roth, Karlsruhe, GER) 150 mM sucrose (Carl Roth, Karlsruhe, GER) pH 4.8
ISH Antibody Buffer	0.05% (v/v) Tween20 1% (w/v) sheep serum (Jackson Immunoresearch, Ely, UK) 1% (w/v) BSA (Sigma-Aldrich, Darmstadt, GER) In PBS
ISH Blocking Buffer	0.1% (v/v) Tween20 2% (w/v) sheep serum (Jackson Immunoresearch, Ely, UK) 1% (w/v) BSA (Sigma-Aldrich, Darmstadt, GER) In PBS

KTBT Buffer	50 mM Tris-HCl (Carl Roth, Karlsruhe, GER) 150 mM NaCl (Carl Roth, Karlsruhe, GER) 10 mM KCl (Carl Roth, Karlsruhe, GER)
Lysis buffer RIP	10 mM Tris-HCl (Carl Roth, Karlsruhe, GER) 10 mM KCl 1.5 mM $MgCl_2$ 0.5 mM LiCl 0.9% NP-40 (Igepal) 1x Protease Inhibitor Cocktail (Roche) 40 U/µL Ribonuclease Inhibitor Ad 10 mL MQ
Protein loading buffer 4 x	5 mL glycerin (Carl Roth, Karlsruhe, GER) 1.5 mL 2-mercaptoethanol (Carl Roth, Karlsruhe, GER) 2 mL 20% (w/v) SDS (AppliChem GmbH, Darmstadt) 1.5 mL MQ One spatula tip bromophenol blue (Carl Roth, Karlsruhe, GER)
Proteinase-K Buffer	5 mL 1 M Tris-HCl (pH 7.4) (Carl Roth, Karlsruhe, GER) 2 mL 0.5 M EDTA (Carl Roth, Karlsruhe, GER) 0.2 mL 5 M NaCl (Carl Roth, Karlsruhe, GER) added MQ to 1 L
RIPA Buffer	50 mM Tris-HCl (Carl Roth, Karlsruhe, GER) 150 mM NaCl (Carl Roth, Karlsruhe, GER) 1% Triton X-100 (Carl Roth, Karlsruhe, GER) 0,1% SDS 0,1% deoxycholate acid (MilliporeSigma, Burlington, USA)
SDS running buffer 10 x	10 g SDS (AppliChem GmbH, Darmstadt) 30.3 g Tris-HCl (Carl Roth, Karlsruhe, GER) 144.1 g glycine (Carl Roth, Karlsruhe, GER) Ad 1 L MQ
Transfer buffer 1 x	3 g Tris-HCl (Carl Roth, Karlsruhe, GER) 14.4 g glycine (Carl Roth, Karlsruhe, GER) 200 mL methanol (VWR, Radnor, USA) Ad 1 L MQ

6.3. Ehrenwörtliche Erklärung

Ich erkläre hiermit, dass ich die vorliegende Arbeit entsprechend den Regeln guter wissenschaftlicher Praxis selbstständig und ohne unzulässige Hilfe Dritter angefertigt habe.

Sämtliche aus fremden Quellen direkt oder indirekt übernommenen Gedanken sowie sämtliche von Anderen direkt oder indirekt übernommenen Daten, Techniken und Materialien sind als solche kenntlich gemacht. Die Arbeit wurde bisher bei keiner anderen Hochschule zu Prüfungszwecken eingereicht. Die eingereichte elektronische Version stimmt mit der schriftlichen Version überein.

Darmstadt, den

.....

Teile dieser Arbeit wurden/werden publiziert in:

Julia Donzelli, Eva Proestler, Anna Riedel, Sheila Nevermann, Brigitte Hertel, Andreas Guenther, Stefan Gattenlöhner, Rajkumar Savai, Karin Larsson, Meike J. Saul: **Small extracellular vesicle-derived miR-574-5p regulates PGE2-biosynthesis via TLR7/8 in lung cancer**, Journal of Extracellular vesicles, October 2021, doi: 10.1002/jev2.12143

Eva Proestler, Julia Donzelli, Sheila Nevermann, Kai Breitwieser, Leon F Koch, Tatjana Best, Maria Fauth, Malin Wickström, Patrick Harter, Per Kogner, Grégory Lavieu, Karin Larsson, Meike J Saul: **The different functionalities of sEV-derived miR-574-5p in PGE2-dependent tumors correlate with the tetraspanin composition of sEV**, Frontiers Pharmacology, in revision

6.4. Danksagung

Ich danke **Dr. Meike Saul**, die mich vor über 4 Jahren in ihrer Gruppe aufgenommen und auch nach meiner Masterarbeit nicht gehen lassen hat. Danke für die schöne Zeit in Deiner Gruppe, für die gute Betreuung, zahlreiche Diskussionen und Dein offenes Ohr bei allen Problemen.

Außerdem möchte ich mich bei **Prof. Dr. Beatrix Süß** für die Unterstützung in den letzten Jahren bedanken, für die fachlichen Diskussionen und die schöne Zeit bei den Winterschools.

Ein großes Dankeschön geht an alle aktuellen und ehemaligen Mitglieder der **AG Süß und AG Weigand**. Danke für die tolle Arbeitsatmosphäre, lustige Mittagspausen, gemeinsame Ausflüge und die schöne gemeinsame Zeit.

Außerdem möchte ich mich bei der **AG Saul**, vor allem bei **Kai, Maria, Leon und Christin** bedanken. Danke, dass ihr mich so unterstützt habt, für die dringend benötigten Kaffeepausen in verwirrten Momenten und für die Zusammenarbeit während der letzten Jahre.

Danke auch an **Dorie**, die mir in meiner Anfangszeit viele Methoden beigebracht hat. Danke für deine fachliche und auch sonstige Unterstützung.

Vielen Dank auch an meine ehemaligen Labornachbarn **Jamina, Anna, Claudi und Chiara**. Die Zusammenarbeit mit euch hat mir immer viel Spaß gemacht.

Ein ganz besonderer Dank geht an **Sheila**. Du warst die beste Masterstudentin, die ich mir hätte wünschen können. Danke für alle fachlichen Anregungen, die großartige Zusammenarbeit, für das Brechen des Triton-Fluchs, für Deine Korrekturen und für die tolle Zeit, die wir gemeinsam hatten.

Und natürlich möchte ich **Julia** danken, die mich von der Idee eine Doktorarbeit zu schreiben überzeugt hat. Ich bin so froh, dass ich damals meine Masterarbeit bei Dir geschrieben habe und dass wir so suuuper als „Team Schmelzbrot“ zusammenarbeiten konnten und es nach wie vor können.

Ein Großes Danke an meine Freunde und Familie. Ein besonderes Dankeschön geht an **Marry, Desi und Angi** für die mittwöchigen Mädelsabende/Therapiestunden und an **Simon** für unsere ausgedehnten Spaziergänge.

Vielen Dank an meine Schwester **Viola**, die mir ein Vorbild in Sachen Disziplin und Ehrgeiz ist und mich in den letzten Jahren immer unterstützt hat und mir zur Seite stand. Danke, dass ich dir immer alles erzählen kann.

Danke an meine Eltern **Maili und Peter**. Danke, dass Ihr mir die Möglichkeit gegeben habt zu studieren und zu promovieren. Danke, dass Ihr mir Rückhalt gebt und mir mit Rat und Tat zu

Seite steht, egal worum es geht. Ich weiß, dass Ihr mich immer bei allem, was ich mir Vornehme unterstützen werdet und ich bin so dankbar, dass ich euch habe. Danke für Alles.

Zuletzt möchte ich mich bei meinem Mann **René** bedanken. Danke für deine Unterstützung und dein Verständnis während meines Studiums. Die letzten 9 Jahre waren turbulent, aber auch großartig und wir haben sie zusammen gemeistert. Ich freue mich auf alles, was noch kommt und ich weiß, dass wir gemeinsam alles schaffen werden.